Seepage Effects on Dune Geometry and Turbulence Flow Characteristics

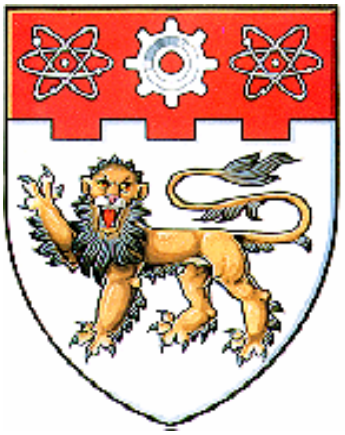

Lu Yan

SCHOOL OF CIVIL & ENVIRONMENTAL ENGINEERING
NANYANG TECHNOLOGICAL UNIVERSITY

2006

Seepage Effects on Dune Geometry and Turbulence Flow Characteristics

Lu Yan

SCHOOL OF CIVIL & ENVIRONMENTAL ENGINEERING

A thesis submitted to the Nanyang Technological University
in fulfillment of the requirement for the degree of
Doctor of Philosophy

2006

ACKNOWLEDGEMENTS

The author would like to express his sincere gratitude to his supervisor, Professor Chiew Yee Meng, for his excellent guidance, patience, and encouragement throughout the execution of the experimental work, the analysis of results and the preparation of this thesis.

Special thanks are expressed to Associate Professor Cheng Nian Sheng for his constant assistance and encouragement from the beginning. Many thanks are expressed to Professor Tay Joo Hwa, Associate Professor Lo Yat Man, Edmond, and Associate Professor Tan Soon Keat for their assistance and encouragement. The author extends his thanks to the technicians in the School of Civil and Environmental Engineering for their help and suggestions in setting up the apparatus and collecting experimental data.

The author is also grateful to Associate Professor Chin Chen Onn for his invaluable comments on this study.

The Research Scholarship offered by Nanyang Technological University is gratefully acknowledged.

Finally, the author deeply appreciates his parents and his wife for their patience, encouragement and support.

CONTENTS

SUMMARY

This study explores how seepage affects the angle of repose of cohesionless sediments, geometrical dimension of dunes, and turbulence characteristics of flows over a stationary two-dimensional dune. Experiments were conducted to achieve the stated objectives except that a theoretical analysis was also carried out to examine seepage effects on the angle of repose of the sediment. In the study, a total of four series of tests were conducted, each with a definite objective.

A review of published studies on flow and sediment transport with seepage is first presented to better understand the state-of-the-art in this area of research. Contradictory results in published literature are highlighted, and the reason for the differences discussed.

The angle of repose of cohesionless sediments in the presence of seepage can be computed using a theoretical expression derived on the basis of the analysis of forces, including seepage force, acting on a single sphere lying on three closely packed spherical particles. The derived relationship between the hydraulic gradient and angle of repose is then reasonably applied to predict the lee-side slope of dunes when the applied seepage rate is known. The results, which were verified with experimental data, show that injection (upward seepage) reduces the angle of repose of sediments and the lee-side slope of dunes, whereas suction (downward seepage) does the opposite.

The variations of the height and length of dunes caused by seepage were then analyzed; they show that the dune height is reduced when injection is present; while suction increases it. Additionally, the response of dune celerity to seepage is also examined. The data show that suction increases the celerity while injection reduces it. These changes may be used to explain why suction appears to increase the wavelength of dunes; whereas injection does the opposite. In conjunction with the finding on seepage effects on dune height and dune celerity, it may be inferred that suction and injection increases and decreases bed-load transport rate, respectively.

The response of the time-average velocity distributions, turbulence intensity distributions and Reynolds shear stress distributions over a single fixed, two-dimensional dune to bed suction was investigated. The results show that suction causes the flow to adhere to the dune-bed boundaries resulting in reduction of the separation length, rendering the streamwise velocity profile to be more uniform. Moreover, suction always produces smaller or more negative vertical velocities in the near-bed region, and decreases both turbulence intensity and Reynolds shear stresses of the flow near to bed. These results confirm that suction can render the turbulent flow in the boundary layer to become less turbulent. The measured data along the single dune show that changes of both turbulence intensity and Reynolds shear stress due to suction are less apparent in the dune trough. The spatially-averaged skin drag calculated from the measured Reynolds shear stress is found to increase with suction. It may also be inferred from this computation that the average bed-load discharge tends to be larger in the presence of suction than that without suction, a result that is consistent with movable bed physical model results.

LIST OF TABLES

LIST OF FIGURES

NOTATION

The following symbols are used in this thesis:

a,b,c = empirical coefficients;

a' = height of separation point from the reattachment point;

A = a function of water surface slope;

b' = flow depth at the crest;

B = roughness function;

cc = sediment concentration in ppm by weight;

c_e = dune migration velocity;

C = 2.7 or 2.2;

C_D = drag coefficient;

C_L = lift coefficient;

C_u = uniform coefficient;

C' = Chezy coefficient;

D = diameter of sediment particles;

D_{16} = 16% by weight of sediment is finer than that indicated;

D_{50} = median diameter of particles;

D_{84} = 84% by weight of sediment is finer than that indicated;

D_{90} = 90% by weight of sediment is finer than that indicated;

D_* = dimensionless grain size;

e_1 and e_2 = moment arms of seepage and submerged weight forces, respectively;

$E, F,$ and G = contact points of the top single particle with the three underlying spheres;

f_* = friction factor;

F_D = drag force;

F_L = lift force;

F_S = seepage force acting on a particle;

g = gravitational acceleration;

g_0 = constant of integration;

g_b = bed-load discharge per unit width per unit time;

$\overline{g_b}$ = average bed-load transport rate between the crests of two neighbouring dunes;

g_s = sediment transport rate;

G' = a transport parameter;

h = water depth;

h_0 = water depth without seepage;

H = dune or ripple height;

H_0 = dune height without seepage;

H_x = developing height of dunes;

i = hydraulic gradient of seepage or 0, 1, …, N-1;

i_c = hydraulic gradient of seepage under quick condition;

I_s, I_0 = energy slope with and without seepage;

J = water surface slope;

k = $(y_1 - y_{0x})/y_x$;

k_s = granular roughness of bed surface;

$K/\overline{K}$ = ratio of the diameter of single grain to the average diameter of the bed grains;

l_s = length of sediment slice;

L = length of seepage zone;

m = exponent =1~2;

n = number of velocity samples or number of particles in the slice;

N = normal force;

$\overline{N}$ = seepage intensity parameter;

O = center of the triangle formed by the centers of the three underlying spheres;

O_0 = center of the triangle formed by the contact points E, F and G;

O_1, O_2, O_3, O_4 = centers of the four spheres;

p = pressure;

P = nominal pivot point;

q_s = seepage discharge;

Q = main flow discharge;

r = a dimensionless index;

R = $|v_s/U|$ = suction rate;

R_{e*} = grain Reynolds number;

R_h = hydraulic radius of the bed;

s = ρ_s / ρ;

S = seepage force acting on particles on the top layer;

S_b = bed slope;

t = time;

T = tangential force;

u = time-averaged streamwise velocity of flow;

u_1, u_x = velocity at y from bed in cross-section at A and B;

u_b = effective velocity acting on particles at the bed;

u_i = instantaneous streamwise velocity of flow;

$u_{\max}$ = maximal streamwise velocity;

u_{r0}, u_{rs} = measured velocities at the reference height without and with suction, respectively;

u_s = slip velocity due to seepage;

u_t = velocity tangential to bed at the dune crest;

u_* = shear velocity;

u_{*0} = shear velocity without seepage;

u_{*c} = critical shear velocity with seepage;

u_{*c0} = critical shear velocity without seepage;

u_{*sf} = skin friction velocity;

u' = rms value of the streamwise velocity fluctuations;

u_s', u_0' = rms value of the streamwise fluctuating velocities with and

without seepage, respectively;

$u_*^{'}$ = $U\sqrt{g}/C^{'}$

U = depth-averaged flow velocity;

U_s, U_0 = average flow velocity with and without seepage, respectively;

U_{0x} = average flow velocity within the depth of y_{xx};

v = time-averaged vertical velocity of flow;

v_i = instantaneous vertical velocity of flow;

v_s = seepage velocity;

v_{sc} = critical seepage velocity under quick condition;

$v^{'}$ = rms value of the vertical velocity fluctuations;

$v_s^{'}, v_0^{'}$ = rms value of the vertical fluctuating velocities with and without seepage, respectively;

W = submerged weight force;

x = streamwise coordinate or distance from the leading edge of seepage zone;

y = normal coordinate or elevation of the sand dune boundary above a horizontal datum;

y_0 = zero-velocity displacement measured from the theoretical bed surface or boundary roughness length;

y_{0x} = depth below which water is removed from the stream between cross-section A and B due to seepage;

y_1, y_x = water depth at cross-section A and B;

y_{xx} = depth below which water is sucked into the bed across the infinitesimal element;

y_s = a reference height at which the interaction due to seepage takes place;

y_* = thickness of the average internal boundary layer;

Y = mobility number;

Y_{cr} = critical mobility number;

Z = h/D;

α = angle of repose of dimensionless sediments or the fully-developed lee-side slope of dunes;

α_0 = angle of repose of sediments without seepage;

α_x = developing angle of the lee-side slope of dunes;

β = coefficient depending on the size of sediment particles which ranges between 0.5 for coarse granular materials and 1 for fine grains;

β' = momentum correction factor;

θ = angle of the bed slope;

λ = dune or ripple length;

λ_r = separation length of flow;

ρ = mass density of fluid;

ρ_s = density of particles;

γ_b = specific weight of bed sediments;

γ_s = submerged specific weight of the particles;

μ = dynamic viscosity of fluid;

μ_f = coefficient of friction between the spherical surfaces;

ν = kinematic viscosity coefficient;

τ = shear stress;

τ_b = bed shear stress;

τ_{b0}, τ_{bs}, = bed shear stress without and with seepage, respectively;

τ_{c0} = critical shear stress without seepage;

τ_{cs} = critical shear stress with seepage;

τ_e = excess shear stress due to suction;

τ_{fd} = form drag;

$\tau_r = -\rho\overline{u'v'}$ = Reynolds shear stress;

τ_{rs}, τ_{r0} = Reynolds shear stress with and without seepage, respectively;

τ_{sf} = spatially-averaged skin friction;

κ = von Karman's constant;

ι = Prandtl's mixing length;

ε = porosity of granular materials;

Γ = a correction factor;

Ξ = $\gamma_s D^3 / \rho\nu^2$;

Ω = $3.38\Xi^{-0.25}$;

Π = Y/Y_{cr} ;

ξ = parameter incorporating the effects of shape and roundness in both particle and bed;

η = parameter incorporating the effects of sorting of the bed grains;

ξ' = 0.8~8;

η' = 0.5~8;

ϕ = location angle depending on the rolling path of the top sphere;

ϕ_{min}, ϕ_{max} = minimum and maximum of ϕ; and

$\sum M$ = sum of moments.

CHAPTER 1

INTRODUCTION

1.1 IMPORTANCE OF SEDIMENT TRANSPORT

Sediment transport has a significant effect on the environment; it plays a very important role in affecting the socio-economic development of the world (Allen 1984; Chien and Wan 1998). Scouring and siltation caused by flowing water can affect infrastructure developments, such as the construction of bridges, roads, railways and other hydraulic structures (Chiew 1995). The economic significance of erosion control is obvious; excessive erosion has a detrimental effect on agricultural production. On the other hand, severe deposition is highly undesirable for navigation. An understanding of sediment transport is essential to solving a wide variety of problems encountered in engineering practice.

A major difficulty in the study of sediment problems lies in the large number of pertinent inter-related variables, such as flow characteristics and sediment properties. The determination of sediment transport rate, for example, is complicated problem due to interactions of these variables. Sediment particles move under the action of a fluid flow; and in turn their movement influences the flow. Such a flow can be quite different from that of clear-water flow. Consequently, after decades of investigation in sediment transport, many unresolved problems remain. There is an urgent need to develop approaches to analyse and understand existing as well as newly identified problems.

1.2 PROBLEMS INVESTIGATED

One aspect of sediment transport that has attracted considerable attention in hydraulic engineering is bedform movement. This is referred to as the collective movement of large number of sediment particles on the channel bed in comparison with the individual movement such as bed load. The flow of water over a sandy bed produces a variety of bed features, of which a detailed description has been given by Allen (1968). If one starts with an erodible plane bed of sand and gradually increases the shear stress or velocity, a progression of bedforms appear as follows: ripples, dunes, transition (washed out dunes), flat bed, antidunes, and chutes and pools. The first two, for which no clear-cut definition exists, are the most common phenomena in natural rivers or streams due to the range of flow

velocity encountered. Dunes can form in a wide range of sediment sizes and grades, from well sorted fine to coarse sands (Allen, 1984) to poorly sorted gravels (Chiew 1991), suggesting common formative processes across a wide range of grain roughness (Bennett and Best, 1995). The formation, persistence and disappearance of bedforms offer a degree of freedom to a river to adapt its friction factor to flow and sediment discharge.

The presence of bedforms will influence the flow close to the bed and, in particular, the intensity of turbulence. The most discriminating features of ripples and dunes are their skewed shape and the presence of eddies in their lees. The abrupt change in the gradient of bedform slope at the crest causes the flow to separate and form an eddy. A kinematic theory that takes into account of the presence of the leeward eddy and the effect of the bedform shape on the flow field was first developed by Mercer (1971). Engel (1981) measured the length of flow separation over dunes. Subsequently, various researchers have investigated the turbulence structure over bedforms experimentally (Nakagawa and Nezu 1987; Espinoza and Martinez 2000) or numerically (McLean and Smith 1986).

Natural streams have bed boundaries composed of permeable material through which mass and momentum transfer occurs continuously. In most cases the magnitude of seepage is small compared with the main channel flow rate. Important consequences of seepage have been identified on (1) the transport of sediment over the porous boundary (Nakagawa et al. 1988); (2) the turbulence characteristics (Chu and Gelhar 1972; Zippe and Graf 1983; Cheng and Chiew

1998a); and (3) flow resistance (Lovera and Kennedy 1969; Bennett 1995). However, very little is known on the effect of seepage on bedform geometry and movement, and near-bed turbulence characteristics, as well as the overall influence on sediment transport rate. In this study, an effort is made to investigate bedform movement under turbulent flow in the presence of seepage. In particular, the study focuses on examining the response of the flow over the dunes to seepage.

1.3 OBJECTIVES OF THE STUDY

In order to understand sediment transport due to flowing water, it is important to elucidate the geometry of bedforms as well as the turbulent characteristics of flow over them. Although numerous laboratory investigations have been performed on sediment transport, most of them have been carried out under conditions without seepage. Because of the wide distribution of permeable materials in natural environments, laboratory experiments on the influence of seepage on flow behaviour and bed configurations are necessary for a better understanding of sediment movement under such conditions.

The present study aims to understand the mechanisms affecting bedform movement and the turbulence characteristics over a porous wave-boundary where seepage is present. The principal objectives of the study are

(1) To review the state-of-the-art knowledge concerning flow and sediment transport with seepage on a flat permeable bed;

(2) To systematically and experimentally investigate how the angle of repose of sediment, the geometry of dunes, the development of dunes, as well as the propagating velocity of dunes are affected by seepage;

(3) To quantify changes of the flow properties over dunes, e.g. time-average velocities, Reynolds shear stresses and the intensities of turbulence, with seepage by comparing to those without seepage; and,

(4) Use these results to obtain insight into the mechanism of sediment transport on a dune-wave bed with seepage.

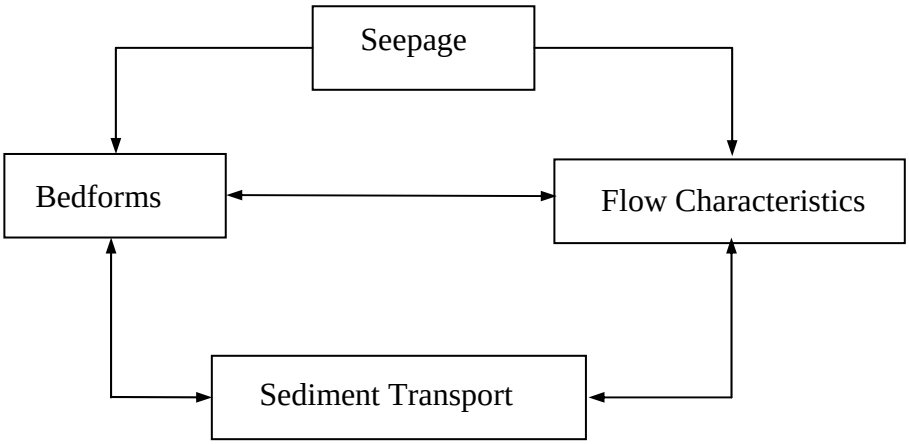

Figure 1.1 Sketch of Interaction Loop

Fig. 1.1 shows the processes using an inter-connected loop that expresses an overall description of the topics described above. First, seepage can influence bedforms and the flow characteristics directly. This leads to changes in the bedform geometry and hence, flow resistance, which in turn affects the flow. These changes have a significant effect on the overall sediment transport rate and behaviour of the flow. The study does not merely identify the processes represented in the boxes in Fig. 1.1, but also attempts to provide a detailed physical understanding and description of the arrows therein, which accounts for seepage effects on each of these processes.

1.4 STUDY OUTLINE

This section summarises the layout of the report. In Chapter 1 the importance of the study and practical applications are presented. Moreover, the objectives of the study are stated, together with a brief overview of the approach of the investigation.

Chapter 2, which is a review of published literature and basic concepts, presents previous experimental, theoretical, and field studies of seepage effects on flows, sediment transport, bedform development, and bedform geometry. Furthermore, some recommendations are provided to shed light on the conflicting results in this area.

Chapter 3 outlines a detailed description of the experimental investigations and equipments used in the study. Included in Chapter 3 is an outline of methodologies

for the measurement of the hydraulic parameters and for the collection of the relevant data in the study.

Chapter 4 presents a theoretical and experimental study to explore the effect of seepage flow on the angle of repose of sediments. The analytical solution relates critical slope to the ratio of the hydraulic gradient of seepage to its critical value under the quick condition by including seepage through a 3-dimensional force analysis. The derived relation, i.e., the force balance model is then verified with experimental data.

Chapter 5 is devoted to the analysis of the experimental data associated with the geometry of dunes subjected to either injection or suction. Dunes will change their shape through a process of reorganization when they move along a seepage zone. The distance-growth of the dune geometry is investigated firstly and then the equilibrium dune dimensions are included in a further analysis of seepage influence on the dune shape.

Chapter 6 deals with the role of boundary suction in turbulent flow over a fixed dune. Detailed measurements of the streamwise and vertical components of velocity over a fixed triangle dune with and without suction identified suction effects on the time-average flow velocities and turbulent characteristics.

Chapter 7 contains the summary, conclusions and recommendations.

CHAPTER 2

REVIEW OF PREVIOUS STUDIES

2.1 INTRODUCTION

Natural streams often comprise of permeable beds in the form of sand particles and gravels. An essential and well-known feature of permeable boundaries is that mass and momentum transfer takes place across the interface between the fluid and porous media. Interactions between turbulent flow and the permeable boundary may result in changes to the structural features of the flow, flow-resistance, sediment transport, and the morphology of alluvial channels, as compared to those with an impermeable boundary.

With the different levels of the free surface in a river and the adjoining groundwater table, two typical seepage flows (suction and injection) may occur through the river

bed. In the case of suction or downward seepage, water seeps out of the river; while with injection or upward seepage, the river receives additional water. In the present study, the direction of seepage flow is assumed to be perpendicular to the dominate time-average channel flow velocity above the boundary.

In most cases, seepage velocity within the porous boundary is small in comparison to the free-stream velocity above the bed. However, this small seepage flow (less than 1% of the free-stream velocity) can have sufficient effects on the flow structure (Schlichting 1979; Prinos 1995; Krogstad and Kourakine 2000; Chen and Chiew 2004a); at the same time it can effect an additional hydrodynamic force on the bed sediment. This, in turn, will significantly affect the processes of sediment transport (Oldenziel and Brink 1974; Nakagawa et al. 1988), such as the incipient motion for sediment entrainment (Cheng and Chiew 1999) and formation of bed features. Other practical examples relate to hydraulic structures used for channel stabilization, bank erosion prevention, and selection of water intakes location. Knowledge of flows over permeable boundaries clearly is not only useful in fundamental research but also has practical importance in engineering applications.

Despite the important influence of seepage on many aspects of practical engineering, relevant information in this area remains extremely scarce. Moreover, results from recent research efforts in this area are often inconclusive and sometimes contradictory. Table 2.1, which summarizes results of important recent findings over the past 35 years, shows these inconsistencies.

Table 2.1 Summary of Results of Previous Studies on Seepage Effects

Source	Flume dimensions		Seepage zone dimensions		Sediment transport rate		Bed shear stress		Turbulence intensity	
	Length (m)	Width (m)	Length (m)	Width (m)	Suction	Injection	Suction	Injection	Suction	Injection
Watters and Rao (1971)	4.6	0.7	1.5	0.7	increase	decrease	-	-	decrease	increase
Oldenziel and Brink (1974)	15	0.5	4	0.5	decrease	increase	-	-	-	-
Willetts and Drossos (1975)	3.6	0.076	0.125	0.076	increase	-	-	-	-	-
Nezu (1977)	-	-	-	-	little effect	little effect	-	-	decrease	increase

Source	Flume dimensions		Seepage zone dimensions		Sediment transport rate		Bed shear stress		Turbulence intensity	
	Length (m)	Width (m)	Length (m)	Width (m)	Suction	Injection	Suction	Injection	Suction	Injection
Richardson et a. (1985)	9.45	0.6	3	0.6	decrease	increase	-	-	-	-
Maclean and Willetts (1986)	5	0.076	5	0.076	-	-	increase	-	-	-
Maclean (1991a)	12	0.3	0.28	0.215	-	-	increase	-	-	-
Maclean (1991b)	5	0.075	0.13	0.075	increase	-	increase	-	-	-
Ramakrishna Rao et al (1994)	14.16	0.615	12.75	0.615	-	-	increase/ decrease	increase/ decrease	-	-
Cheng (1997)	7.6	0.21	0.5	0.21	-	increase	-	decrease	-	increase

Source	Flume dimensions		Seepage zone dimensions		Sediment transport rate		Bed shear stress		Turbulence intensity	
	Length (m)	Width (m)	Length (m)	Width (m)	Suction	Injection	Suction	Injection	Suction	Injection
Cheng and Chiew (1998a)	30	0.7	2	0.7	-	-	-	decrease	-	increase
Cheng and Chiew (1998b)	30	0.7	2	0.7	-	-	-	decrease		-
Cheng and Chiew (1999)	7.6	0.21	0.5	0.21	-	increase	-	decrease	-	-
Ramakrishna Rao & Nagaraj (1999)	3.6	0.1575	2.4	0.1575	increase	decrease	increase/ decrease	increase/ decrease	increase	decrease
Chen and Chiew (2004a)	30	0.7	2	0.7	-	-	increase	-	-	-
Chen and Chiew (2004b)	30	0.7	2	0.7	-	-	-	-	decrease	increase

The objective of this chapter is to review the state-of-the-art knowledge concerning flow and sediment transport with seepage. This chapter first presents published results on the variation of flow velocity and turbulence in the presence of bed seepage. Bed shear stresses induced by bed seepage and their implications on sediment transport is then examined. Conflicting results are highlighted, and the reason for the differences discussed. Finally, the findings on bedform geometry with or without seepage are described.

2.2 VELOCITY DISTRIBUTION SUBJECT TO SEEPAGE

The well-established law of the wall was originally derived for the inner layer of turbulent shear flows, and is widely used in boundary layer, pipe and open-channel flows. In the presence of seepage, the flow structure near the boundary and thus the distribution of the streamwise velocity are significantly modified. For example, the no-slip boundary condition that is commonly used in fluid mechanics for solid impermeable walls may not work if seepage occurs at the bed.

In the presence of boundary mass transfer, velocity profiles have been reported to be different from the logarithmic law in the field of aerodynamics. Various analytical models have been proposed, e.g. those by Clarke et al. (1959), Willetts and Drossos (1975) and Schlichting (1979). Velocity measurements over the seepage zone in open channel flow have been performed by Maclean (1991a), Cheng and Chiew (1998a, b), and Chen and Chiew (2004a).

For a two-dimensional flow over a horizontal bed, the streamwise momentum equation can be expressed as

$$u\frac{\partial u}{\partial x}+v\frac{\partial u}{\partial y}=-\frac{1}{\rho}\frac{\partial p}{\partial x}+\frac{1}{\rho}\frac{\partial \tau}{\partial y} \tag{2.1}$$

where u, v = streamwise and vertical velocity, respectively; τ = shear stress; p = pressure; and ρ = mass density of fluid. For the vertical velocity, application of the equation of continuity leads to

$$v=v_s \tag{2.2}$$

in which v_s = seepage velocity. Moreover, by ignoring terms involving the x-derivatives, Eq. (2.1) can be simplified to

$$v_s\frac{du}{dy}=\frac{1}{\rho}\frac{d\tau}{dy} \tag{2.3}$$

Additionally, based on Prandtl's mixing-length concept

$$\tau=\rho\iota^2\left(\frac{du}{dy}\right)^2 \tag{2.4}$$

with $\iota=\kappa y$, where κ = von Karman constant ≈ 0.41, one gets

$$\frac{du}{dy}=\sqrt{\frac{\tau}{\rho}}\frac{1}{\kappa y} \tag{2.5}$$

Eqs. (2.3) and (2.5) can be used to derive the velocity profile for open channel flows subject to seepage if boundary conditions are known. For the case of zero seepage, i.e. flows over an impermeable bed, the well-known law of the wall can be derived from Eq. (2.5) alone by assuming that τ is constant, leading to

$$\frac{u}{u_*} = \frac{1}{\kappa} \ln \frac{y}{y_0} \tag{2.6}$$

where $u_* = \sqrt{\tau_b / \rho}$ = friction velocity, τ_b = boundary shear stress, and y_0 = zero-velocity displacement measured from the theoretical bed surface. If an equivalent roughness height k_s is used, y_0 can be expressed as

$$y_0 = k_s \exp(-\kappa B) \tag{2.7}$$

where k_s can be taken as $2 D_{50}$, D_{50} = median diameter of sediment particles, and B = roughness function, being taken as 8.5 for a completely rough flow.

2.2.1 Flow with Injection

In the case of injection, integration of Eq. (2.3) with $\tau = \tau_b$ at $u = 0$ results in

$$\tau = \tau_b + \rho u v_s \tag{2.8}$$

Substituting (2.8) into (2.5) and noting that $\tau_b = \rho u_*^2$, one gets

$$\frac{2}{v_s}\left(\sqrt{u_*^2 + u v_s} - u_*\right) = \frac{1}{\kappa} \ln \frac{y}{y_0} \tag{2.9}$$

which can be rearranged as (see Schlichting 1979; Cheng and Chiew 1998b)

$$\frac{u}{u_*} = \frac{1}{\kappa} \ln \frac{y}{y_0} + \frac{v_s}{4u_*}\left(\frac{1}{\kappa} \ln \frac{y}{y_0}\right)^2 \tag{2.10}$$

Cheng and Chiew (1998b) reported that Eq. (2.10) compares well with their experimental data. Such an example is reproduced in Fig. 2.1 for the case of v_s/u_* = 0.137. Fig. 2.1 also shows that the commonly-used log-law (2.6) deviates considerably from the measured velocity profile.

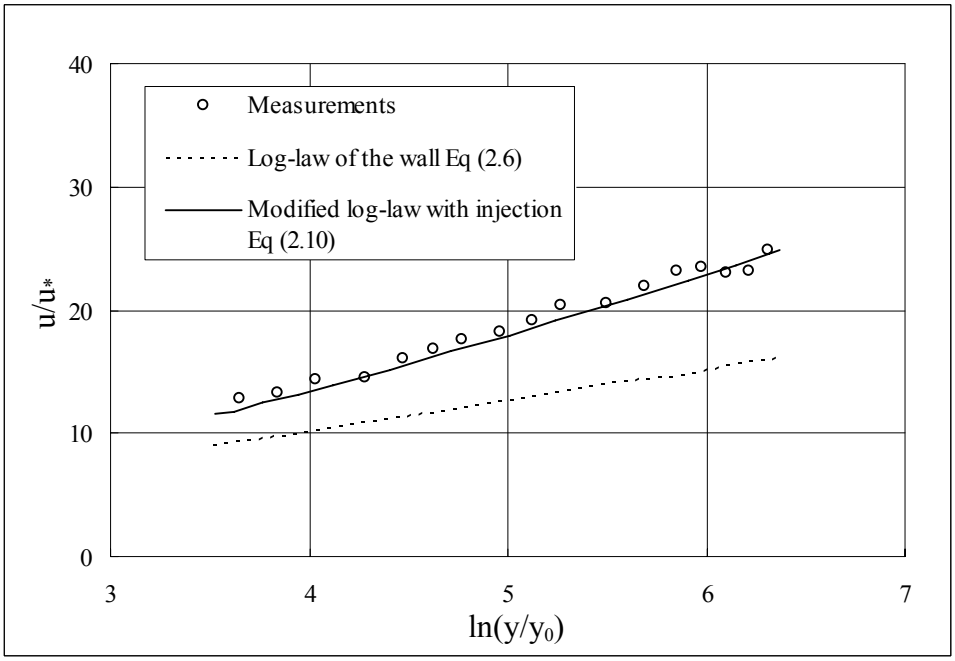

Figure 2.1 Comparison of Experimental Data with Modified Log-Law with Injection (Cheng and Chiew, 1998b)

Substituting Eq. (2.7) into Eq. (2.10) leads to

$$\frac{u}{u_*} = \frac{1}{\kappa}\ln\frac{y}{k_s} + B + \frac{v_s}{4u_*}\left(\frac{1}{\kappa}\ln\frac{y}{k_s} + B\right)^2 \qquad (2.11)$$

It is of interest to note that with the assumption of uniform suction Eq. (2.11) was also derived by Schlichting (1979) using Prandtl's mixing-length theory. In fact,

this equation can be regarded as a generalization of Eq. (2.6), the latter being applicable only for impermeable beds. The experimental data by Rotta (1966) agrees well with Eq. (2.11) in the case of both injection and suction if a suitable value of B is found. In the case of injection only, Cheng and Chiew (1998b) proposed that B is related to v_s/u_* for the completely rough regime in the form

$$B = \frac{8.5}{1 + v_s/u_*} \tag{2.12}$$

The value of the roughness function with injection is apparently smaller than that with zero-seepage flow, and reverts to 8.5, a commonly accepted value in the literature when the seepage velocity vanishes.

It may be worthwhile noting that in deriving Eq. (2.10) or (2.11), Prandtl's mixing-length theory which is widely used in smooth wall flow has been inherently adopted for flow with seepage. Since the mixing length varies with different boundary conditions, the validation of this assumption may be questionable.

2.2.2 Flow with Suction

In the case of suction, the velocity distribution over a flat bed is schematically shown in Fig. 2.2, with the support of flow visualization by Willetts and Drossos (1975). A modified one-seventh power law was proposed to describe the streamwise velocity profile as

$$\frac{u}{u_{\max}} = k\left(\frac{ky + y_{0x}}{y_1}\right)^{1/7} \tag{2.13}$$

$$k = \frac{y_1 - y_{0x}}{y_x} \tag{2.14}$$

where y_{0x} = depth below which water is removed from the stream between the two sections; and $u_{\max}$ = the maximum velocity which occurs at distance y_1 from the bed. The experimental data measured using a hot-wire anemometer in a wind tunnel by MacLean (1983) fit well with this profile. One main drawback of the method is that many assumptions are needed to compute y_{0x}. In general a power law velocity profile, $\frac{u}{u_{\max}} = \left(\frac{y}{y_1}\right)^{1/n}$, is often employed in many engineering applications. The exponent, n, is a function of the Reynolds number which varies with the stream velocity. However, it is common to apply $n = 7$ in a wide range of flows (Willetts and Drossos, 1975). In the presence of seepage, errors produced by the estimation may not be negligible. Moreover, the power law cannot be used to calculate the bed shear stress because it gives an infinite velocity gradient at the bed.

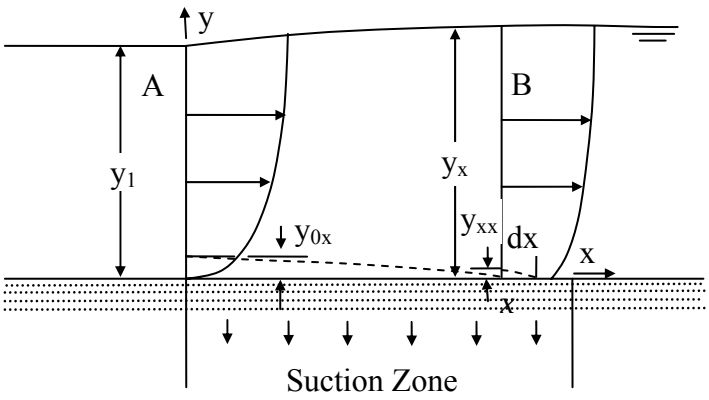

Figure 2.2 Velocity Profile with Suction

Eight years after his original work, Maclean (1991a) presented another study on open channel flow velocity over a zone of rapid infiltration. In the latter paper, he argued that Eq. (2.11) is not valid for the description of the velocity distribution when suction velocity is high ($\frac{v_s}{u_*} \sim 2$) because the x-derivatives ($\frac{\partial p}{\partial x}, \frac{\partial u}{\partial x}$), which are ignored in deriving Eq. (2.11), are no longer negligible. Moreover, he defined an inner boundary layer close to the bed to describe the velocity profile subjected to seepage. Based on experimental data, he concluded that the flow structure in the inner boundary layer, is significantly different from that described by Eq. (2.11), but above the inner layer, the velocity profile is still logarithmic if a suitable value is chosen for the roughness function, B.

More recently, an approach similar to that proposed by Cheng and Chiew (1998b) was used by Chen and Chiew (2004a) to derive the velocity profile for flows

subjected to suction. They assumed that the boundary occurs at $y = -y_0$ instead of $y = 0$, as is the case for an impermeable bed (see Fig. 2.3).

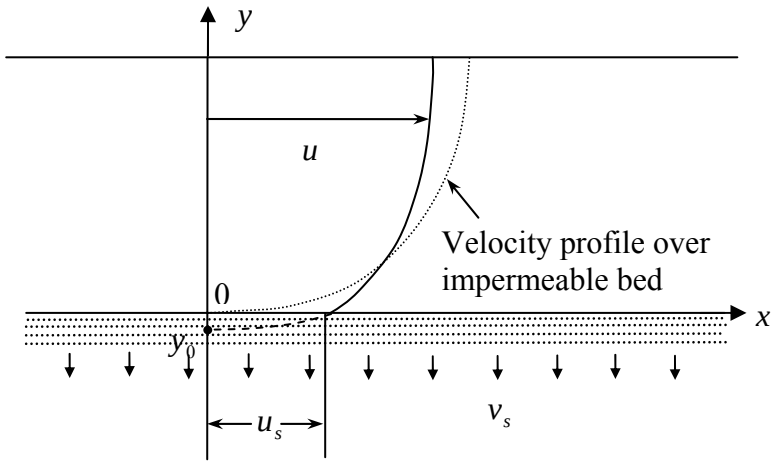

Figure 2.3 Schematic Diagram of Velocity Profile over Permeable Bed with Suction

Since the mixing length, ι varies with different boundary conditions, as a first approximation they expressed it as

$$\iota = \kappa(y + y_0) \tag{2.15}$$

With this consideration, Eq. (2.5) can be rewritten as

$$\frac{du}{dy} = \sqrt{\frac{\tau}{\rho}} \frac{1}{\kappa(y + y_0)} \tag{2.16}$$

Integration of Eq. (2.3) from y = 0 to y = y with the condition of $u = u_s$ and $\tau = \tau_b$ at the bed yields

$$\tau = \tau_b + \rho u v_s - \rho u_s v_s \tag{2.17}$$

Here, the bed surface is taken as the reference level at which the flow has a slip-velocity of u_s. Substituting (2.17) into (2.16) with $\tau_b = \rho u_*^2$ one gets

$$\frac{du}{dy} = \frac{\sqrt{u_*^2 - u_s v_s + u v_s}}{\kappa(y + y_0)} \tag{2.18}$$

Integration of (2.18) from y = 0 to y = y gives

$$\frac{2}{v_s}\left(\sqrt{u_*^2 - u_s v_s + u v_s} - u_*\right) = \frac{1}{\kappa}\ln\frac{y + y_0}{y_0} \tag{2.19}$$

Eq. (2.19) can be rewritten as follows

$$\frac{u - u_s}{u_*} = \frac{1}{\kappa}\ln\frac{y + y_0}{y_0} + \frac{v_s}{4u_*}\left(\frac{1}{\kappa}\ln\frac{y + y_0}{y_0}\right)^2 \tag{2.20}$$

With y_0, u_*, and u_s determined experimentally, Chen and Chiew (2004a) reported that Eq. (2.20) may be used to describe the measured profiles. Their measurements also confirmed the existence of the slip velocity and a significant increase in the near bed velocity. An example velocity profile for $|v_s/U| = 1.53\%$ at x = 100 cm is reproduced in Fig. 2.4, where U is average flow velocity. This result is consistent with that obtained by MacLean (1991a), who showed an acceleration of flow close to the bed and a deceleration of flow near the free surface.

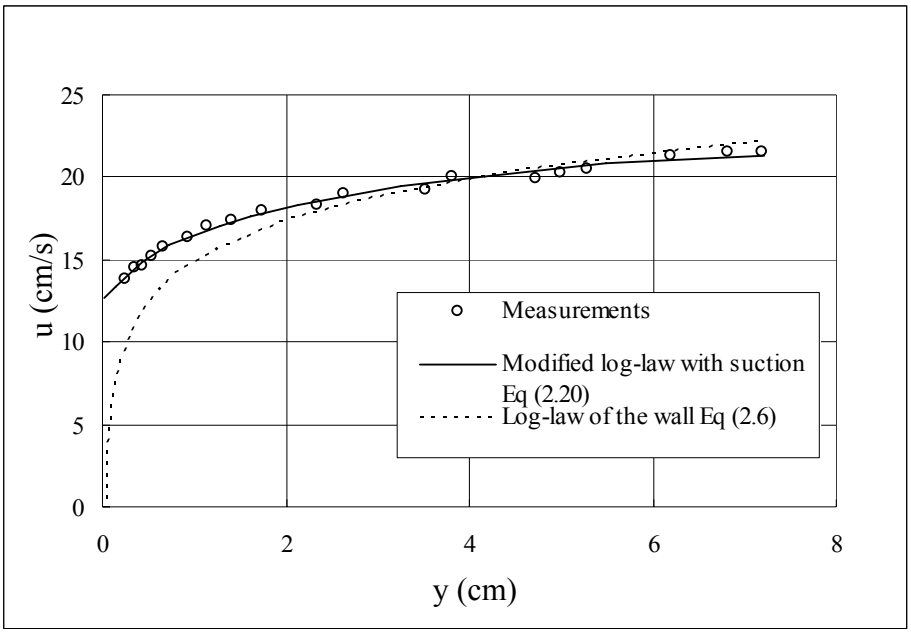

Figure 2.4 Comparison of Experimental Data with Modified Log-Law for Suction (Chen and Chiew, 2004a)

2.3 TURBULENCE INTENSITY SUBJECT TO SEEPAGE

Although turbulence intensity in impervious open channel flow has been studied extensively, how it responds to seepage is not clearly understood. Based on a study of the fluid dynamic forces acting on a typical bed particle, Watters and Rao (1971) concluded that suction decreases turbulent fluctuations in the flow field resulting in less momentum exchange between fluid particles; while the opposite is true for the case of injection. An extreme case was found in their study showing that with strong suction the particle boundary layer changes from turbulent to laminar condition.

All three components of turbulence intensities in open-channel flow for both injection and suction were measured by Nezu (1977). His experimental data showed that seepage has a significant effect on the turbulence level, i.e. turbulence intensities increase with injection and decrease with suction.

Other studies on the response of a turbulent boundary layer to seepage, either through porous strips or open slots, generally supported the observation that injection enhances (Krogstad and Kourakine 2000; Kim and Sung 2003), while suction diminishes turbulence intensities (Antonia and Zhu 1995).

Detailed experimental investigations on injection effects on open-channel flow were conducted by Cheng (1997) using an acoustic Doppler anemometer (ADV). Based on an extensive experimental study, he observed an increase of the rms values of velocity fluctuations near the bed although little change was detected near the water surface. This behavior, which was also observed by Nezu, is in agreement with general expectation. Since seepage interacts with the main channel flow immediately near the bed, the turbulence intensities are expected to change more readily near the bed than those near the water surface.

A series of experiments were performed by Ramakrishna Rao and Nagaraj (1999) to investigate the effect of seepage on the behavior of turbulence characteristics. Velocity fluctuations were measured using a hot film anemometer on a plane and non-transporting bed for both suction and injection. They concluded qualitatively that turbulence intensities were higher for suction than for injection or no-seepage.

It is interesting to note that the results of Ramakrishna Rao and Nagaraj are contrary to the findings of the other researchers mentioned earlier. It is not possible to make any judgment on these findings before further rigorous investigation are conducted. However, a plausible explanation for this contradiction may be due to the measurement techniques and instrumentation since hot film probes are known to be inadequate for turbulence measurement in regions of high turbulence levels.

The experimental data of Chen and Chiew (2004b) collected using the same flume as that used by Cheng (1997) showed that both the horizontal and vertical turbulence intensities decrease with suction. Similar to those observed with injection, the changes are significantly more apparent near the bed level than near the water surface.

2.4 BED SHEAR STRESS SUBJECT TO SEEPAGE

Detailed investigations of flow and sediment movement in an alluvial stream require an accurate evaluation of the bed shear stress or shear velocity. The latter, which is the most fundamental velocity scale for near-bed flows, can be determined using different methods. One typical approach is to measure the water surface slope under uniform flow conditions, which can then be used to compute the bed shear stress or shear velocity. Besides this, the shear velocity may also be determined from the measured velocity distribution in conjunction with the logarithmic law, or

inferred from the measured Reynolds shear stress distribution. Finally, one can measure the bed shear stress directly with a Preston tube. However, almost all these methods fail to work in the presence of seepage. This is because bed seepage can invalidate both flow uniformity and the no-slip condition at the boundary. Consequently, other approaches have been used to determine bed shear stresses on a permeable boundary (Oldenziel and Brink 1974; Maclean and Willetts 1986; Maclean 1991b; Ramakrishna Rao et al. 1994; Cheng and Chiew 1998b; Chen and Chiew 2004a).

Oldenziel and Brink (1974) calculated the change in bed shear stress due to suction and injection by considering the excess bed shear stress arising from three factors: (1) the variation of energy slope; (2) the difference in momentum flux for the two end cross sections of a seepage zone; and (3) the additional momentum losses due to mixing of channel flow and seepage. In computing the additional momentum losses, they introduced a reference height, y_s at which this interaction takes place

$$y_s = \frac{2}{3}\left(\frac{\mu L v_s}{\tau_{b0}}\right)^{1/2} \tag{2.21}$$

where L = length of the seepage zone; v_s = seepage velocity; μ = dynamic viscosity of fluid; and τ_{b0} = bed shear stress without seepage. Comparing the situations with and without seepage, the following equation was finally obtained

$$\tau_{bs} - \tau_{b0} = \rho g h(I_s - I_0) - 2\rho U_0 v_s - \frac{2}{3}\Gamma \rho v_s \left(\frac{L\tau_{b0} v_s}{\mu}\right)^{1/2} \tag{2.22}$$

where I_s, I_0 = energy slope with and without seepage, respectively; U_0 = average flow velocity without seepage; h = water depth; τ_{bs} = bed shear stress with seepage;

and Γ = a correction factor. The correction for additional loss due to the mixing of discharges has to be determined by experiment. Moreover, this method is practical only when the energy slope is measured accurately.

The idea of Oldenziel and Brink was later adopted by Willetts and Drossos (1975) for flow subjected to suction. In their study, the streamwise velocity profile in the suction zone was described using the modified seventh power law (Eqs. (2.13) and (2.14)) discussed earlier (also see Fig. 2.2). Furthermore, the value of y_{0x} was determined by assuming that the water removed between two sections per unit time was equal to the flow rate within the depth y_{0x}. Finally, the excess shear stress due to suction was calculated as

$$\frac{1}{2}\rho g {y_1}^2 + \frac{1}{2}x(y_x - y_1)\rho g S_b - \frac{1}{2}\rho g {y_x}^2 - \int_0^x \tau_e dx = \rho \int_0^{y_x} {u_x}^2 dy - \rho \int_0^{y_1} {u_1}^2 dy \qquad (2.23)$$

where S_b = bed slope; u_x, u_1 = velocity at y from bed in cross-section at B and A, respectively; and τ_e = excess shear stress due to suction. A numerical method is necessary to solve Eq. (2.23).

The results computed using this model showed a sudden increase in the shear stress at the leading edge of the suction zone, whereas the experimental observation indicated a relatively gentle increment (Maclean 1983). A further modification of this method was proposed by Maclean and Willetts (1986) and Maclean (1991b) by assuming that the excess bed shear stress due to suction was equal to the momentum given up by the fluid as it entered the bed. By considering the infinitesimal element in the section of x shown in Fig. 2.2, the excess bed shear stress is given by

$$\tau_e dx = \rho U_{0x}^2 y_{xx} \tag{2.24}$$

where y_{xx} = depth below which water is sucked into the bed across the infinitesimal element, and U_{0x} = average flow velocity within the depth of y_{xx}. By consideration of continuity, the following expression was obtained

$$\tau_{bs} = \tau_{b0} + \rho U_{0x} v_s \tag{2.25}$$

Maclean (1991b) reported that Eq. (2.25) overestimated the bed shear stress. By observing the initiation of indicator grains whose critical shear stress had been predetermined in uniform flow, Maclean and Willetts (1986) measured the bed shear stress with and without suction. The so-measured shear stresses were found to increase with the suction velocity ratio, as shown in Fig. 2.5. However, it must be noted that the incipient motion of sediment particles subject to bed seepage should be different from that without seepage because different hydrodynamic forces are involved. This aspect will be further discussed in a latter section in this review. It may be inferred from the above discussion that the results of Maclean and Willetts (1986) could be questionable.

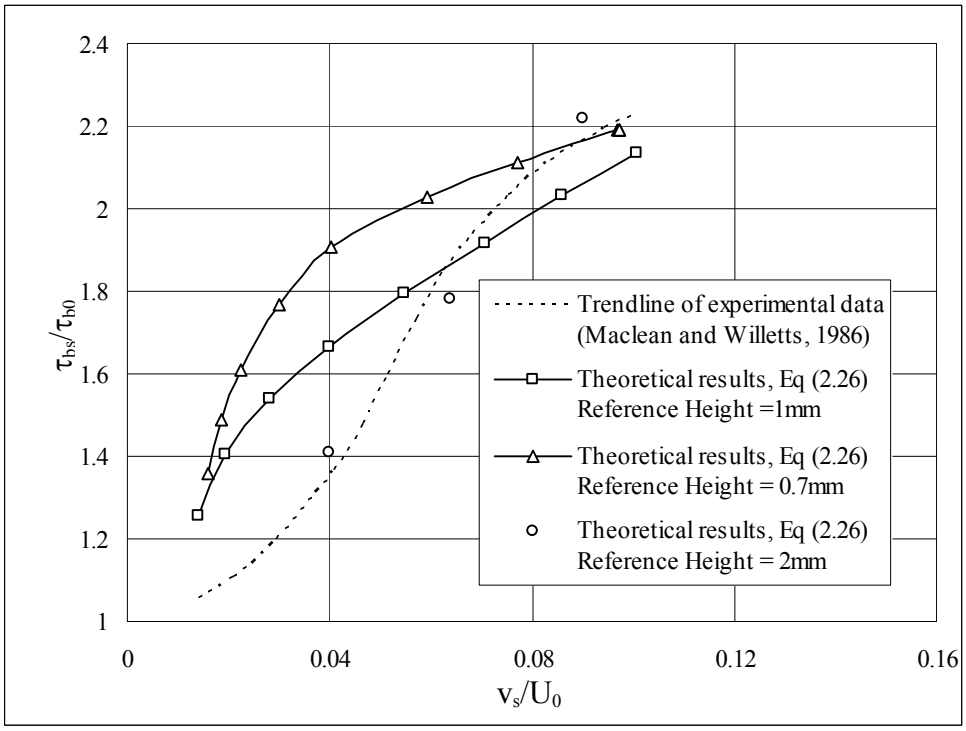

Figure 2.5 Comparison of Bed Shear Stress Computed Using Method of Reference Height (MacLean, 1991a, b)

To obtain bed shear stresses from the flow velocity, MacLean (1991b) also proposed an alternative approach by relating the bed shear stress to the square of the water velocity at a given reference height above the bed.

$$\frac{\tau_{bs}}{\tau_{b0}} = \frac{u_{rs}^2}{u_{r0}^2} \tag{2.26}$$

where u_{r0}, u_{rs} = velocities measured at the reference height without and with suction, respectively. This approach was found to give a reasonable fit with the experimental data. However the choice of the reference height was arbitrary, which had significant effects on the results (see Fig. 2.5).

Conducting a series of laboratory experiments, Ramakrishna Rao et al. (1994) observed that the variation of bed shear stress resulting from seepage depends on the critical shear stress without seepage, the sediment concentration and seepage velocity. Two empirical relationships were presented to estimate the variation for the flow with and without sediment transport, respectively. In the case of a non-transporting bed, the ratio of bed shear stress with and without seepage was expressed as

$$\frac{\tau_{bs}}{\tau_{b0}} = \left(\frac{\tau_{b0}}{\tau_{c0}}\right)^{-C\overline{N}} - \overline{N} \tag{2.27}$$

where $\overline{N} = \frac{2\rho U_s v_s}{\tau_{b0}}\left(\frac{R_h}{h}\right)$ = seepage intensity parameter (v_s takes negative for suction); U_s = average flow velocity with seepage; h = water depth; R_h = hydraulic radius of the bed after smooth wall correction; and C = 2.7. However, the C-value was later revised by Ramakrishna Rao and Nagaraj (1999) to be 2.2, based on a wider range of experimental data. In the case of a transporting sand bed, the following relationship, which is valid only for suction, was proposed

$$\frac{\tau_{bs}}{\tau_{b0}} = \left(\frac{600}{cc}\right)^{1.75\overline{N}} + \overline{N} \tag{2.28}$$

where cc = sediment concentration in ppm by weight. It is of interest to note that one can see from Eqs. (2.27) and (2.28) that both injection and suction can cause an increase or decrease in the bed shear stress, an anomaly that will be discussed in a latter section.

By integrating the continuity and momentum equations with the appropriate boundary conditions, Cheng and Chiew (1998a) derived the following equation to evaluate the shear velocity:

$$\tau_{bs} = -\rho g h \frac{dh}{dx}\left(1 - \frac{\beta' U^2}{gh}\right) - 2\beta' \rho U v_s \qquad (2.29)$$

in which U = depth-averaged streamwise velocity; h = flow depth and $\beta' = \left(\int_0^h u^2 dy\right) \Big/ (hU^2)$ = momentum correction factor. The bed shear stresses derived based on the momentum integral equation in Eq. (2.29) compare well with the results determined from the measured Reynolds shear stress distribution (Cheng 1997). Clearly, this approach depends on accurate measurements of the water surface slope in the case of seepage. Another method was proposed by Cheng and Chiew (1998b) for evaluating the bed shear stress by directly fitting the modified logarithmic law for injection (2.10) or (2.11) to the velocity measurements. To avoid the effect of uncertainties involved in near-bed velocity measurements, the depth-averaged velocity is used instead by integrating Eq. (2.10) from y_0 to h, which leads to (noting $y_0/h << 1$)

$$\frac{U}{u_*} = \frac{1}{\kappa}\left(\ln\frac{h}{y_0} - 1\right) + \frac{v_s}{4\kappa^2 u_*}\left[\ln^2\frac{h}{y_0} - 2\left(\ln\frac{h}{y_0} - 1\right)\right] \qquad (2.30)$$

It is noted that an iterative procedure is necessary to evaluate the shear velocity with Eq. (2.30) because y_0 is dependent on B, and thus on the shear velocity. This approach was used by Cheng and Chiew (1998b) to evaluate the bed shear stress distribution over an injection zone, as shown in Fig. 2.6.

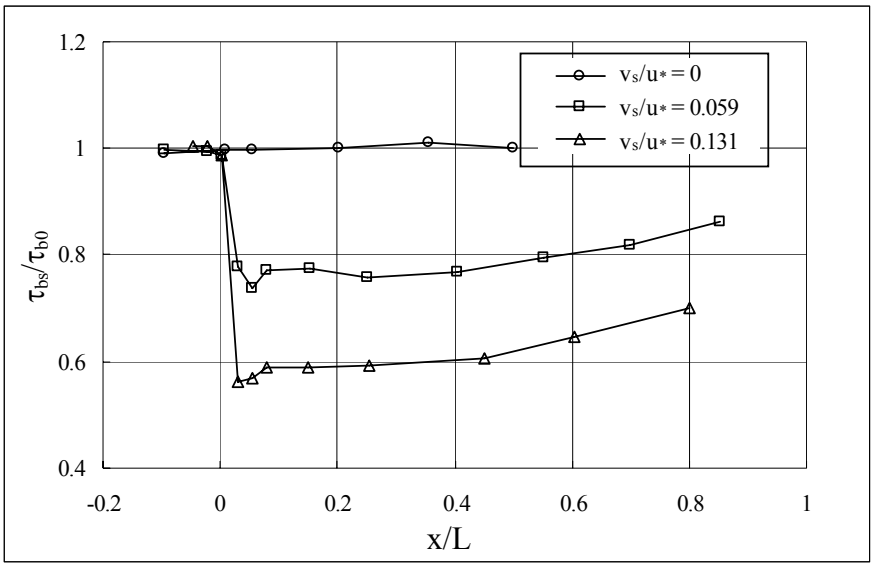

Figure 2.6 Bed Shear Stress Distribution over Injection Zone (Cheng and Chiew, 1998)

Fig. 2.6 also shows that the shear stress reduces markedly at the beginning of the injection zone and the reduction becomes more apparent for higher seepage intensity. However, a gradual increase of bed shear stress has been found toward the downstream end of the injection zoon; the reason for this gradual increase can be attributed to the influx of mass to the main flow. Based on this result, it can be deduced that injection effects on bed shear stresses are related to two important features. First, it alters the flow configuration near the bed resulting in a sudden reduction of the bed shear stress directly. Second, it introduces additional mass to flow, which gives an increase in water depth and water surface slope, thus causing an increase in the bed shear stress indirectly.

The effect of mass (introduced by injection or suction) may be substantiated by the experimental results of Ramakrishna Rao et al. (1994), who conducted their tests in a flume with a seepage zone with length = 12.75 m. This is much longer than that used by Cheng and Chiew (1998a, b), which is only 2 m long. The additional discharge influx to the main flow will likely increase the resulting bed shear stress. This may be one of the reasons why their results are contrary to general accepted norm, which states that injection tends to reduce bed shear stress. In the limiting condition where the length of the seepage zone approaches infinity, it may not be erroneous to infer that the bed shear stress will also become excessively large. It is worthwhile to note that it is hard to keep the uniformity of seepage along such a long seepage zone (12.75m); this could be another reason for the deviation of the experimental results of Ramakrishna Rao et al. (1994) from the general accepted norm.

Suction effects on bed shear stress in open-channel flow were experimentally investigated by Chen and Chiew (2004a). As was discussed in the earlier section on velocity distributions, the modified logarithmic law, i.e., Eq. (2.20) for suction includes three unknown parameters y_0, u_s and u_*. To determine the shear velocity, the measured velocity profiles were compared to Eq. (2.20). A software package (Matlab) was used to fit the experimental data to a second-order polynomial function to determine the best values for the three parameters, including the shear velocity. Their result on the bed shear stress distribution over the suction zone is reproduced in Fig. 2.7. For comparison, the data of Cheng and Chiew (1998b) obtained for injection are superimposed in the figure, in which the injection and

suction rates are represented by positive and negative numbers, respectively. For the suction case, the data also shows significant reduction in the shear stress. This phenomenon is similar to that observed with injection; decrease in the bed shear stresses may largely be due to the reduction of mass caused by suction. An interesting phenomenon of their data is another reversal of bed shear stresses at around $x/L = 0.3$. This second reversal is not seen with data associated with injection, and the reason for its occurrence is as yet unknown.

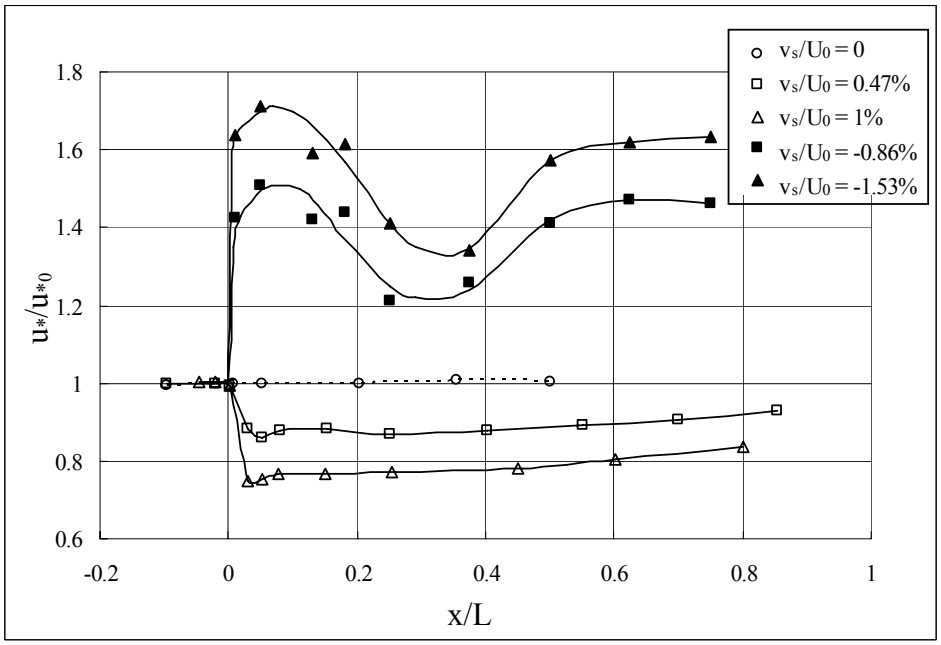

Figure 2.7 Bed Shear Stress Distribution over Injection and Suction Zone (Cheng and Chiew, 1998b; Chen and Chiew, 2004a)

By fitting the experimental data of the dimensionless shear velocity $\frac{u_*}{u_{*0}}$ with relative suctions, Chen and Chiew (2004a) presented an empirical equation as

$$\frac{u_*}{u_{*0}} = 0.073\left|\frac{v_s}{U_0}\right|^3 - 0.44\left|\frac{v_s}{U_0}\right|^2 + 0.9\left|\frac{v_s}{U_0}\right| + 1 \qquad (2.31)$$

where, u_{*0} = local shear velocity without seepage. This approach shows that the rate of increase of shear velocity is much bigger when $\left|\frac{v_s}{U_0}\right| < 0.6\%$ than that when $\left|\frac{v_s}{U_0}\right| > 0.6\%$ (Fig. 2.8).

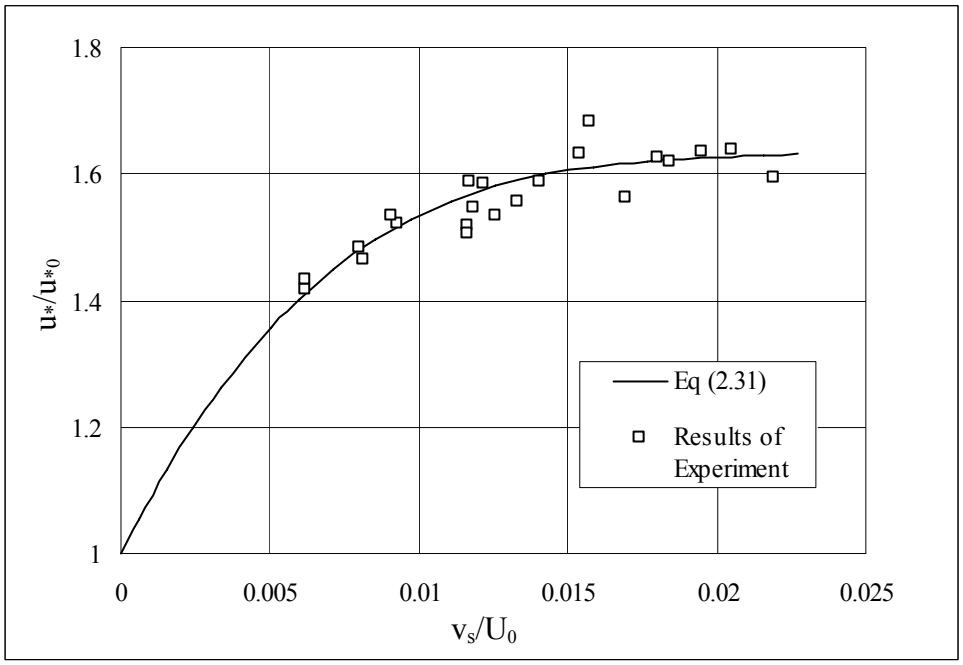

Figure 2.8 Relationship between Shear Velocity and Suction Velocity Ratios (Chen and Chiew, 2004a)

Unfortunately, all the suction velocities in their studies are more than 60% of the depth-averaged stream velocity due to experimental set-up and no verification can

be done for small values of seepage rate. Further accurate measurement at small values of suction velocities is necessary to verify the empirical equation.

The data of Cheng and Chiew (1998a, b) for injection and Chen and Chiew (2004a) for suction, respectively are re-plotted in Fig. 2.9. In this figure the value of the shear velocity for the respective seepage rate refers to that measured at the centre of the seepage zone, i.e., 1 m from its leading edge. At this location, the data show a clear increase and decrease of shear velocity for suction and injection, respectively. It, however, does not reveal how mass addition (due to injection) and extraction (due to suction) would influence shear velocities. In other words, the data in Fig. 2.9 should only apply to a relatively short seepage zone, and not a long one.

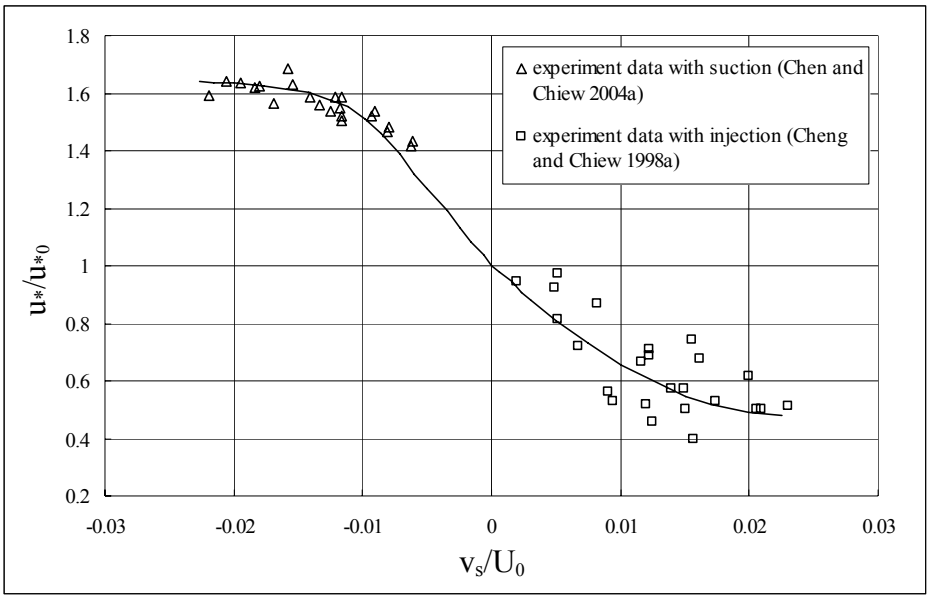

Figure 2.9 Effect of Injection and Suction on Shear Velocity

2.5 STABILITY OF BED PARTICLES SUBJECT TO SEEPAGE

Despite that existing data are generally incomplete and inconsistent, published studies have shown that the open-channel flow characteristic can be significantly modified by seepage. One may infer from this result that sediment transport theories developed without consideration of seepage effects are not applicable for cases with suction or injection. Current research results in this respect are, however, still very rudimentary. They are largely related to the simple case of incipient sediment motion.

Since the boundary flow condition varies with seepage, bed particles are subject to additional hydrodynamic forces besides drag and lift forces. Cheng and Chiew (1999) performed a force analysis for the threshold condition of sediment movement by including an additional force due to injection. With reference to a spherical particle at the incipient condition on a slope as shown in Fig. 2.10, an equilibrium consideration of various forces acting on the particle results in

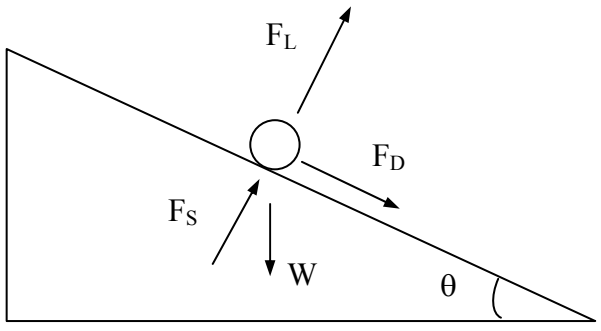

Figure 2.10 Forces Acting on a Sphere Resting on the Bed

$$\tan\alpha = \frac{F_D + W\sin\theta}{W\cos\theta - F_L - F_S} \tag{2.32}$$

where $W = (\rho_s - \rho)g\frac{\pi D^3}{6}$ = submerged particle weight; $F_D = C_D\frac{\pi D^2}{8}\rho u_b{}^2$ = drag force; $F_L = C_L\frac{\pi D^2}{8}\rho u_b{}^2$ = lift force; $F_S = \frac{i\rho g\pi D^3}{6(1-\varepsilon)}$ = seepage force; C_D, C_L = drag and lift coefficients, respectively; D = diameter of particle; ρ_s = density of particle; i = seepage hydraulic gradient; ε = porosity; and u_b = effective velocity acting on particles at the bed. Furthermore, the effective velocity was related to the shear velocity in the following form

$$u_b = \frac{u_{*c}}{\sqrt{f_*}} \tag{2.33}$$

where f_* = friction factor; and u_{*c} = critical shear velocity with seepage. Comparing the situation with and without seepage, one gets

$$\left(\frac{u_{*c}}{u_{*c0}}\right)^2 = 1 - \frac{i}{i_c} \tag{2.34}$$

where $i_c = (1-\varepsilon)(\rho_s - \rho)/\rho$ for a horizontal bed, which describes a quick condition. If the hydraulic gradient is related to seepage velocity, Eq. (2.34) can be rewritten as

$$\left(\frac{u_{*c}}{u_{*c0}}\right)^2 = 1 - \left(\frac{v_s}{v_{sc}}\right)^m \tag{2.35}$$

where v_{sc} = critical seepage velocity under quick condition; and m = 1-2, which depends on the characteristics of sediments. Eq. (2.34) or (2.35) shows the relationship between the critical shear velocities with and without injection under the threshold condition for sediment transport. Increasing the hydraulic gradient or injection velocity results in a reduction of the critical shear velocity and vice versa.

Eq. (2.35) compares well with the experimental data of Cheng and Chiew (1999), which are re-plotted in Fig. 2.11. Later, Cheng (2003) derived an alternative expression for computing the critical shear stress reduced by upward seepage, where the Eugen equation was used to describe the relationship between the seepage velocity and seepage-related hydraulic gradient. More recently, Dey and Zanke (2004) presented an analytical model and their results were verified using the data of Cheng and Chiew (1999).

Ramakrishna Rao and Nagaraj (1999) assumed that the critical shear stress due to suction τ_{cs} is related to both the bed shear stress without seepage τ_{b0} and the critical shear stress without seepage τ_{c0}, as

$$\ln\left(\frac{\tau_{b0}}{\tau_{c0}}\right) = -0.2525\left(\frac{\tau_{cs}}{\tau_{c0}}\right)^{-2.917} \qquad \text{for } \tau_{b0}/\tau_{c0} < 1 \tag{2.36}$$

where τ_{cs} = critical shear stress with seepage; and τ_{c0} = critical shear stress without seepage, which may be computed using the Shields diagram. In their experiments, the values of τ_{cs}/τ_{c0} varied from about 0.6 to 1.4, showing that suction can significantly affect the critical condition for sediment entrainment. By relating the critical shear stress with suction to the seepage intensity parameter $\overline{N}$ defined in Eq.(2.27), Eq. (2.36) is modified to

$$\frac{\tau_{cs}}{\tau_{b0}} = \left(\frac{\tau_{b0}}{\tau_{c0}}\right)^{-2.2\overline{N}} - \overline{N} \qquad \text{for } \tau_{b0}/\tau_{c0} < 1 \tag{2.37}$$

In the above analysis, Ramakrishna Rao and Nagaraj (1999) further assumed that $\tau_{bs} = \tau_{cs}$ and $C = 2.2$. Eqs. (2.36) and (2.37) may be used to calculate the critical shear stress with suction for any given particles if the initial bed shear stress is

known. In the case of injection, the following equation was fitted to their experimental data

$$\ln\left(\frac{\tau_{b0}}{\tau_{c0}}\right) = 0.2525\left(\frac{\tau_{cs}}{\tau_{c0}}\right)^{1.68} \qquad \text{for } \tau_{b0}/\tau_{c0} > 1 \qquad (2.38)$$

A significant variation in τ_{cs}/τ_{c0}, from about 0.5 to more than 2, was shown in their investigation, which indicates that injection can significantly affect the critical condition for sediment entrainment. However, no method was proposed in their studies to relate the critical shear stress with injection to the seepage intensity parameter, $\overline{N}$.

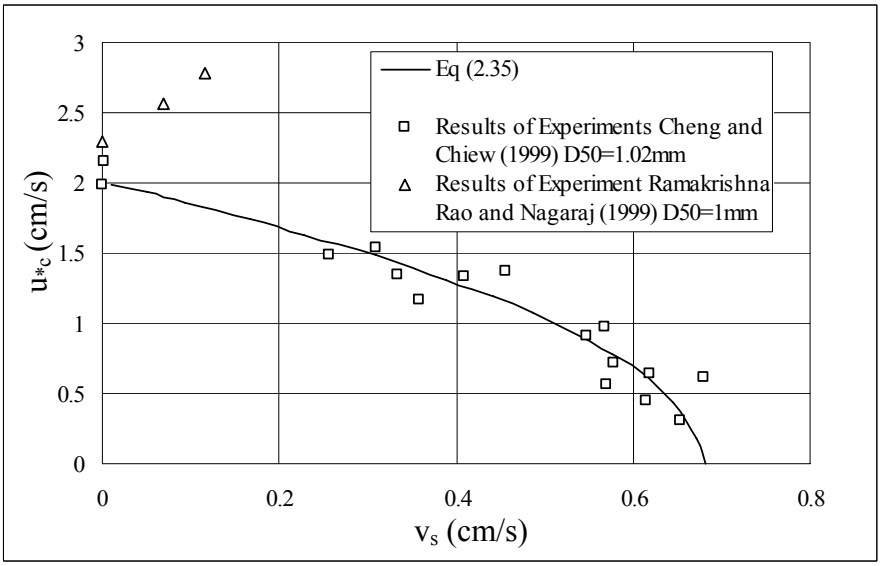

Figure 2.11 Comparison of Experimental Results on Threshold Condition for Sediment Entrainment

It is of interest to note that the value of τ_{cs}/τ_{c0} can be more or less than unity for both cases of suction and injection in the study by Ramakrishna Rao and Nagaraj

(1999), whereas those by Cheng and Chiew (1999), i.e., Eq.(2.35), Cheng (2003) and Dey and Zanke (2004) showed that τ_{cs}/τ_{c0} is always less than unity in the case of injection. Ramakrishna Rao and Nagaraj argued that in the presence of injection, the resistance decreases due to the reduction of effective weight of bed particles, and the hydrodynamic forces acting on the bed particles also reduce due to the decrease in the near-bed velocity as well as turbulence intensity; the opposite trend holds for suction. Therefore, it appears that the threshold of sediment movement is dependent on variations in both changes in the effective particle weight and hydrodynamic forces. No satisfactory explanations are given at this stage, although it does not appeal to common sense that injection should cause an increase in the threshold condition for sediment entrainment.

The experimental data of Ramakrishna Rao and Nagaraj (1999), which were collected in tests conducted with a similar grain size as those conducted by Cheng and Chiew (1999), are superimposed in Fig. 2.11. The figure shows that the two sets of experimental results are very different, even for their trend. One possible explanation could be the magnitude of the seepage rates used in the two studies; the seepage velocities used for the experiment conducted by Cheng and Chiew are much higher than those used by Ramakrishna Rao and Nagaraj.

It must be stated that these results are affected to some extent by the length of seepage zone. Since the bed shear stress is not uniform along the seepage zone (see Fig. 2.7) due to the variation of main flow discharge resulting from mass transfer associated with either injection or suction, it is questionable to use any average

value, such as average transport rate, or that measured in center of seepage zone to define the threshold of sediment movement. To further illustrate this, it may be worthwhile to conduct a thought experiment, whose setup is schematically shown in Fig. 2.12. The 2m-long-seepage zone is divided into 5 sections evenly. Each section is covered by same uniform sediment particles that are color-coded.

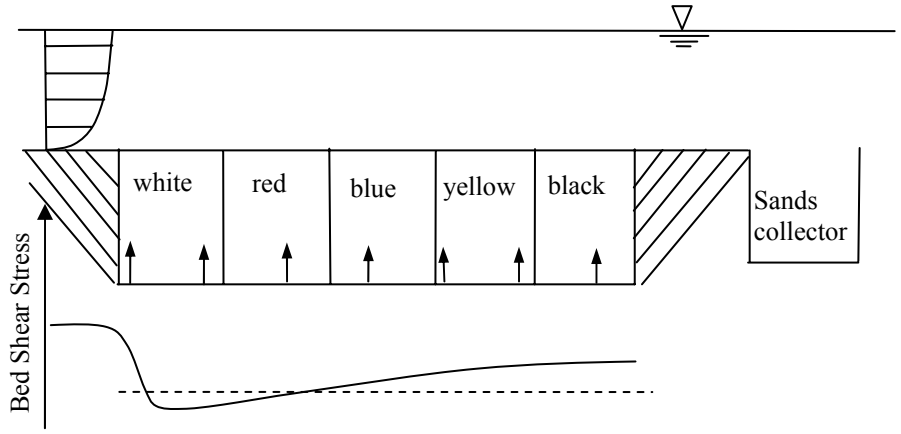

Figure 2.12 Thought Experiment Setup for Study of Incipient Motion of Sediment with Seepage

In order to examine the incipient motion criterion, the sediment particles that are entrained are collected in a box placed downstream of the test section. For a given water depth and main flow discharge, either injection or suction is introduced, together with the adjustment of the tail gate to achieve the incipient condition. Here, weak particle movement is used to define the initiation of sediment movement. For the case of injection for example, the variation of bed shear stress (Fig. 2.6) presented by Cheng and Chiew (1998b) along the seepage zone is superimposed in

Fig. 2.12 to aid discussion. The imaginary threshold shear stress for sediment entrainment is also shown in Fig. 2.12 as a dashed line. With these considerations, the amount of sediment particles collected at the downstream end of the seepage zone may reasonably be shown in Fig. 2.13.

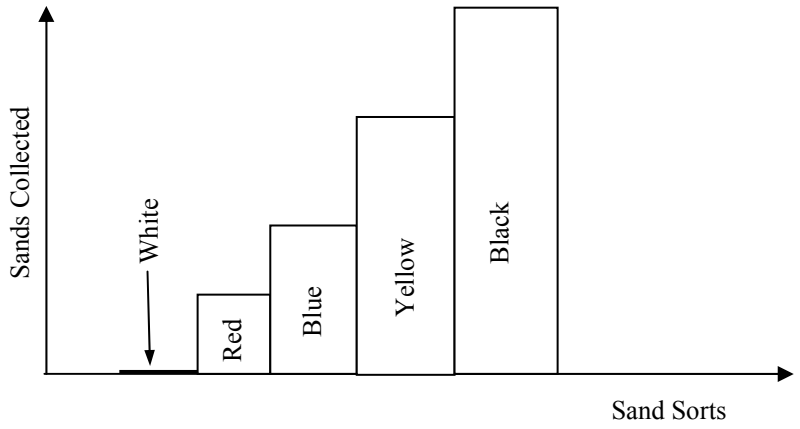

Figure 2.13 Schematic Diagram of Quantity of Sediment Particles Collected

Fig. 2.13 shows that the quantity of the different color particles collected are different. This is because the bed particles in the seepage zone are identical except for their color, thus their respective critical shear stress must remain the same. However, the bed shear stress experienced by each of these color-coded sediment particles is different dependent on their location in the seepage zone as the distribution of bed shear stress along the zone changes. Therefore, it is not reasonable to define the incipient condition by considering the average transport rate at a particular location in the seepage zone. Additionally, it is questionable that the threshold of sediment initiation is dictated by the bed shear stress at the center

of the seepage zone. As a minimum, this thought experiment highlights the limitation of published results. Additional experiments and analyses clearly are necessary.

The experimental results of Ramakrishna Rao and Nagaraj (1999) showed that injection increases the stability of bed particles while suction does the opposite. This is in agreement with the findings of some earlier researchers (Harrison 1968; Willets and Drossos 1975), but contrary to findings of more recent studies (Oldenziel and Brink 1974; Richardson et al. 1985; Cheng and Chiew 1999; Cheng 2003; Dey and Zanke 2004). A summary of these contradicting results is showed in Table 2.1; an attempt to explain the contradiction is discussed below.

In general, the stability of bed particles is controlled by the effective weight and bed shear stress, both of which are modified by seepage, as illustrated in Fig. 2.14. In the figure, a positive (+) and negative (-) sign denotes an increase and decrease in particle stability, respectively. The presence of suction can cause an increase in the effective weight of the bed particles because it acts downwards while injection has the opposite effect. As discussed previously, suction or injection, respectively, increases or decreases the bed shear stress. Fig. 2.14 shows a graphical representation of the influence of the effective weight and shear stresses on bed particles stability. In quadrant 2, the stability of bed particles is always reduced due to the increase of bed shear stress and the decrease of effective weight of bed particles. In quadrant 4 on the other hand, the stability of bed particles is always enhanced due to the reduction of bed shear stress and the increase of effective

weight. While the above inference is rational, it has no real physical meaning because it is impossible to introduce both injection and suction at the same time. The other two quadrants are, however, more realistic. Quadrant 1 depicts the condition where suction increases the effective weight of bed particles, thus enhancing the stability of bed particles; on the other hand, suction also has the tendency to increase the bed shear stress and as a result reduces the stability of bed particles. With this combined effect, it is not immediately clear whether the stability of bed particles is finally enhanced or reduced. Similarly, in quadrants 3 injection decreases the effective weight resulting in the reduction of the bed particle stability, and at the same time it also decreases the bed shear stress resulting in an increase of stability. From this consideration, it is clear that the stability of bed particles is dependent on the relative magnitude of these two opposing effects. For instance, in the experiments of Ramakrishna Rao and Nagaraj's (1999), as a result of the decrease of effective weight due to injection, the stability of the bed particles is reduced, but it is offset by the reduction of bed shear stresses. The final stability of the bed particles is dependent on which effect is more dominant. If the reduction in weight is more than the decrease in the bed shear stress, the stability of the sediment particle will reduce; a condition designated by the shaded portion in quadrants 3. Similarly, suction increases the effective weight, thereby leading to an increase in the bed particle stability, but it is offset by the increase of bed shear stresses. If the increase in weight is less than the increase in the bed shear stress, the stability of the sediment particle will reduce, as indicated by the shaded portion in quadrants 1. The above reasoning may be an explanation to account for the contradictory findings in published literature. This hypothesis, including the idea

illustrated in Fig. 2.14, is only conceptual presently; more experiments are needed to prove the explanation and investigate the imaginative dashed line shown in the figure.

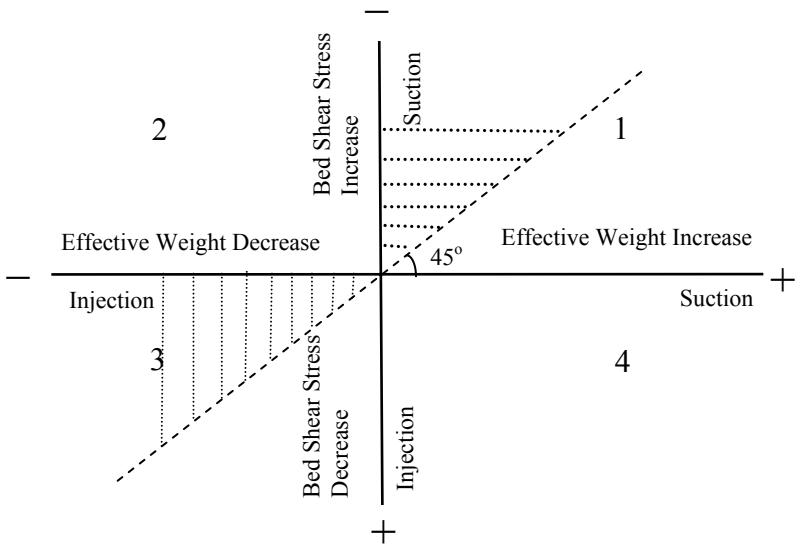

Figure 2.14 Quadrant Analysis of Bed Particle Stability Due to Seepage

2.6 BEDFORM DEVELOPMENT AND GEOMETRY

Once the threshold of initiation of cohesionless sediment motion is exceeded, bed particles are transported at a rate that increases with the flow strength. Under certain conditions, the sediment bed possesses transversely oriented wave-like features.

Based on a large data set collected from laboratory flumes, Simons and Richardson (1961) presented a classification of bedforms which has been widely accepted (see

Fig. 2.15). The most important bedforms are ripples, dunes, plane bed, and antidunes. To be consistent with the objective of this study, more attention in this section is placed on dunes.

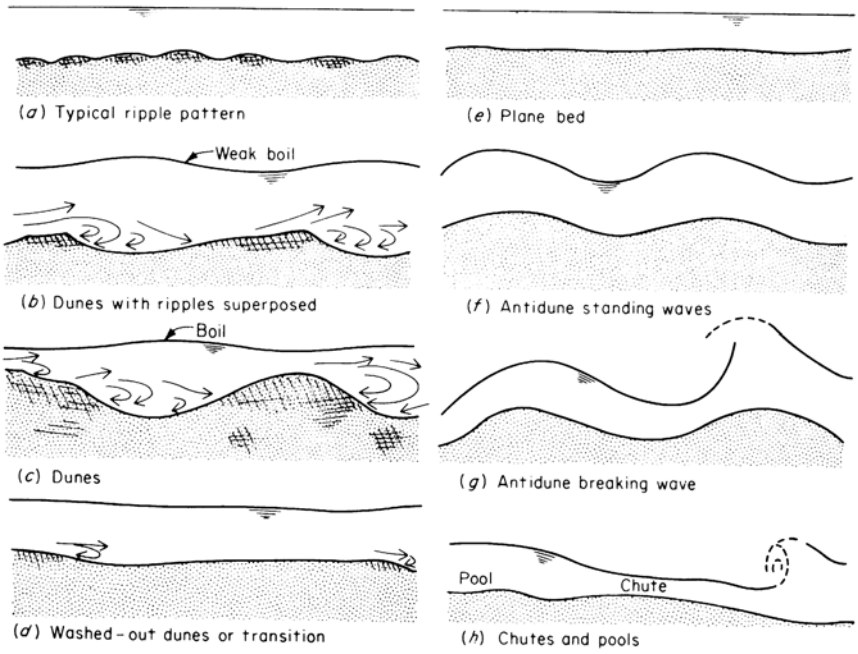

Figure 2.15 Idealized Bedforms in Alluvial Channels
(Simons and Richardson, 1961)

2.6.1 Development of Bedforms

For the last four decades a considerable amount of research has been performed on the formation of bedforms in erodible channels, with varying degrees of success. Concepts of bedform initiation on plane granular surfaces involve mainly the influence of boundary defects, either pre-existing ones or those directly induced by the flow. Today, many researchers agree that the process of bed wave formation is

a problem of instability. Kennedy (1963) presented a pioneering work on this problem using the potential flow analysis. A series of assumptions were introduced to linearize the analysis in a two-dimensional, inviscid flow. i.e., the bed undulation is assumed to have a sine curve configuration and the bed wave height is small compared to the wavelength and water depth. Kennedy's stability analysis approach was later followed and extended by Reynolds (1965), Engelund (1970), and Fredsϕe (1974), Parker (1975), Richards (1980) and others. Many of these studies were reviewed by Kennedy (1969), and later by Engelund and Fredsϕe (1982). In this section, emphasis is put on the results obtained over the past two decades.

Owing to the inherent assumption of small sand-wave heights, stability analyses based on potential flow theory have accordingly not been able to adequately explain the mechanics of the development of bed-waves of finite heights. In contrast, the idea of unification and reorganization was introduced by Raudkivi and Witte (1990), to show that bedform celerity decreases with increasing bedform height. The numerical results given by the bedform unification models were later verified by Coleman and Melville (1994, 1996) on the basis of an extensive series of bedform development experiments.

The development of bedforms toward the equilibrium condition involves the action of strongly non-linear effects. Hence, linear analyses cannot be used to study this problem, and other weakly or fully non-linear theories have been developed for this purpose (Fredsϕe 1974; Ji and Mendoza 1997). By expanding in terms of the dune

amplitude to flow depth ratio, Fredsϕe (1974) extended his linear theory to a second-order approximation, and reasoned that the asymmetry growth of the bedforms is induced by the phase shift between erosion and the mean velocity. The comparison between the non-linear and linear models by Ji and Mendoza (1997) indicates that the former predicts more reasonable dune length.

Another alternative technique to study bedform development is that proposed recently by Landry and Werner (1994), and Niño, et al. (2002), which makes use of discrete computer models to simulate individual particle motion based on a set of simple rules. This set of rules intends to represent the fundamental aspects of the physical processes related to the transport of particles over a bedform comprising similar particles. In these simulations bedforms emerge naturally from the interaction of transported particles and the bed. This approach has the advantage of being simple but at the same time capable of simulating complicated non-linear processes.

2.6.2 Geometric Characteristics of Bedforms

The form resistance due to bedforms, caused by local flow separation and recirculation, can be significant and is dependent on their dimensions as well as on flow and sediment characteristics. Because of the importance of bedform resistance in determining the overall resistance in sand bed flows, the prediction of bedform geometry is essential for estimating flow resistance and water levels during floods

in rivers. The physics of these features has fascinated researchers and applied mathematicians; extensive research has been undertaken in the past on the mechanics and prediction of bedform geometry in alluvial channels with varying degrees of success.

2.6.2.1 Ripple

Ripples are the smallest bed configurations. The size of the ripples is assumed to be independent of flow depth. Using laboratory data, Yalin (1977a) proposed an empirical formula to evaluate the average ripple length, λ

$$\lambda = 1000D \tag{2.39}$$

where D = representative diameter of granular material. Using dimensional analysis, Yalin (1977b) further proposed that the length of a ripple is a function of the grain Reynolds number, Re_*, to which he (1985) added the dimensionless parameter reflecting the nature of granular material and fluid, $\Xi = \gamma_s D^3/(\rho\nu^2)$, in which γ_s = the submerged specific weight of the particles, ρ = the density of fluid, and ν = kinematic viscosity coefficient i.e.,

$$\frac{\lambda}{D} = f(\mathrm{Re}_*, \Xi) \tag{2.40}$$

Graphically the experimental data obtained by different authors showed a family of curves due to different value of the dimensionless variable Ξ. Yalin further incorporated the influence of Ξ in Re_* as

$$\frac{\lambda}{\Omega D} = f(\Omega \mathrm{Re}_*) \tag{2.41}$$

In which Ω is empirically determined as

$$\Omega = 3.38\Xi^{-0.25} \tag{2.42}$$

In this way the family of curves was simplified into a single curve pattern. Further analyses arising from the curve show that the value of λ/D must be expected to be within the interval

$$600 < \frac{\lambda}{D} < 2000 \tag{2.43}$$

Data on ripple length show a dependence on grain size. Raudkivi (1997) proposed a simple relationship between λ and D_{50} by fitting the published data associated with ripple length as a first approximation.

$$\lambda = 245 D_{50}^{0.35} \tag{2.44}$$

where, D_{50} = median diameter of particles. This is consistent with the relationship proposed by Baas (1993)

$$\lambda = 75.4 \log D_{50} + 197 \tag{2.45}$$

where D_{50} and λ are in mm.

The data on ripple heights H is remarkably consistent. The bulk of data are in the range of $12.5 \le H \le 18$ mm with an average of about 15 mm. Baas (1993) also proposed an expression for the ripple height

$$H = 3.4 \log D_{50} + 18 \tag{2.46}$$

or

$$H = 18.16 D_{50}^{0.097} \tag{2.47}$$

where H and D_{50} are in mm. In the ripple height description of Yalin (1985), by introducing the mobility number $Y = \frac{\rho u_*^2}{\gamma_s D}$, its critical value Y_{cr}, and the relative intensity of the flow $\Pi = \frac{Y}{Y_{cr}}$, he reasoned that λ/D should be considered as

$$\frac{\lambda}{D} = f_{\Delta}(\Pi;\Xi) \tag{2.48}$$

The data on λ/D versus Ξ for $Z = h/D > 600$ show the value, λ/D, decreases with the increasing values of Ξ, where h = mean water depth. For the steepness of bed features Yalin (1977b) also deduced from dimensional reasoning that

$$\frac{\lambda}{H} = \varphi\left(\frac{Y}{Y_{cr}};\mathrm{Re}_*;Z\right) \tag{2.49}$$

in which H = the height of a dune or ripple, and Re_* = grain Reynolds number. Thus, if ripple λ/H is independent of flow depth and they occur at small and near constant Re_* then

$$\frac{\lambda}{H} = \varphi\left(\frac{Y}{Y_{cr}}\right) \tag{2.50}$$

Also the ripple steepness can be drawn from Eq. (2.45) and Eq. (2.46) as

$$\frac{\lambda}{H} = 0.074 D_{50}^{0.253} \tag{2.51}$$

2.6.2.2 Dunes

Dunes, which are generally larger and more two-dimensional bed features, develop at higher bed shear stress than ripples. The size of a dune is closely related to water depth. Yalin (1972) addressed the problem of the scale of two-dimensional ripples and dunes from a hydraulic standpoint. Arguing that the mean bed shear stress in the trough of the bed feature must be in the same order as the shear stress at the threshold of particle motion, τ_{c0}, he reasoned from dimensional and empirical considerations that:

$$\frac{H}{h} = \frac{1}{6}\left(1 - \frac{\tau_{c0}}{\tau_{b0}}\right) \tag{2.52}$$

in which τ_{b0} is the overall mean bed shear stress. Since τ_{c0} is never vanishingly small compared to τ_{b0}, the ripple or dune height cannot exceed one-sixth of the mean water depth. Yalin further reasoned that the dune length is approximately 2π times the water depth. On the other hand, Allen (1984) stated that in deep flows (h > 10 m) a better fit is given by

$$\lambda = 1.16h^{1.55} \tag{2.53}$$

Fredsϕe (1980) worked out a simple model to calculate the dune shape by relating the local dune height H to the local sediment transport rate, g_s through the equation of continuity, as

$$g_s = c_e H(1-\varepsilon) \tag{2.54}$$

where c_e is the dune migration velocity and ε the porosity of granular material.

van Rijn (1982) analysed experimental dune data from 84 flume experiments with a fairly large range of grain size, $0.19mm \le D_{50} \le 2.3mm$, and 22 field experiments with a range of $0.49mm \le D_{50} \le 3.6mm$. The dune height was related to the dimensionless grain size D_*, and a transport parameter G'

$$D_* = D_{50}\left[\frac{(s-1)g}{\nu^2}\right]^{\frac{1}{3}} \tag{2.55}$$

$$G' = \left[\left(u_*'\right)^2 - u_{*c}^2\right]/u_{*c}^2 \tag{2.56}$$

in which, $s = \rho_s/\rho$, ρ_s, ρ = sediment density and fluid density, respectively, g = acceleration of gravity, $u_*' = U\sqrt{g}/C'$, $C' = 18\log(12R_h/3D_{90})$ = Chezy-coefficient, R_h = hydraulic radius of the bed, D_{90} = 90% passing bed particle

diameter, and u_{*c} is obtained from the Shields threshold criterion. Thus, with an assumption that for $G^{'} \le 0$ and $G^{'} \ge 25$ the bed is almost plane, van Rijn proposed

$$\frac{H}{h} = 0.11\left(\frac{D_{50}}{h}\right)^{0.3}\left(1-e^{-0.5G^{'}}\right)\left(25-G^{'}\right) \tag{2.57}$$

$$\frac{H}{\lambda} = 0.015\left(\frac{D_{50}}{h}\right)^{0.3}\left(1-e^{-0.5G^{'}}\right)\left(25-G^{'}\right) \tag{2.58}$$

Accordingly, the expression for the bedform length L can be derived from Eq.(2.57) and (2.58), as

$$\lambda = 7.3h \tag{2.59}$$

which is close to the abovementioned result of Yalin, $\lambda = 2\pi h$.

The applicability of van Rijn's method was extended by Julien and Klaassen (1995) for the prediction of dune height and length in large rivers during floods. Since large sand-bed rivers do not necessarily achieve a plane bed when G = 25, they suggested

$$H = \xi^{'} h\left(\frac{D_{50}}{h}\right)^{0.3} \tag{2.60}$$

$$\lambda = \eta^{'} H\left(\frac{h}{D_{50}}\right)^{0.3} \tag{2.61}$$

where $0.8 < \xi^{'} < 8$ and the average value 2.5, and $0.5 < \eta^{'} < 8$ with average value 2.5. Note that $\lambda = \xi^{'}\eta^{'}h$ is obtained from Eq. (2.60) and Eq. (2.61). One may use $\lambda = 6.25h$ as a reasonable first approximation, which is close to Eq. (2.59).

Using a physical argument, Yalin (1972) and Yalin and Karahan (1979) deduced that the height-wavelength ratio of ripples and dunes is a bell-shaped function of the

mean bed shear stress, with a maximum steepness at an intermediate stress within an appropriate stress range. Fredsøe (1975) used the principle of similarity to obtain the following relationship, restricted to dunes:

$$\frac{H}{\lambda} = \frac{1}{8.4}\left(1 - \frac{0.6}{Y} - 0.4Y\right)^2 \tag{2.62}$$

where the numerical quantities are partly empirical.

More recently, Haque and Mahmood (1986) have shown that the limiting steepness of ripples and dunes can be determined analytically if the bed material moves essentially as bedload. Based on the assumption that the sediment transport rate is taken as proportional to some power, *r*, of the local velocity, i.e., $\left(\frac{u}{u_t}\right)^r = \frac{y}{a'}$, the relationship between the limiting steepness of bedforms and the relative depth of flow for various values of r is presented analytically, as

$$\frac{a'}{\lambda} = 0.4(r)^{-1.178}\left[1 - \exp\left(-2.5\frac{b'}{\lambda}\right)\right] \tag{2.63}$$

in which u = local velocity, u_t = velocity tangential to bed at the crest, y =coordinate of a point on the bedform surface, a' = the height of separation point from the reattachment point, b' = flow depth at the crest, and r = a dimensionless index.

However, it is not frequent in nature that sediment particles are never transported as suspension in the flow. To consider the effect of suspended sediment, Haque and Mahmood (1987) further extended the mathematical formulation to include

sediment diffusion. Subsequently, the governing equations of convection-diffusion of suspended sediment in two-dimensional flow fields over ripples or dunes were solved using the finite-element method. The result showed the significant effect of flow velocity and particle fall velocity on bedform lengths.

Another distinguishing method was presented by Karim (1999) who adopted the concept which relates energy loss due to form drag to the head loss across a sudden expansion in open channel flows. A relationship, which can be applied to various bedforms, i.e., ripples, dunes, and transitional bed regimes, was proposed as,

$$\frac{H}{h} = \left[\frac{\left\{ I_0 - 0.0168 \left(\frac{D_{50}}{h} \right)^{0.33} \cdot F_r^{\,2} \right\} \left(\frac{\lambda}{h} \right)^{1.20}}{0.47 F_r^{\,2}} \right]^{0.73} \tag{2.64}$$

in which I_0 is the energy slope. The equation can be solved directly for H/h, using appropriate relations for λ/h, depending on the bedform type. In Karim's analysis, the result of Yalin (1972) for ripples length and the result of Julien and Klaassen (1995) for dunes length were used.

2.6.3 Seepage Effects on Bedforms

Very few studies on changes of bedforms in flows over a porous boundary subjected to seepage exist. Amongst the studies that can be found in the literature is one by Harrison (1968), who noted that the angle of repose of the downstream face of the bedforms increased by 10^o for suction and decreased by 9^o for injection.

Richardson et al. (1985) proposed that the stream power, $\tau_b u$, in which τ_b is the total bed shear stress and u the mean velocity, increased with injection. As a result, the increase in stream power modifies the bedform. However, no quantitative descriptions on bedform geometry were documented in their studies.

2.7 SUMMARY

Published works that deal with seepage effects on open-channel flow and sediment transport are limited. It is evident from changes of the flow velocity distributions, bed shear stresses and erosion rate due to seepage that the interaction between flow and permeable boundary is significantly influenced by seepage. Many of these interactions outlined in Fig. 1.1 are still not clear presently.

Many attempts have been made to characterize the mean flow on a porous bed (e.g., Willetts and Drossos 1975; Schlichting 1979; Maclean 1991a; Cheng and Chiew 1998a, b and Chen and Chiew 2004a). Notwithstanding the hypotheses and conjectures, what exists depicts well the alteration of the flow velocity induced by seepage.

Most previous experimental studies of injection or suction have shown that when injection is applied, turbulence intensities are enhanced (Watters and Rao 1971; Nezu 1977; Cheng 1997). On the other hand, suction diminishes turbulence

intensities (Watters and Rao 1971; Nezu 1977; Chen and Chiew 2004a). Ramakrishna Rao and Nagaraj (1999), however, showed the reverse trend.

Detailed investigations of flow and sediment movement in alluvial stream require an accurate evaluation of the bed shear stress or shear velocity. For point-source seepage, it alters the flow configuration near the bed resulting in a sudden modification of the bed shear stress directly; for seepage with long streamwise extent, the effect of mass (introduced by injection or suction) also needs to be considered (Ramakrishna Rao et al. 1994).

The issues of whether seepage reduces or enhances sand-bed stability are still matters of considerable debate. Table 1 clearly shows many of these discrepancies. For example, some studies (Oldenziel and Brink 1974; Richardson et al. 1985) suggested that injection increases bed erosion, whereas suction tends to inhibit sediment motion. On the other hand, other researchers suggested a completely opposite result, stating that suction increases sediment transport rate (Willetts and Drossos 1975), while injection inhibits the motion of bed particles (Watters and Rao 1971).

Although few studies on seepage effects on bedforms in the literature (Harrison 1968; Richardson et al. 1985) have been reported, no quantitative descriptions on bedform geometry were documented. Considerable work is still needed to explore and better understand the phenomenon, especially for the dune-boundary flow. The

principle inference of this chapter is that the complex interactions defined in Fig. 1.1 caused by seepage raise many important issues that require further research.

CHAPTER 3

EXPERIMENTAL APPARATUS AND MEASUREMENT TECHNIQUES

3.1 INTRODUCTION

As discussed in Chapter 2, the influence of seepage on bedform geometry, turbulence characteristics over dunes and sediment transport rate are very complex and are presently poorly understood. In this experimental study, emphasis is placed on investigation of bedform geometry and the turbulence features of flows over a permeable boundary subjected to seepage, and their implications on sediment transport rate. Comparisons are made between these measurements and those conducted on a non-porous boundary to highlight seepage effects.

A series of experimental studies are carried out at the Hydraulics Modelling Laboratory, Nanyang Technological University to examine how seepage affects the angle of repose of sediments, shape of dunes, and the time-average flow velocities and turbulence fields over a fixed, two-dimensional dune. The experimental program for this study consists of four fundamental series of tests with definite objectives:

The first series (Series-A) aims to investigate the permeability of granular materials used in the study. The "non-Darcy" law, which is used to determine the relationship between the seepage hydraulic gradient and seepage velocity in the granular particles, is verified. Furthermore, the critical hydraulic gradient under the quick condition for all sediment samples used is determined in this series of tests. The results of Series-A are applied in the subsequent data analysis.

The second series of tests (Series-B) is designed to study the influence of seepage on the angle of repose of sediments and to verify the theoretical relationship between the dimensionless seepage hydraulic gradient and the angle of repose. The experimental data in the first two series are analysed and presented in Chapter 4.

In the third series of experiments (Series-C), measurements of the geometry of dunes with and without seepage are performed to identify how seepage affects the shape of dunes. Additionally, the celerity of propagating dunes at various seepage rates is investigated. The analyses of the experimental results associated with the

third series are presented in Chapter 5, in which changes of the dune height, lee-side slope, and wavelength caused by seepage, are discussed.

The last series of tests (Series-D) deals with the role of bed seepage in turbulent flow over a fixed, two-dimensional dune. Only suction effects are examined, and the velocity field is measured using a Laser Doppler Anemometer (LDA). In order to avoid complications and ambiguities imposed by the mobile boundary, artificial dunes fixed in typical natural form are constructed in the flume. Detailed measurements of the streamwise and vertical components of velocity over a fixed triangle dune with and without suction identify the suction influence on the time-average and fluctuating characteristics. The results from Series-D tests, including the implication on sediment transport, are presented in Chapter 6.

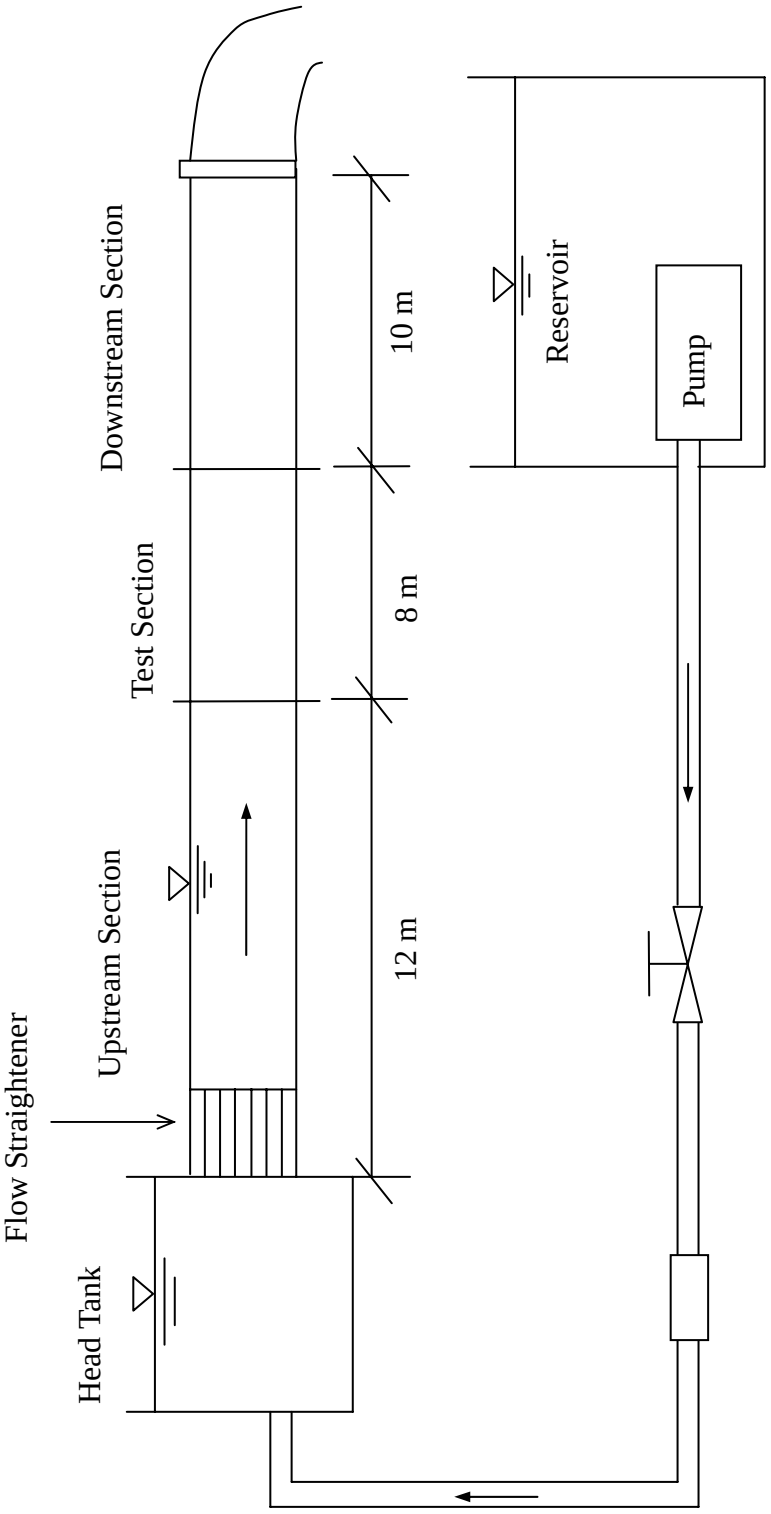

Figure 3.1 Schematic Diagram of Open Channel Flume

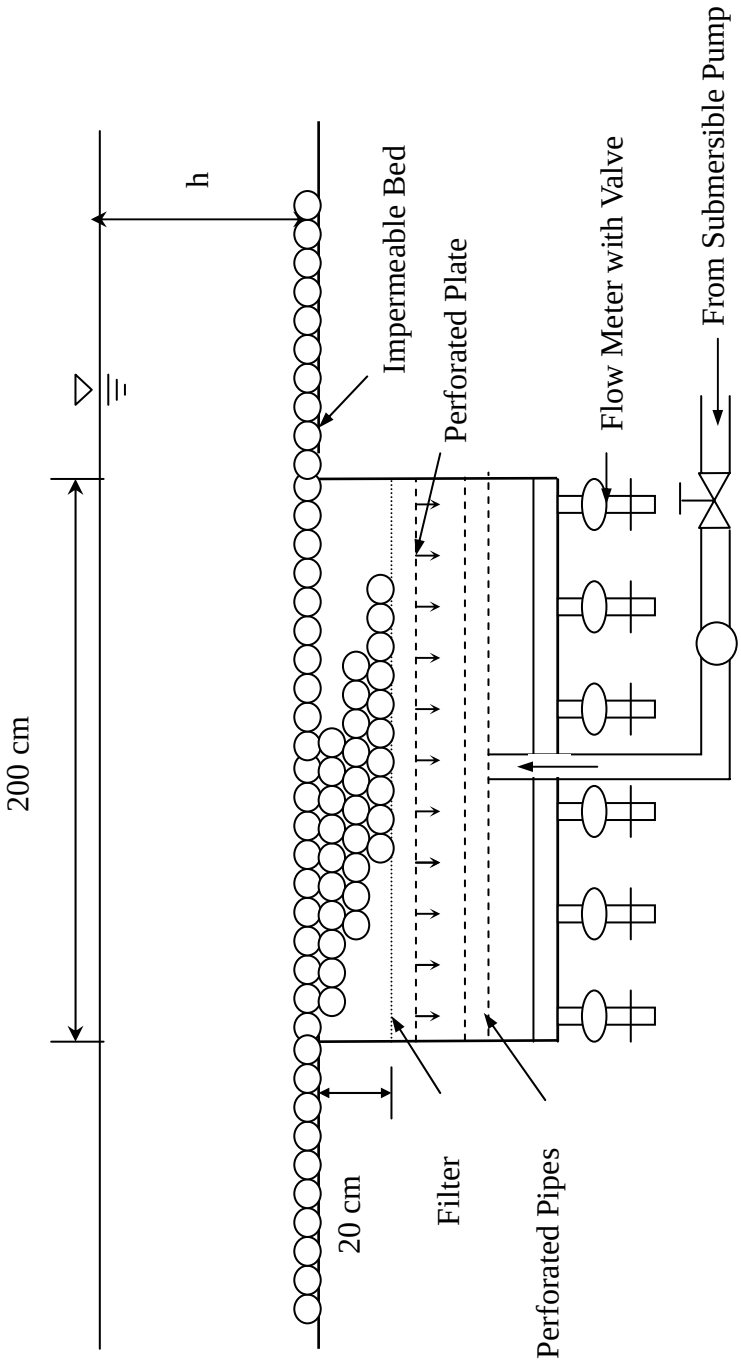

Figure 3.2 Schematic Diagram of Test Section

3.2 EXPERIMENTAL APPARATUS

3.2.1 Open-Channel Flume

The experimental equipment includes an open-channel flume and a seepage conduit. The glass-sided horizontal flume, which is 30 m long, 0.7 m wide and 0.6 m deep, is supported on a steel truss. Fig. 3.1 shows the schematic diagram of the flume and its auxiliary facilities.

Fig. 3.1 shows how the flume is divided into three reaches: upstream section, test section, and downstream section. Water is supplied to the flume using a submersible pump installed in the laboratory reservoir. The flume pumping system is capable of recirculating up to 200 L/s of water. The flow rate in the flume, monitored by the use of an electromagnetic flow meter, is controlled using a speed inverter and valve. At the entrance to the flume, flow straighteners are installed to ensure uniform flow conditions and to minimize large scale turbulence and circulations. The 12-m-long upstream reach together with the head tank (see Fig. 3.1) permits the stabilization of the flow.

Located at the middle reach with length = 8 m is the test section that includes a seepage zone in the form of a recess. The seepage zone, where either upward or downward seepage can be introduced, is 2 m long, 0.2 m deep, and spans the width of the flume. The seepage zone is designed to ensure uniform seepage velocity over the entire area of the seepage zone. The setup of the seepage recess is schematically shown in Fig. 3.2. The permeable bed in the seepage zone is levelled to the

elevation of the neighboring bed. Sand is placed on top of a filter net, which in turn, overlays a perforated metal plate. The use of the filter net prevents the sediment particles from falling down to the bottom of the recess, which may clog the pipes. Water is allowed to seep through the perforated plate, filter net and sand layer to ensure uniform seepage flow within the granular materials.

In the case of suction, twelve identical pipes, each with a valve and a flow meter to control and monitor the suction discharge, are fixed onto the bottom of the recess to drain water out uniformly. On the other hand, a separate submersible pump installed in the laboratory reservoir is used to supply injection; its flow discharge is determined by a speed inverter and valve, which is monitored using a flow meter. Before water seeps into the granular materials, it is first pumped through the perforated pipes with identical diameter holes to ensure uniform seepage velocity in the entire seepage zone.

The downstream reach occupies the last 10 m of the flume. It serves as an outlet section to minimize backwater effects on the test zone. A tailgate weir, which is constructed at the end of the flume, allows adjustment of the water depth.

3.2.2 Seepage Conduit

The permeability tests for granular materials used in this study (Series-A) are performed in a clear Perspex seepage conduit as shown in Fig. 3.3. The rectangular conduit has a cross-section of 14 cm by 21 cm, and a height of 80 cm. A perforated plate at the bottom of the conduit is applied to support the sediment samples. The use of a special filter, whose permeability is better than that of the sediment particles tested, overlying the plate permits the formation of uniform seepage into the granular materials. Water is pumped from the low end of the conduit into a chamber, before it seeps into sediment sample. Four manometers connected to the conduit are used for piezometric head measurements.

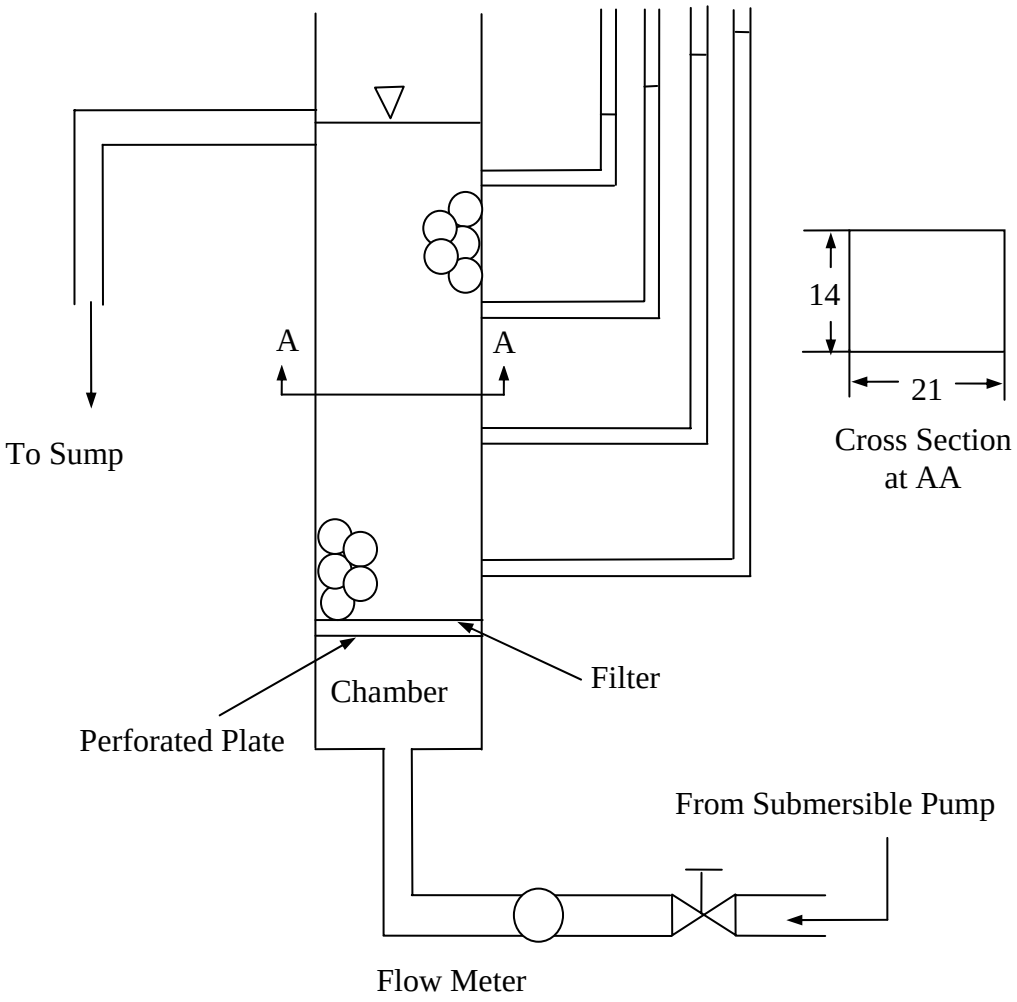

Figure 3.3 Schematic Sketch of Seepage Conduit

3.2.3 Setup for Sand Feeding

Experiment Series-B is performed in the seepage zone of the 30-m long flume to investigate the influence of seepage on the angle of repose of the sediment. When collecting the relevant data in the presence of seepage, the depth of water in the flume is kept constant. To this end, water seeping into the flume is drained over the tailgate in the case of injection; and additional water is supplied to the flume in the case of suction.

To minimize the influence of any streamwise velocity, which might be induced by seepage on the slope of the sand heap in the test of Series-B, specially-designed equipment is used to feed sediments during the test (see Fig. 3.4). The equipment comprises three parts:

(1) A Perspex box which has the same width as the flume, is used to encase the sand heap from the effect of flow;

(2) Conduit A, which is a circular cylinder with diameter = 10 cm, penetrates through the top of the Perspex box. This is to avoid disturbances created by the surface flow on the sediment particles as they dropped into the Perspex box;

(3) Conduit B has a diameter slightly larger than that of the test sediment. It is concentric with Conduit A, with its lower end located just above the water surface. This minimises the forces of the falling sediment particles from exerting on the sand heap.

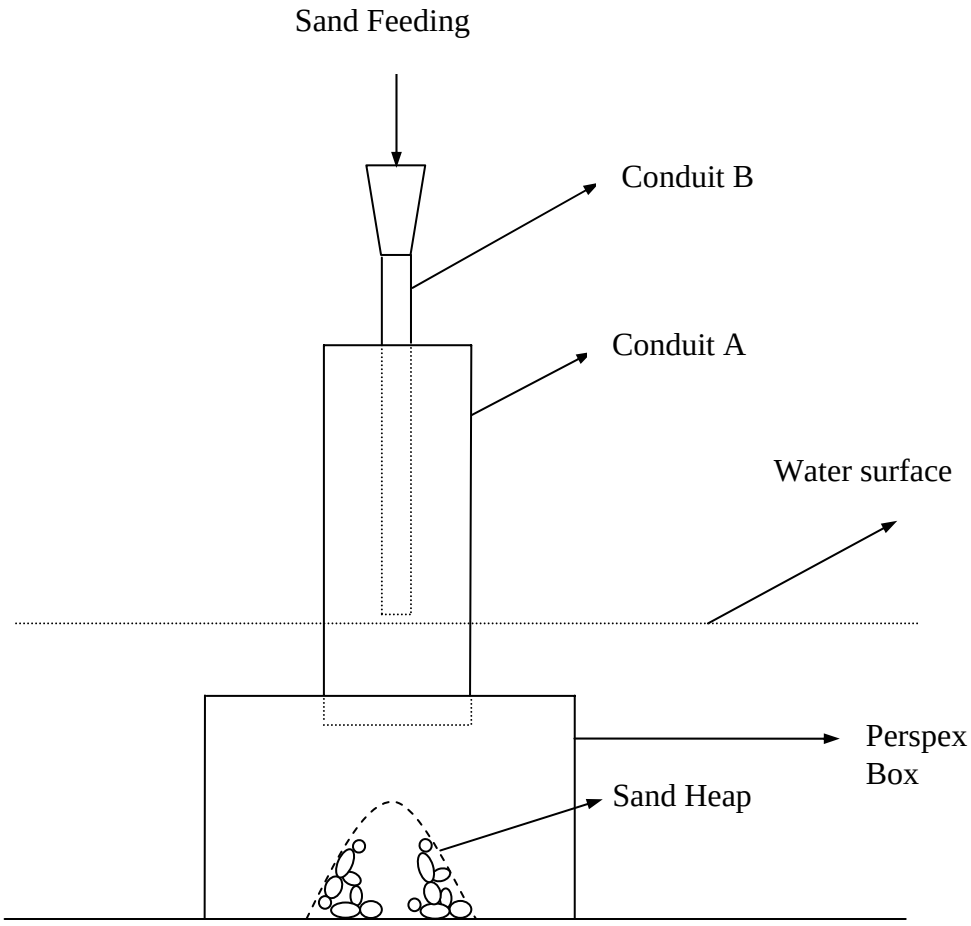

Figure 3.4 Experiment Setup Used to Determine Angle of Repose of Sediments

3.3 BED MATERIALS CHARACTERISTICS

3.3.1 Definitions

Sediment characteristics are defined by size, shape, fall velocity, specific gravity, porosity and geometric standard deviation. Of all the properties of sediment particles, the size of the sediment is the most commonly used in sediment transport studies. The two main methods for determining particle size distributions (from which sediment size can be obtained) are sieve analysis, for particles larger than approximately 0.06 mm; and hydrometer analysis, for smaller particles. In the latter, the size of a particle is equivalent to the diameter of a sphere that settles in water at the same velocity as the particle. In sieve analysis, the granular material is shaken in a series of sieves with square openings of a specified size. As such, the size of the particle is based on the side dimension of a square hole of the sieve. Thus, the size of a sediment particle is closely related to the analysis method.

Garde and Ranga Raju (1977) and Shen and Julien (1993) defined sieve diameter of a sediment particle as the square size opening in a sieve through which a given sediment particle will just pass. However, the sediment particles in a riverbed consist of different shapes, ranging from round to flat and needle-like. Due to the extreme irregularity in shape and size, this arbitrary definition of size actually means that only some dimension of a particle, which can slip through a square hole, is measured. Additionally, Shen and Julien (1993) stated that in most studies it has been shown that the sieve diameter is 90% of the nominal diameter. In most cases a

series of sieves is used for the separation of sediment particles into various size grades provided that the particles are larger than 0.0625 mm in diameter.

3.3.2 Size Distribution of Sediment Particles

Since both flow resistance and sediment movement are directly related to sediment size distribution, it is imperative that one can obtain such values accurately (Vanoni, 1975). In this study, the sieve analysis method is used to determine the size distribution of the sediment particles; in which a series of sieves are fitted one over another with the mesh size decreasing in the downward direction. A sediment sample is placed on the top sieve and the sieve column is shaken using a mechanical shaking machine.

A total of three sets of fairly uniform sediments are tested in the study. Fig. 3.5 shows the particle size distribution curves obtained by plotting the percentage by weight passing through each sieve in a sieve analysis. Various characteristic grain diameters such as D_{50} and D_{90} can be obtained from these curves. A granular material composed entirely, or almost entirely, of particles of a particular size is called uniform. Using D_{16}, D_{50} and D_{84}, uniformity coefficient, or geometric standard deviation C_u, is defined by:

$$C_u = \frac{1}{2}\left(\frac{D_{84}}{D_{50}} + \frac{D_{50}}{D_{16}}\right) \tag{3.1}$$

Table 3.1 shows the results of the sieve analysis, and some other properties of the tested sediment particles. The median grain diameters are 0.9 mm, 1.41 mm and 1.64 mm, with respective geometric standard deviation, C_u, of 1.27, 1.17, and 1.23 which shows the uniformity of each sediment used.

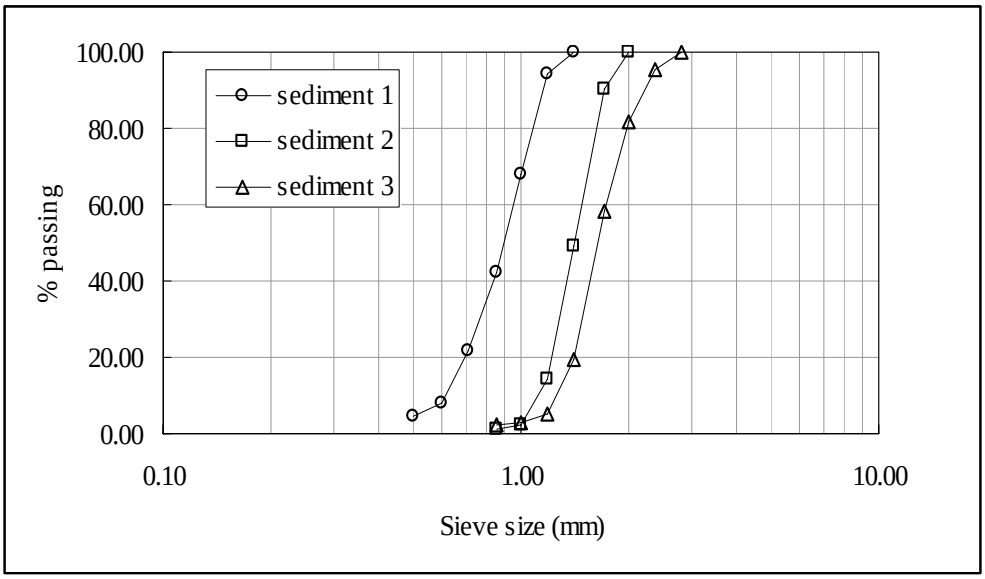

Figure 3.5 Grain Size Distributions of Sediment Samples

Table 3.1 Properties of Sediments Used in the Study

No.	Median Grain Diameter (mm)	Uniformity Coefficient	Porosity	Specific Gravity
1	0.9	1.27	0.47	2.62
2	1.41	1.17	0.44	2.55
3	1.64	1.23	0.46	2.62

3.3.3 Porosity of Sediments

Porosity, which is a macroscopic porous medium property, is the percentage of voids in the total space occupied by a known number of sediment particles. In nature, porosity depends not only on the size, uniformity, and shape of particles, but also on the pattern of deposition. Loose packing occurs when sediments settle from suspension in still water. When seepage is concerned, the porosity of the granular material becomes very important when compared with other properties of the sediment particles. Since seepage flows through voids of the sediment particles directly, porosity is one of the dominant factors governing seepage properties such as seepage gradient and quick condition (refer to Chapter 4).

Numerous methods have been developed for determining porosity in the literature. In this study, porosity is calculated using the volume of sand particles and the total volume of the sediment sample with a known weight. Since the experimental procedure has a significant effect on porosity due to compaction or consolidation, the same experiment for a given sediment sample is repeated several times. The average value of porosity for each sediment sample is used for subsequent data analysis. The computed porosity values of the sediments are also included in Table 3.1.

3.3.4 Specific Gravity

The specific gravity of the sediment particles is also an important parameter, which is defined as the ratio of the sediment density and the fluid density. Natural quartz sediment has a specific gravity of 2.65. In this study, the specific gravity of the sediment samples is determined from the measured sediment weight and volume. Similar to the measurement of porosity, the experimental procedure is repeated several times to minimize the effects caused by compaction or consolidation. The specific gravity of the sediments used in the study is shown in Table 3.1.

3.4 MEASUREMENT TECHNIQUES

3.4.1 Flow Velocity and Turbulence Measurement

A Dantec two-component fiber optic Laser Doppler Anemometer (LDA) is used to measure the velocity and turbulence of the flow over the artificial fixed dune in Series-D (see Fig. 3.6). The LDA, operated in back-scatter mode, has a lens with a focal length of 400 mm. Velocities are obtained by measuring the Doppler shift in the frequency of light scattered by a particle following the flow when it passes through the intersection of two beams of coherent light. Four beams of 100 mW argon-ion laser converge to define a very small measuring volume of 0.12 mm × 0.12 mm × 2.5 mm, thereby providing a good spatial resolution. For measuring particle velocity, the effective length of the volume is 0.12 mm according to the principles of LDA. Nelson et al. (1993) reported that the mixing length for a uniform boundary layer, $\iota = \kappa y$, fits reasonably well with the measurement data for turbulence over bedforms. Noting that $\kappa \approx 0.41$ and taking $y = 1mm$ as an example, the mixing length gives a value of 0.41 mm which is much higher than the effective length 0.12 mm. This fact indicates that the measuring volume of LDA could satisfy the requirements of measurement in the present experiment. The small measuring volume in combination with fast signal processing electronics also permits high bandwidth, time-resolved measurement of fluctuating velocities, providing excellent temporal resolution. Moreover, its non-intrusive principle and directional sensitivity make it very suitable for applications with reversed flows associated with dunes.

Usually the temporal resolution is limited by the concentration of seeding rather than the measuring equipment itself. Ideally, the seeding particles should be small enough to follow the flow, yet large enough to scatter sufficient light from the LDA probe to obtain good output. In the present study, the flow is seeded with 45 μm diameter TiO_2 powder, which is sufficiently small when compared with the mixing length or the measuring volume and provides data rate of between 20 and 100 Hz. The sampling time for each point is at least 5 minutes; this allows acquisition of sufficient data (more than 5000) for reliable results. In an LDA study of the backward-facing step flow Adams and Eaton (1988) pointed out with more than 2000 samples that the statistical uncertainty was estimated to be less than 1% throughout the flow. Experience with the LDA for studying sediment-laden flows (Lyn 1988, 1992) showed that the uncertainties are estimated to be 1%, 5% and 10% for the mean velocities, turbulence intensities, and Reynolds shear stresses, respectively, except for those in the region very near the bed. For the turbulence over dunes investigated in this study, the uncertainties are generally regarded to be in a similar range. However, in the recirculation region a higher level of uncertainty may be expected. The laser-optics probe is mounted on a high-precision, electronically controlled traverse system so that the predetermined measurement locations can be positioned easily with an accuracy of ± 0.1 mm.

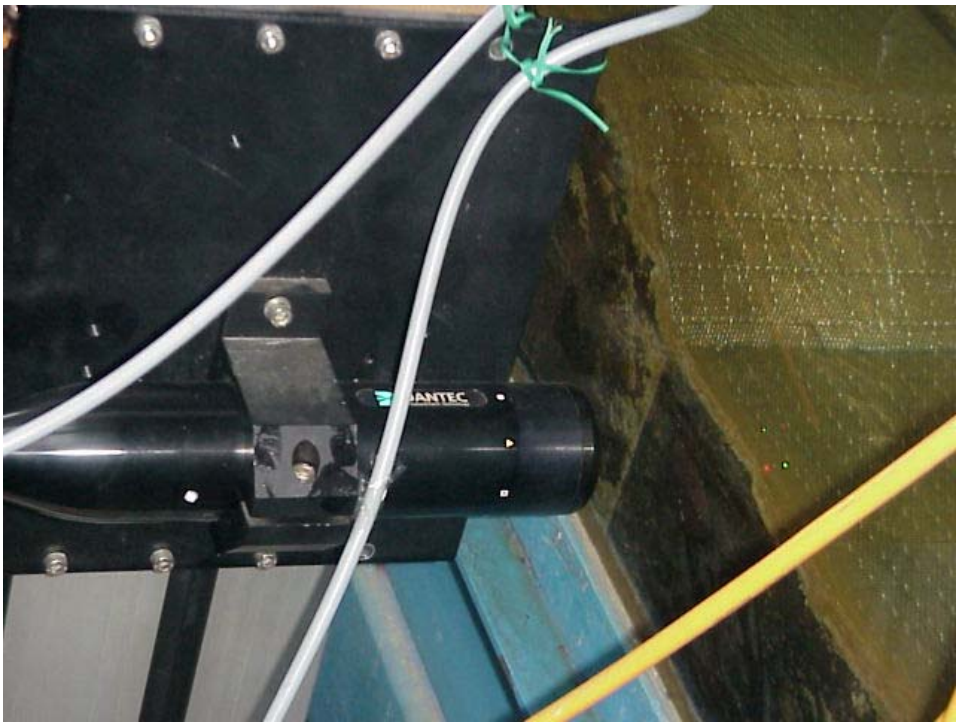

Figure 3.6 Photo of LDA Probe

With the aid of BSA flow software (Dantec) and a micro computer, the following statistical parameters can be calculated using the measured velocity data. The formulas for calculating the time-averaged streamwise and vertical velocities, u and v respectively at a single location are as follows:

$$u = \frac{1}{n}\sum_{i=0}^{n-1} u_i \tag{3.2}$$

$$v = \frac{1}{n}\sum_{i=0}^{n-1} v_i \tag{3.3}$$

where n is the number of velocity samples, and u_i and v_i are the instantaneous streamwise and vertical velocities, respectively. The root-mean-square values of the streamwise and vertical components of velocity are

$$u' = \left[\frac{1}{n}\sum_{i=0}^{n-1}(u_i - u)^2\right]^{0.5} \tag{3.4}$$

$$v' = \left[\frac{1}{n}\sum_{i=0}^{n-1}(v_i - v)^2\right]^{0.5} \tag{3.5}$$

where, u' = rms value of the streamwise velocity, and v' = rms value of the vertical velocity. The formulas for determining the Reynolds stress are

$$-\overline{u'v'} = \frac{1}{n}\sum_{i=0}^{n-1}(u_i - u)(v_i - v) \tag{3.6}$$

$$\tau_r = -\rho\overline{u'v'} \tag{3.7}$$

where, τ_r = Reynolds shear stress. More details on the LDA apparatus and the BSA flow software are given by Durst et al. (1987) and Dantec (2000).

3.4.2 Water Surface Slope Measurement

When seepage occurs through the bottom of an open channel flow, it has an influence on the water surface slope over the seepage zone. Water surface elevations are measured along the flume centreline from the leading edge to the downstream edge of the seepage zone using a point gauge with a vernier scale. This gauge, capable of measuring the water level with an accuracy of ± 0.5 mm, is fixed on a movable device mounted on the flume. The mean water surface slope is then evaluated from the linear approximation of these elevations within the seepage zone.

This slope in the seepage zone is used to estimate the spatially-averaged mean bed shear stress in the latter analysis in Chapter 6, from

$$\tau_b = \rho g h J \tag{3.8}$$

where ρ = fluid density, g = gravitational acceleration, h = mean water depth, and J = mean water surface slope.

3.4.3 Dune Dimensions Measurement

3.4.3.1 Electronic Bed Profiler

An electronic bed profiler (Fig. 3.7), together with a data-recorder (Fig. 3.8), is used to measure the geometrical dimensions of bedforms as well as the angle of repose of sediments. The distance between the probe tip of the profiler and the bed surface is kept constant, which may adjust continuously from 0.5 mm to 5 mm to satisfy the requirement of different experiment conditions. To avoid disturbance by the probe on the measurement, especially for tests in Series-D, a larger distance is chosen. The use of a motor mounting device enables the profiler to be moved to any test location for measurement of the dune geometrical dimensions. During the experiment, the profiler moves along the centreline of the flume in the streamwise direction at a predetermined speed that is controlled by the motor; while the probe adjusts itself up and down depending on the geometry of the dune. Therefore, the path of the probe represents the geometrical shape of the dune. Real-time electronic signals are sent to a data-recorder and transformed to digital signals, from which the

geometrical dimensions can be obtained using a pre-calibrated curve. The resolution of the measurement is ±0.2 mm.

Figure 3.7 Photo of Bed Profiler

Figure 3.8 Photo of Data-Recorder

3.4.3.2 Real-Time Data-Recorder

A compact, lightweight and portable double-channel recorder shown in Fig. 3.8 is used to record the electronic signals, associated with the geometrical dimensions of the dune, from the bed profiler. It features a recording section that uses a thermal dot array and a liquid-crystal display, and is capable of real-time recording of the measured data. Its wide dynamic range from 50mV to 200V permits the accurate display of the dune geometry with fairly large range of dimensions. The signals received from the electronic bed profiler are digitized and then printed on plotting

paper. The paper feed speed could be adjusted to suit the specific requirement and has been pre-calibrated. With the calibration curve, the geometrical dimensions of the dune can be determined from the plotted curves.

CHAPTER 4

ANGLE OF REPOSE OF SEDIMENTS WITH SEEPAGE

4.1 INTRODUCTION

Slope stability of non-cohesive sediment is a fundamental problem in both hydraulics and soil mechanics. Under a static condition, the angle of repose is the steepest angle at which the sediment particles can stay without motion. One of the most common methods used to investigate slope stability is to consider the initiation of motion of sediment particles. To this end, numerous researchers have theoretically analyzed forces acting on, and moment about a sediment particle to determine the angle of repose. On the other hand, laboratory experiments have also

been conducted to empirically achieve the same objective. Often times, both these approaches are used concurrently to verify the results.

Eagleson and Dean (1959) conducted a series of experiments in which the angle of repose of spherical particles resting on two different types of natural sand, with median diameter = 1.83 mm and 0.79 mm were determined. Their experimental data showed that the angle of repose for the top spheres with various sizes and densities ranged from nearly 50^0 to less than 20^0. Miller and Byrne (1966), on the other hand, performed experiments to examine particle-shape effects on the angle of repose and proposed an empirical equation for predicting the angle of repose as $\alpha = \xi\left(K/\overline{K}\right)^{-\eta}$, in which α = the average angle of repose of a single particle on a rough bed; $K/\overline{K}$ = the ratio of the diameter of single grain to the average diameter of the bed grains; ξ = a parameter incorporating the effects of shape and roundness in both particle and bed; and η = a parameter incorporating the effects of sorting of the bed grains. All these studies were conducted under conditions where seepage is absent. If seepage is present, the sediment particles experience an additional hydrodynamic force, which renders a more complex boundary condition for slope stability consideration. Very few studies have been done to explore the response of the angle of repose to seepage flow. Amongst the studies that can be found in the literature is the one by van Rhee and Bezuijen (1992), who proposed two stability criteria, namely, the continuum mode and single-particle mode to account for sandy slope stability in the presence of seepage. Based on their experimental results, they concluded that for injection, the continuum mode theory governs the failure process,

whereas in the case of suction, the failure mode can be described by the single-particle mode theory.

Seepage through boundaries of alluvial channels, rivers and streams is a common occurrence due to porosity of the granular material. Water is continuously seeping into or out of the channel bed and banks because of the different level between the free water surface in the channel and the adjoining groundwater table resulting in suction or injection. A thorough literature search shows that very few studies have been conducted to date to investigate the influence of seepage on the angle of repose of cohesionless sediment. The difference in the results associated with the angel of repose, even in the condition of without seepage, is quite large, which is possibly due to the various experimental methodologies applied besides the difference in the properties of sediments.

The objective of this chapter is twofold: (1) by including seepage in a 3-dimensional force analysis, to theoretically examine its influence on the critical sandy slope; a general expression for the angle of repose is proposed to account for the effect of seepage hydraulic gradient; and (2) to conduct a series of laboratory experiments to verify the theoretical result.

4.2 THEORETICAL CRITICAL SLOPE

For a sandy slope consisting of non-cohesive uniform spherical sediments in which the particles are subjected to seepage alone, i.e., without any surface flow; the geometrical layout of and forces acting on the sediment particles on the top layer is shown in Fig. 4.1. The figure shows how in a three-dimensional configuration, one sphere (Sphere 1) is located on top of three other spheres. At the onset of motion, Sphere 1 experiences seepage force F_S, submerged weight force W, normal force N and tangential force T from either Sphere 3 or Sphere 4 or both (no reaction forces from Sphere 2 is considered because they are zero when Sphere 1 is just about to move). Two modes of movement may be taken by Sphere 1: sliding or rolling. If Sphere 1 is sliding down, $T = \mu_f N$, where μ_f is coefficient of friction between the spherical surfaces. Ling et al. (1992) studied a similar problem in which the driving force on the sphere is gravity only. They numerically solved the equations of motion and found that when motion just begins, the sphere starts with rolling because T is usually much smaller than μ_f N. In fact, sliding is limited to consuming up to only about 1% of the kinetic energy of the sphere. In light of the results of their study, rolling is assumed in the present analysis.

In the three dimensional configuration, the reaction forces lie on the edges of a tetrahedron formed by the points of contact of the spheres and the center of gravity of Sphere 1 (Figs. 4.2a and 4.2b). Points E, F and G are the contact points of the top single particle with the three underlying spheres; Points O_1, O_2, O_3 and O_4 are the centers of the four spheres; and Points O and O_0 are the centers of the triangle formed by the centers of the three underlying spheres and that formed by the contact

points E, F and G, respectively. When Sphere 1 is just about to move, the moment equation about a nominal pivot point P (see Figs. 4.2a and 4.2b) can be written as

$$\sum M = F_S \cdot e_1 - W \cdot e_2 = 0 \tag{4.1}$$

$$e_1 = O_1 P \cdot \sin\phi \tag{4.2}$$

$$e_2 = O_1 P \cdot \sin(\phi - \alpha) \tag{4.3}$$

in which e_1 and e_2 are the moment arms of seepage and submerged weight forces, respectively.

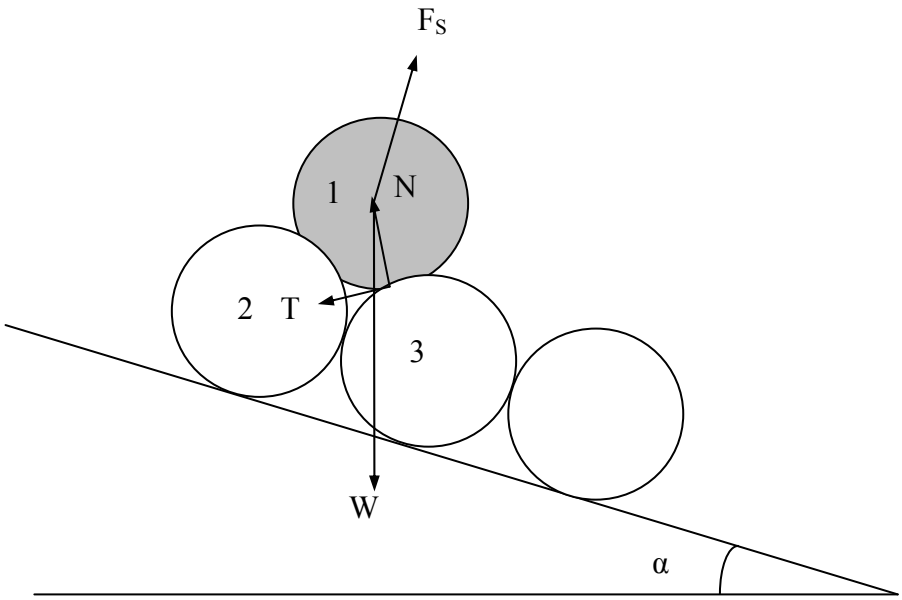

(a) Elevation View

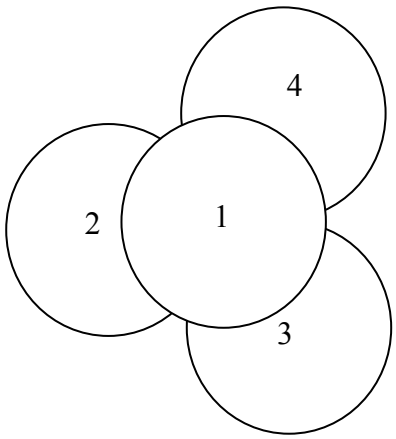

(b) Plan View

Figure 4.1 Forces Acting on a Single Sphere

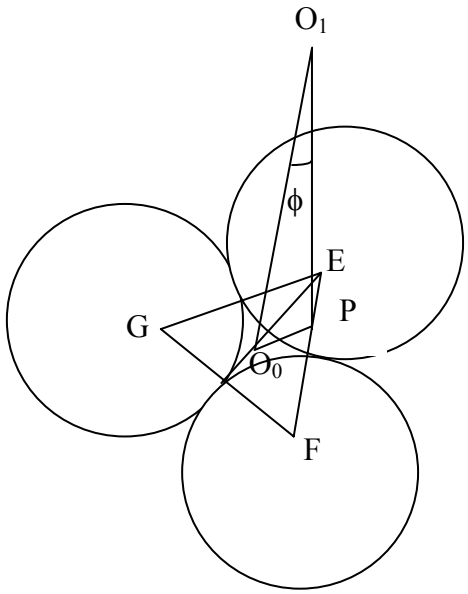

(a)

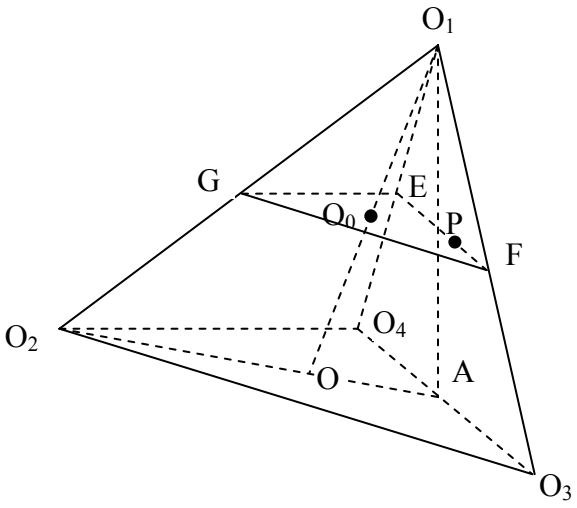

(b)

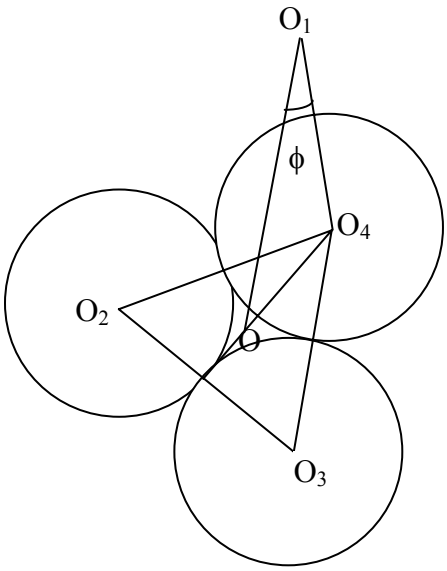

(c)

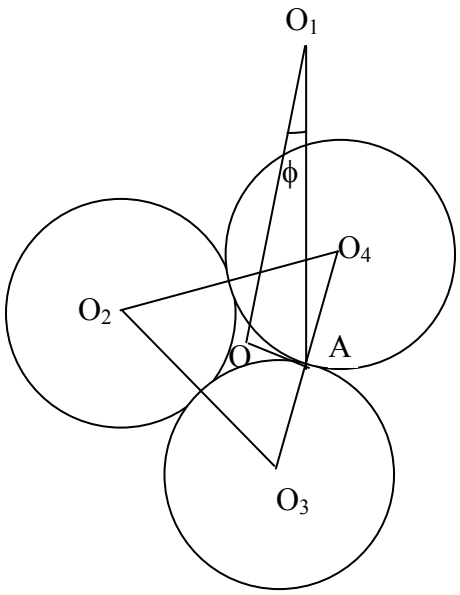

(d)

Figure 4.2 Geometrical Relationships of Spheres with Different Orientations

The magnitude of e_1, e_2 and ϕ is determined by the position of the pivot point P. Depending on the orientation of the bed particles, Sphere 1 can roll over the valley formed by the two particles, roll over the summit of a single particle, or anywhere in between these two locations. This means that any point along the line EF can be the nominal pivot point over which the sphere rolls. Two extreme cases are considered herein in order to determine the average value of ϕ as follows (see Figs. 4.2c, 4.2d):

Case 1: Sphere 1 rolls over the summit of one of the underlying spheres, say along OO_4 in the vertical plane (Fig. 4.2c). In this case, $\phi = \phi_{max}$, and is the maximum. Based on the geometrical relationships,

$$\tan\phi_{max} = \frac{OO_4}{OO_1} = \frac{\sqrt{2}}{2} \tag{4.4}$$

Case 2: Sphere 1 rolls over the valley formed by Spheres 3 and 4, along OA in the vertical plane (Fig. 4.2d). In this case, $\phi = \phi_{min}$, and is the minimum value. Similarly, geometrical consideration yields

$$\tan\phi_{min} = \frac{OA}{OO_1} = \frac{\sqrt{2}}{4} \tag{4.5}$$

The actual angle ϕ could be any value between ϕ_{max} and ϕ_{min}, depending on which path the sphere takes. As a first approximation, we take the average of the ϕ-values for which Sphere 1 rolls over three points on the line O_3 O_4, i.e., Points O_4, A and O_3. With this assumption,

$$\tan\phi = \frac{\tan\phi_{max} + \tan\phi_{min} + \tan\phi_{max}}{3} = \frac{5}{6}\tan\phi_{max} \tag{4.6}$$

since $\tan\phi_{max} = 2\tan\phi_{min}$.

Therefore,

$$\tan\phi = \frac{5\sqrt{2}}{12} \text{ or } \phi = 30.51^0 \tag{4.7}$$

By substituting Eqs. (4.2), (4.3) and (4.7) into Eq. (4.1), one gets

$$F_S = \frac{\sin(\phi-\alpha)}{\sin\phi}W = \frac{\sin(30.51^\circ-\alpha)}{\sin 30.51^\circ}W = 1.97\sin(30.51^\circ-\alpha)W \tag{4.8}$$

The submerged weight of the top sphere is given by

$$W = \frac{\pi}{6} D^3 (\rho_s - \rho) g \tag{4.9}$$

where D = diameter of the particle, and equals to D_{50} of the test material; ρ_s = mass density of sediment; ρ = mass density of fluid; and g = gravitational acceleration.

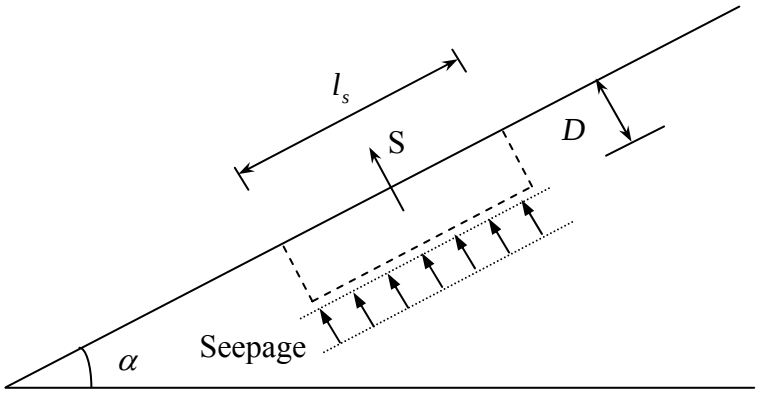

Figure 4.3 Analysis of Seepage Force on a Slice

If the hydraulic gradient is taken as positive for injection, the force exerted by seepage on a sediment slice with volume of $D \times D \times l_s$ (see Fig. 4.3) on the top layer of the slope can be derived by using Darcy's law with the assumption of uniform seepage therefore seepage force in the slope:

$$S = i \rho g D^2 l_s \tag{4.10}$$

where i = hydraulic gradient of seepage. Since the volume occupied by the sediment particles over an arbitrary length, l_s is $D \times D \times l_s$, the number of particles in this layer is

$$n = \frac{6l_s(1-\varepsilon)}{\pi D} \tag{4.11}$$

where ε = porosity of the sediment. Thus, the seepage force acting on a particle can be computed by dividing (4.10) with (4.11)

$$F_S = \frac{i\rho g \pi D^3}{6(1-\varepsilon)} \tag{4.12}$$

In the case of coarse particles, there is no or negligible pressure gradient on the upper half of the particles at the top layer of the slope (van Rhee and Bezuijen 1992); therefore, the hydraulic gradient of seepage flow has effect only on the lower half of the top particles. To account for this, a coefficient β is added to (4.12) resulting in

$$F_S = \frac{i\rho g \pi D^3 \beta}{6(1-\varepsilon)} \tag{4.13}$$

where β is dependent on particle size, and ranges between 0.5 for coarse granular materials and 1 for fine grains. For simplification, the average value of β (= 0.75) is used to compute the seepage force exerting on the top particle

$$F_S = \frac{i\rho g \pi D^3}{8(1-\varepsilon)} \tag{4.14}$$

Substituting Eqs. (4.9) and (4.14) into Eq. (4.8) leads to

$$i = 2.63(1-\varepsilon)\frac{\rho_s - \rho}{\rho}\sin(30.51^\circ - \alpha) \tag{4.15}$$

Eq. (4.15) implies that for the case without seepage, the maximal slope angle, i.e., the angle of repose of the uniform spherical particle is 30.51^o. It is comforting to

note that this value is consistent with the angle of repose cited in the literature for well-rounded sand.

Das (1979) and Cheng and Chiew (1999) described a quick condition for a horizontal bed, as

$$i_c = (1-\varepsilon)\frac{\rho_s - \rho}{\rho} \tag{4.16}$$

Under the quick condition, the seepage force acting on a particle resting on a horizontal bed just balances its submerged weight force.

Dividing Eq. (4.15) by (4.16), one gets

$$\frac{i}{i_c} = 2.63\sin(30.51^\circ - \alpha) \tag{4.17}$$

Eq. (4.17) describes the relationship between the dimensionless hydraulic gradient of seepage and the critical slope, comprised of identical uniform particles, on which the top particle can stay without motion. Seepage can increase or reduce the angle of repose of sediments depending on its flow direction, which is clearly shown in Fig. 4.5.

Hydraulic Gradient

The hydraulic gradient that sustains the movement of water through the porous medium is related to the seepage velocity. In most practical cases in soil mechanics the assumption of a linear relationship between velocity and hydraulic gradient based on Darcy's law is valid because laminar flow condition is present. However, if the flow velocity through coarse granular materials is comparatively large,

nonlinear relationships could be present, as is proposed by many researchers to account for the transitional and turbulent seepage. Kovács (1981) grouped these nonlinear relationships into two main categories:

(a) Binomial form

$$i = av_s + bv_s^2 \tag{4.18}$$

(b) Power form

$$i = cv_s^m \tag{4.19}$$

in which v_s = seepage velocity; a, b, c = empirical coefficients; and m = exponent which ranges between 1 and 2.

In this study, Eq. (4.19) is used to delineate the nonlinear relationship between the seepage velocity and the hydraulic gradient and the empirical coefficients, c and m, are determined experimentally for each sediment sample.

4.3 EXPERIMENTAL PROCEDURE

Two series of experiments (Series-A and Series-B) are conducted to investigate the influence of seepage on angle of repose of sediments. The experimental setup and apparatus for the two tests have been introduced in Chapter 3. A total of three sets of fairly uniform sediments, whose properties are shown in Table 3.1 and Fig. 3.5, are tested.

Series-A is performed in a seepage conduit (see Fig.3.3) to test the permeability of sediments used in the study, i.e., empirically identify the parameters in Eq. (4.19) and the following test procedure is adopted:

(1) Before commencement of the test, the sediments in the seepage conduit are first soaked for a period and stirred to release all air bubbles which may affect the permeability of sediments significantly;

(2) Water is pumped into the conduit slowly and the discharge is increased gradually to a predetermined value. For obtaining a steady state, the seepage flow lasts for a period of time. The steady state is identified if the piezometric heads are observed to be constant;

(3) Upon flow stabilization, the piezometric heads are recorded for subsequent computation of the hydraulic gradient;

(4) Adjust the seepage discharge, and then steps (2) and (3) are repeated. Observation is made on the mobility of the sand grains as the seepage velocity is increased gradually until the occurrence of the quick condition or the attainment of the maximum velocity.

In this way a series of hydraulic gradients are obtained for the sediments.

The experimental procedure used in the Series-B is summarized as follows:

(1) Water is first filled into the flume and the required water depth is kept constant by adjusting the tailgate;

(2) Using the setup specially-designed for sediment feeding (see Fig.3.4), Sand is dropped into the flume at the test zone to form sand heaps with a suitable height.

The geometrical dimensions of the sand heaps are then measured using the electronic bed profiler (see Fig. 3.7);

(3) Suction or injection is slowly introduced to the flume and increased gradually to the predetermined value;

(4) When the steady state is reached, more sediment particles are added to the heap to ensure that the slope angle is the maximum because the sand slope may be affected during introduction of seepage or suction. To ensure that the water level in the flume is a constant during the experiment, additional water is supplied to and superfluous water drained over the tailgate for tests associated with suction or injection, respectively;

(5) The geometry of the slopes is measured by the bed profiler and recorded by the data-recorder (see Fig. 3.8) for the seepage rate;

(6) Change the seepage discharge gradually and then steps (3)-(5) are repeated for each seepage rate.

4.4 EXPERIMENTAL RESULTS AND ANALYSIS

The values of c and m in Eq. (4.19) are first determined by plotting the experimental data collected from Series-A in Fig. 4.4. The data show that the hydraulic gradient and seepage velocity fit well with the exponential function. In Fig. 4.5, the results of the angle of repose arising from the test conducted in Series-B are plotted against the seepage hydraulic gradients for the three sediments used.

The data show that the presence of seepage has a significant influence on the angle of repose of the sediment: injection decreases the angle of repose while suction has the opposite effect. The theoretical Eq. (4.17) is also superimposed in Fig. 4.5. Although the experimental data consistently fall above, its trend is almost parallel to, the theoretical equation. To account for the constant shift of the data, Eq. (4.17) can reasonably be adjusted by simply changing the coefficient from 30.51 to 34, resulting in a modified equation below:

$$\frac{i}{i_c} = 2.63\sin(34^\circ - \alpha) \tag{4.20}$$

A possible reason why the experimental data do not agree with the theoretical equation is that the sediment particles in the test are neither uniform nor spherical; The choice of β = 0.75 in the computation is quite arbitrary; Moreover, the assumption of uniform seepage force for deriving theoretical equation may not be reached in the experiments. Eq. (4.20) is also superimposed in Fig. 4.5, and it compares better with the experimental data.

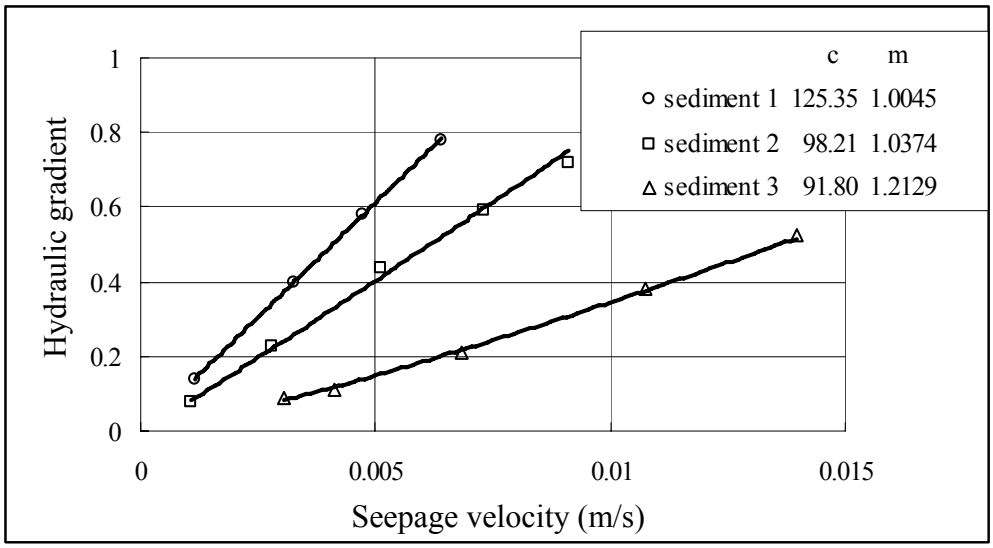

Figure 4.4 Nonlinear Relationship between Hydraulic Gradient and Seepage Velocity

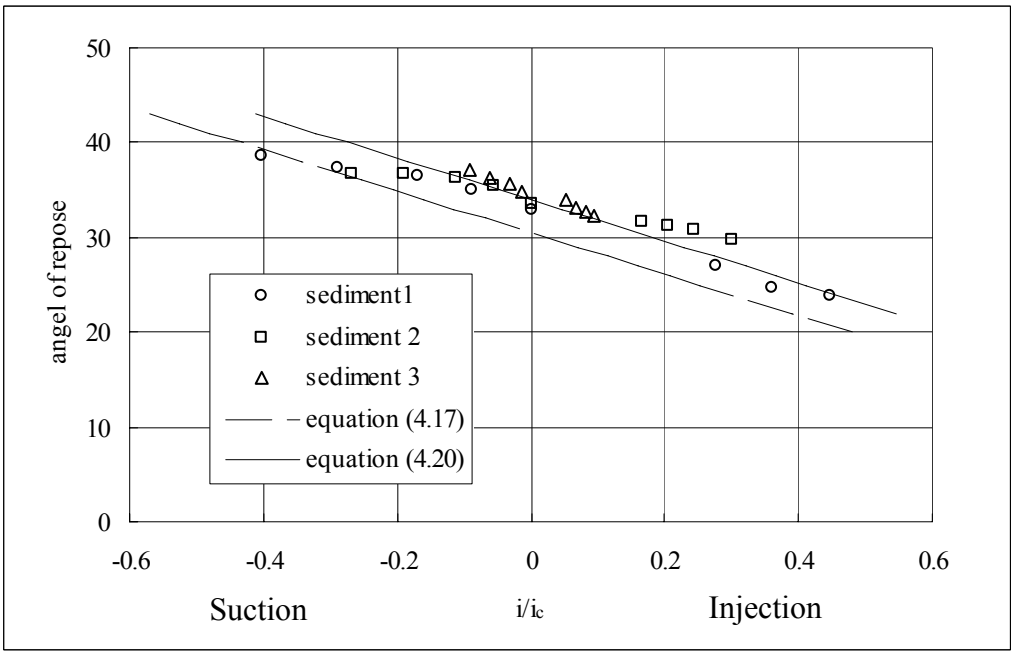

Figure 4.5 Influence of Seepage on Angle of Repose

4.5 COMPARISON WITH OTHER MODES

van Rhee and Bezuijen (1992) proposed two stability criteria, namely, the continuum mode and single-particle mode to account for sandy slope stability in the presence of seepage. Based on their experimental results, they concluded that for injection, the continuum mode theory governs the failure process, whereas in the case of suction, the failure mode can be described by the single-particle mode theory. The work of van Rhee and Bezuijen is used to compare with the results of this study.

By analyzing the force equilibrium of a slice on the top of a slope, the continuum mode was derived as (for a brief description of the continuum theory see Terzaghi and Peck, 1967; van Rhee and Bezuijen, 1992):

$$i = (1-\varepsilon)\frac{(\rho_s - \rho)}{\rho}\frac{\sin(\alpha_0 - \alpha)}{\sin(\alpha_0)} \tag{4.21}$$

where the hydraulic gradient is taken as positive for injection and negative for suction; and α_0 = angle of repose of sediments without seepage.

In the light of the work of Lambe and Whitman (1979), van Rhee and Bezuijen (1992) analyzed the stability of a single grain on a slope and proposed the single-particle mode:

$$i = \frac{4}{3}\frac{(\rho_s - \rho)}{\rho}\frac{\sin(\alpha_0 - \alpha)}{\sin(\alpha_0)} \tag{4.22}$$

These two stability mode have the same form, the only difference being the coefficients.

The maximum slope of sediments with seepage was also investigated experimentally by van Rhee and Bezuijen (1992). The median grain diameter of the sand in their tests was 0.2 mm and the angle of repose without seepage for this sand = 37^0. The data of their experiments are reproduced in Fig. 4.6, together with the continuum mode and the single-particle mode. Eq. (4.20) with the critical seepage hydraulic gradient = 0.8 is superimposed in the figure for comparison. Fig. 4.6 shows that the curves of the continuum mode and the single-particle mode meet at the zero-seepage point, with the present Eq. (4.20) lying in between. The results clearly reveal that the experimental data of van Rhee and Bezuijen (1992) fit Eq. (4.20) fairly well for both injection and suction.

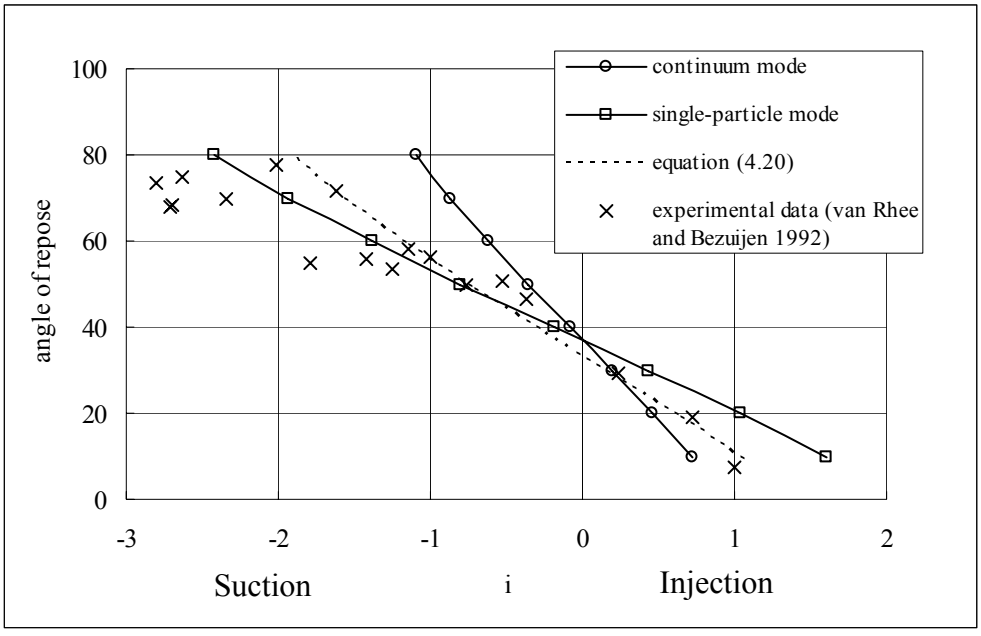

Figure 4.6 Comparison of Criteria for Critical Slope Angle with Seepage

4.6 SUMMARY

The influence of seepage on the angle of repose of uniform spherical sediments is examined in this chapter. The relationship between the hydraulic gradient and angle of repose is first established by analyzing the forces, including the seepage force, exerting on a single sphere resting on three packed spherical particles. The equation derived shows that injection reduces the angle of repose of sediments, whereas suction does the opposite.

To relate the hydraulic gradient to the seepage velocity for the porous medium consisting of coarse sediment particles, parameters of the exponential function are first determined experimentally. The empirical relationship is applied to another series of experiments in which the influence of seepage on the angle of repose is investigated. All experimental data reasonably support the theoretical equation derived for the angle of repose with seepage, when the coefficient in the equation is slightly modified to account for sediment shape and uniformity effects.

This chapter also draws a comparison between the theoretically derived equation in this study and the experimental results of van Rhee and Bezuijen (1992). It clearly shows that the equation in this study can describe both the injection effect on the critical slope angle, similar to the continuum mode, and the suction effect, similar to the single-particle mode.

CHAPTER 5

SEEPAGE INFLUENCE ON DUNE GEOMETRY

5.1 INTRODUCTION

The formation of bed features such as dunes in unidirectional current is a common phenomenon that gives rise to diverse practical problems. This is because resistance to flow in such a condition can be an order of magnitude larger than flat bed conditions. The magnitude of flow resistance on a dune bed is not only dependent on flow and sediment characteristics, but also on dune dimensions. Owing to the dominance of bedform resistance, the prediction of bedform geometry is essential for estimating flow resistance and the rate of sediment transport in rivers. Extensive studies on dunes and ripples in alluvial channels have been undertaken

with varying degrees of success, but their scope has often been restricted to impermeable boundaries. Significant early contributions were made by Kennedy (1963), who analyzed potential flow over sinusoidal bedforms; and Yalin (1977a) who developed dune height relations as functions of bed shear stress and other variables.

Although the magnitude of natural seepage flow is often small in relation to the total flow, the effect produced by it can be significant on sediment transport (Willets and Drossos 1975; Cheng and Chiew 1999), the stability of bed and bank (Shen 1971), and turbulence characteristics (Nezu 1977; Cheng and Chiew 1998a; Chen and Chiew 2004b). A thorough literature search shows that very few studies have been conducted to date to investigate the influence of seepage on bedform geometry. The principle objective of the present study is to develop certain concepts with sufficient experimental verification on how seepage affects dune geometry.

In this chapter, a brief description of experimental procedure used in Series-C experiments is followed by a detailed description of experimental results which include the distance-growth of lee-side slope and height of dunes along the seepage zone, the modification of dune geometry caused by seepage flow; the variation of propagating celerity of dunes with seepage. After that, the implication of sediment transport is analyzed.

5.2 EXPERIMENTAL PROCEDURE

The principal objective of the experiments in Series-C is to investigate the influence of both injection and suction on the dune geometry. The experimental setup and apparatus for the test have already been outlined in Chapter 3. Herein, only the procedures applied in this series are presented and the experimental flow parameters are illustrated in this section. In Series-C, Only the sediment with $D_{50} = 0.9mm$ is used as test material.

Series-C experiments are performed in the 30-meter-long open-channel flume. The experimental procedures applied are summarized as follows:

(1) Before each run is started, the sand bed, including the seepage zone, is first leveled to the elevation of the neighbouring impermeable bed, but not packed;

(2) The inlet discharge is then slowly introduced and gradually increased to the predetermined value. By adjusting the tailgate, a suitable value of the water depth is obtained so that dunes are dominant in the flume;

(3) Once the predetermined main flow state is obtained, the required seepage flow, either suction, injection or no-seepage is introduced. During the experiment, the transport of sediment in the flume is kept in equilibrium using the sand pump to recirculate the sediment particles. It is necessary to run the flume for a long period of time, say at least 4 hours, in order to permit the stabilization of flow and the formation and development of dunes in the flume;

(4) After reaching the steady state, the height of dunes is measured using the electronic bed profiler along the seepage zone. In the measurement, it is necessary to trace each dune as it propagates from upstream to downstream of

the seepage zone because the dimension of dune changes continuously through the seepage zone until reaching its equilibrium state. In other words, the heights of dunes at numerous locations upstream and downstream of, and in the seepage zone are documented. For each run, at least 10 dunes past the seepage zone are investigated to obtain the mean value so that the dune geometrical dimensions can be quantified in statistical terms;

(5) Also the propagating celerity of dunes is measured by the use of a stopwatch and a common scale. Similar principles in the measurement of dune geometry are adopted;

(6) The water depth at the test section is measured from the water surface to the mean bed level using a depth gauge at the center of seepage gallery;

(7) This procedure is repeated for different original water depths and various seepage rates including the no-seepage condition. Altogether, a total of 14 runs are documented in this study.

Table 5.1 summarizes the flow variables of all the experiments conducted in Series-C. In the table, the seepage discharge, q_s, is taken as positive for injection and negative for suction; Q is the main flow discharge; h_0 is the water depth without seepage, and is measured from the water surface to the mean bed level; h is the water depth with seepage at the centerline of seepage zone; D_{50} is the median grain diameter of the bed sediments used in the experiment; and x is the distance measured from the leading edge of the seepage zone and is taken as negative for distances upstream of the leading edge.

Table 5.1 Summary of Experimental Data

Run No	Q (L/s)	q_s (L/s)	h_0 (cm)	h (cm)	D_{50} (cm)	x (cm)
1	80	-1.21	23.4	23.5	0.09	-70~250
2	80	-2.83	23.4	23.2	0.09	-70~250
3	80	-4.01	23.4	23.0	0.09	-70~250
4	80	0	23.4	23.4	0.09	-70~250
5	80	2.61	23.4	23.9	0.09	-70~250
6	80	3.52	23.4	24.5	0.09	-70~250
7	80	4.39	23.4	25.0	0.09	-70~250
8	80	-0.87	18.6	18.3	0.09	-70~250
9	80	-2.01	18.6	18.7	0.09	-70~250
10	80	-2.56	18.6	18.2	0.09	-70~250
11	80	0	18.6	18.6	0.09	-70~250
12	80	2.57	18.6	19.1	0.09	-70~250
13	80	3.47	18.6	19.7	0.09	-70~250
14	80	4.47	18.6	20.4	0.09	-70~250

5.3 EXPERIMENTAL RESULTS AND ANALYSIS

5.3.1 Distance-Growth of Dune

When a dune moves into the seepage zone, its shape changes due to the seepage force. This eventually leads to the formation of an equilibrium shape for a given seepage rate if the seepage gallery is long enough. To investigate the seepage effect on the shape of dunes, it is necessary to compare the equilibrium data related to dune geometry between in the case of seepage and in the case of non-seepage. To this end, the results on the distance-growth of dune geometry along the seepage gallery are first proposed.

If x = 0 and x = L = 2 m represent the beginning and end of the seepage zone, the growth of the lee-side slope α_x with suction and injection is shown in Figs. 5.1(a) and 5.1(b), respectively; where α_x and α is the developing and developed lee-side slope of the dune, respectively. Similarly, the development of the dune height H_x along the seepage zone is shown in Figs. 5.2(a) and 5.2(b), where H_x and H is the developing and developed height of the dune, respectively.

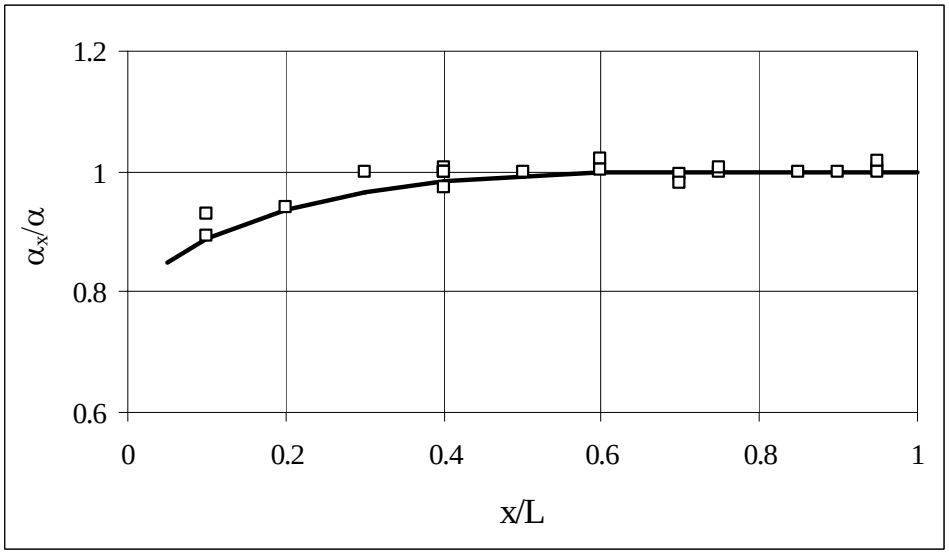

Figure 5.1(a) Development of Lee-side Slope of a Dune with Suction

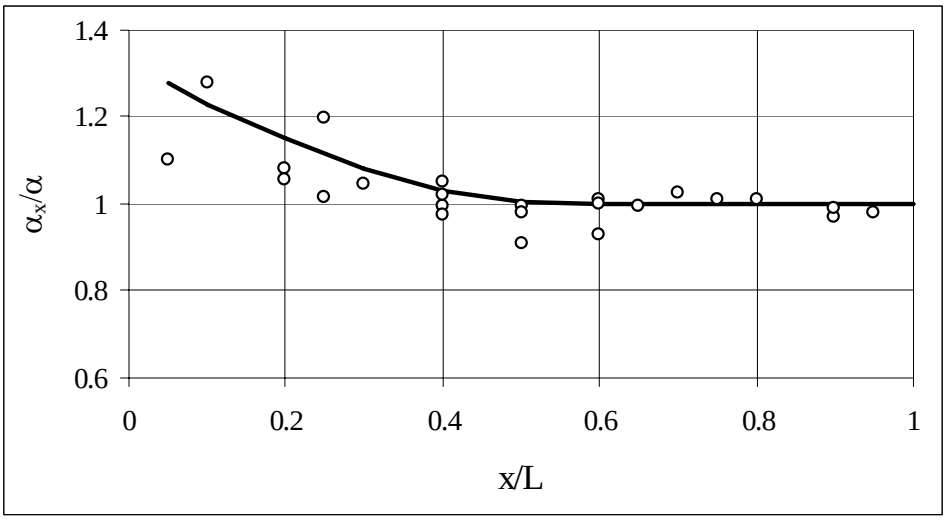

Figure 5.1(b) Development of Lee-side Slope of a Dune with Injection

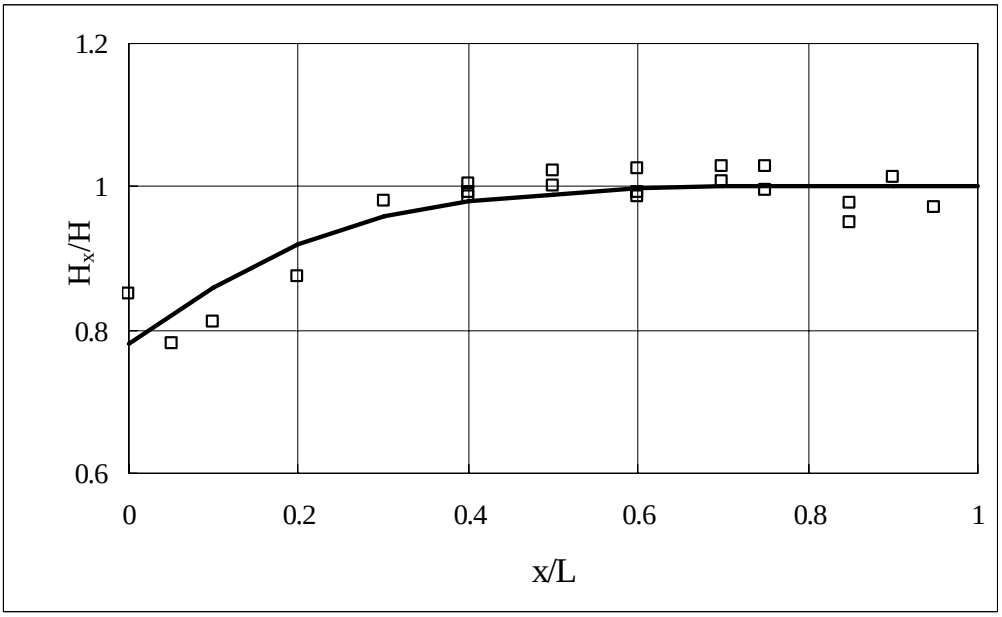

Figure 5.2(a) Development of Dune Height with Suction

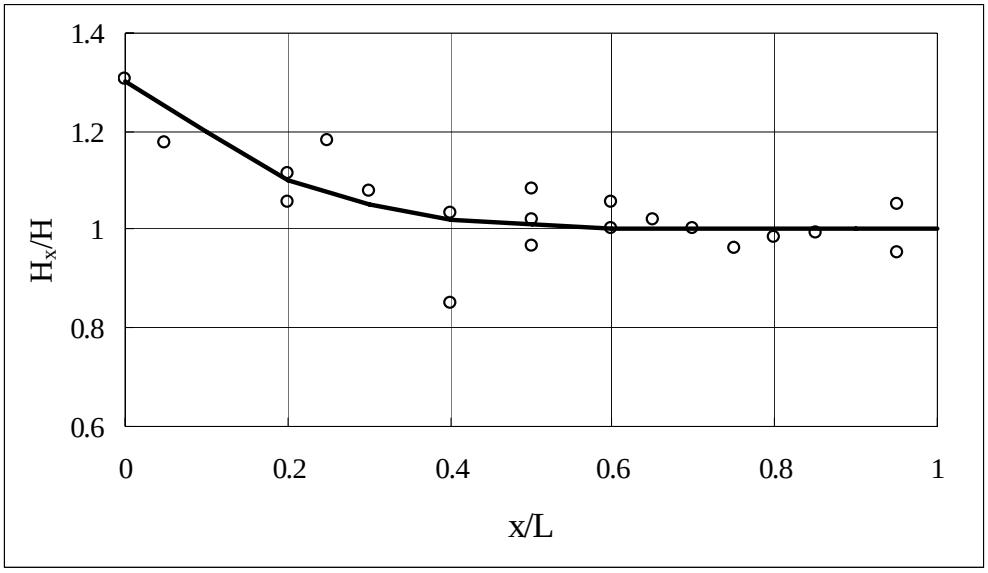

Figure 5.2(b) Development of Dune Height with Injection

The curves in Figs 5.1 and 5.2 show that the seepage zone is long enough for the dunes to reach their fully developed stage for given seepage rates. In subsequent analyses of the effect of seepage on dune height, only the equilibrium dune data, i.e., the fully developed lee-side slopes of dunes, α and fully developed height H, with the corresponding seepage rates, are used.

5.3.2 Seepage Influence on Lee-Side Slope of Dune

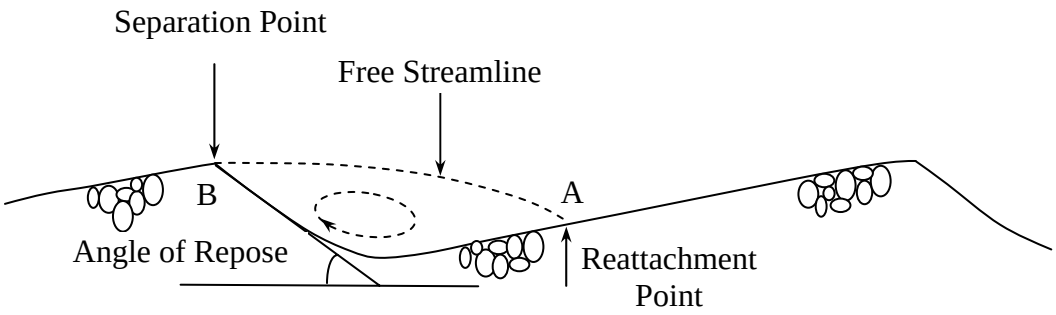

Figure 5.3 Schematic Sketch of a Dune

The distinguishing features of dunes are generally characterized by a slightly curved upstream surface and a downstream slope approximately equal to the angle of repose of the sediment making up the dune (see Fig. 5.3). The abrupt change in the surface gradient at the crest causes the flow to separate and to form an eddy in the

lee of the bedform. The eddy has an important influence on shaping the dune profile, especially on the lee-side slope. Under the combined effects of both the flow and the eddy, the lee-side slope is approximately equal to the angle of repose of the sediment particles. Moreover, the experimental data associated with the lee-side slope of dunes indicates that the lee-side slope of dunes becomes steeper or gentler due to suction or injection, respectively. The same tendency has been found in the angel of repose when seepage is introduced in the former chapter. Therefore, it is reasonable to assume that in the case of seepage the stable lee-side slope of a dune inclines at the angle of repose with the same seepage rate, i.e., Eq. (4.20) derived in Chapter 4 is a reasonable approximation for the lee-side slope of dunes in the presence of seepage.

With these considerations in mind, the curve characterizing Eq. (4.20) is re-plotted in Fig. 5.4 and the experimental data, associated with the fully developed lee-side slope of dunes, are produced in the same figure. For a better comparison of the results of the lee-side slope with those of the angle of repose, the data from Series-B are also presented in this figure. It is clear that all experimental data fit well with Eq. (4.20); this indicates that the presence of seepage has a similar influence on the lee-side slope of dunes as that on the angle of repose of the sediments.

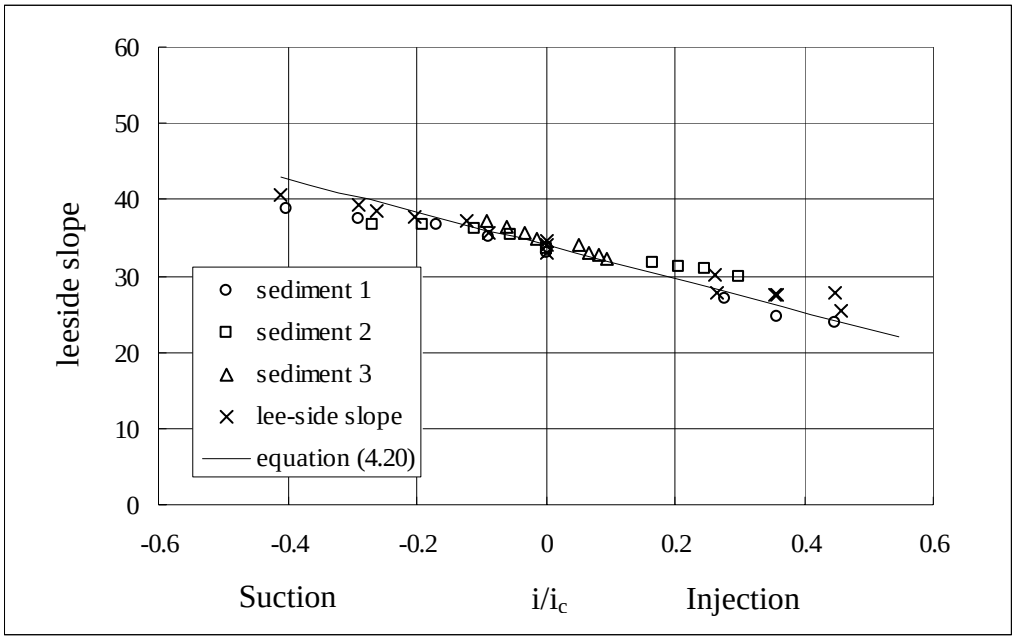

Figure 5.4 Seepage Influence on Lee-Side Slope of Dunes

5.3.3 Seepage Effect on Dune Height

With regard to the seepage effects on the height of a dune, the experimental data of the ratio of the developed dune height to water depth h are plotted against the dimensionless seepage hydraulic gradient in Fig. 5.5, where h_0 is the water depth without seepage. It shows that the height of the dune is reduced when injection is present; while suction increases it.

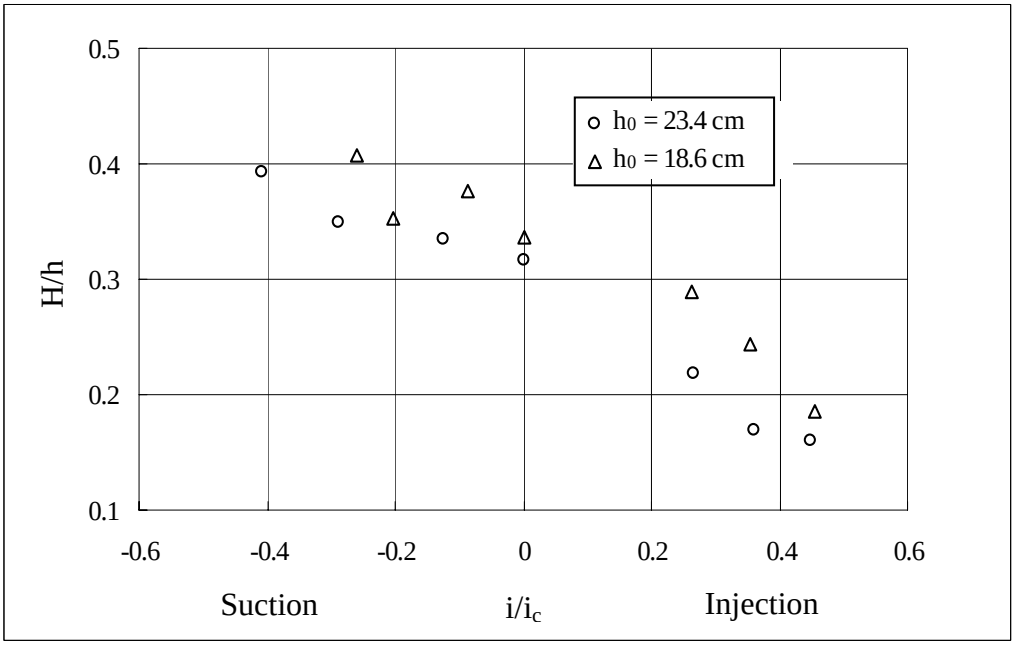

Figure 5.5 Seepage Effects on Dune Height with Undisturbed Flow Depth as the Third Variable

The data reveal that the relative dune height, H/h, is also affected by initial water depth without seepage, h_0. Fig. 5.5 shows that the data points corresponding to the two different values of h_0 used in the study tend to form their own curves. In fact, under the condition of different upstream water depths, one may get dunes with different heights in the case of no-seepage. Considering this, the effect of water depth without seepage may be incorporated in the undisturbed dune height without seepage, H_0 by using H_0 as the normalizing variable. Fig. 5.6, presents the results of this endeavor, clearly shows that the data collapse well to form one unique curve.

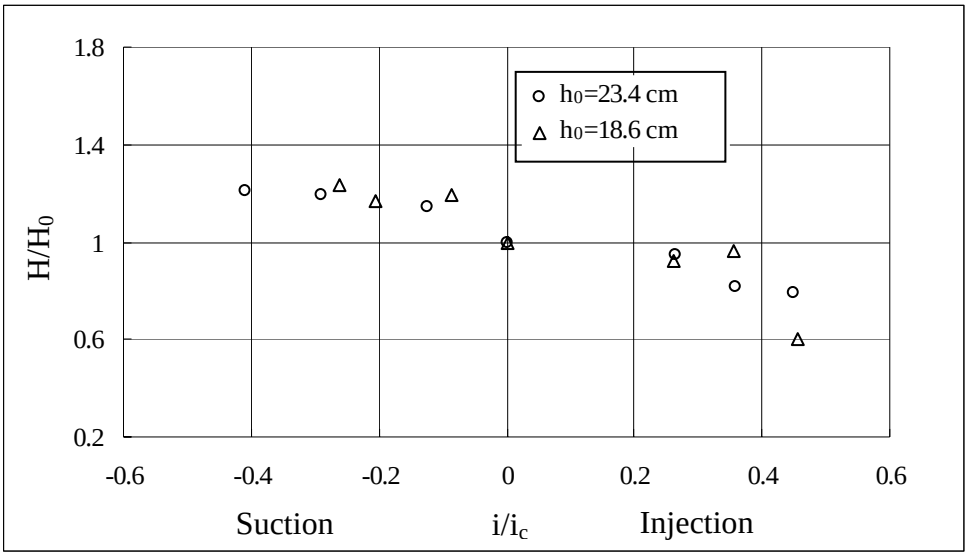

Figure 5.6 Collapsed Plot of Variation of Dune Height with Seepage

5.3.4 Assessment of Minimum Length of Seepage Zone

Figs. 5.1 and 5.2 depict the growth of dunes along the seepage zone. The data clearly show that the dunes may not reach their fully developed stage if the seepage zone is not long enough. In other words, a certain length of the seepage zone is necessary to ensure the equilibrium height and lee-side slope of the dune are achieved for a given seepage rate. However, one cannot determine the length of the seepage zone required for the dunes to reach their equilibrium state using the figures plotted previously. To overcome this limitation, the data associated with the distance-growth of dunes along the seepage zone are re-plotted in Figs. 5.7(a) and

(b) in which the distance, x is normalized with the height of the fully developed dunes instead of the total length of the seepage zone used in the experiment.

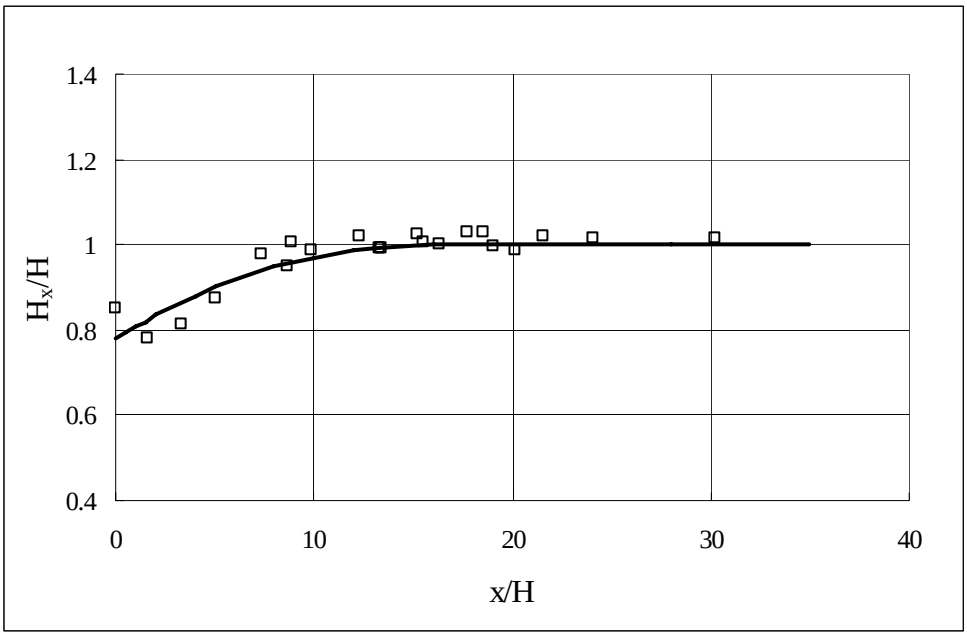

Figure 5.7(a) Development Length of Dune Height under the Influence of Suction

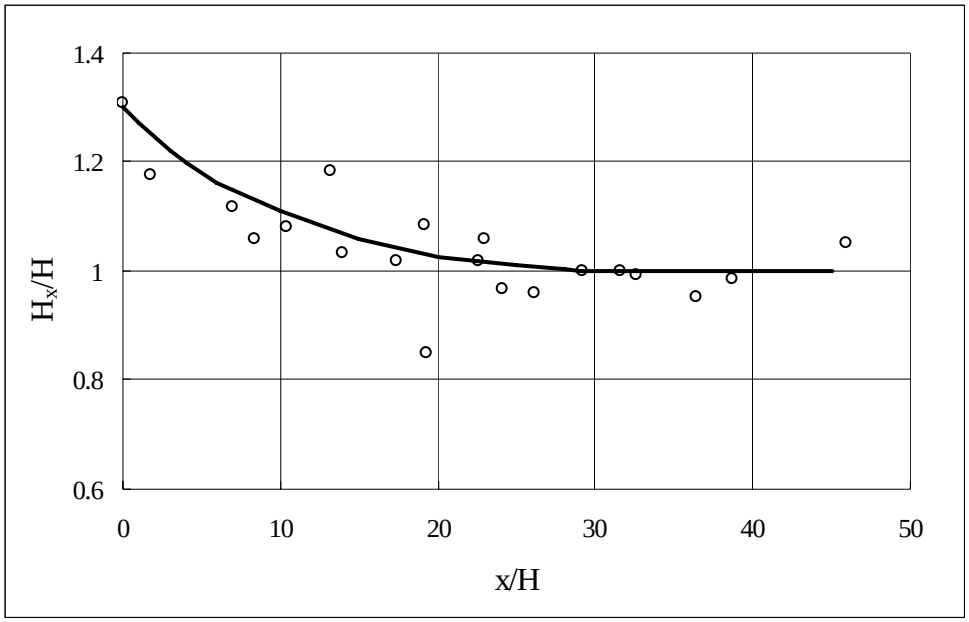

Figure 5.7(b) Development Length of Dune Height under the Influence of Injection

Figs. 5.7(a) and (b) show that the length needed to reach the fully developed stage for suction and injection is approximately 20 and 30 times the height of the fully developed dunes for a given seepage rate, respectively. Since the distance-growth of the lee-side slope of dunes in the seepage zone is almost the same as that of the dune height (see Figs. 5.1 and 5.2), the minimal length of the seepage zone for the lee-side slope growth is identical with that for the dune height growth for both injection and suction.

5.3.5 Seepage Effect on Dune Wavelength

It is necessary to state at the outset that under the flow conditions used in this study, the wavelength of dunes formed in the flume is fairly long with a typical value of approximately 1.4m. However, the length of the seepage gallery of the flume is only 2 m. Because of the limitation of the experimental apparatus, it may not be appropriate to categorically conclude that the seepage zone is long enough for the wavelength to reach its equilibrium value. Although no equilibrium data can be obtained from the experiments, it is observed that suction appears to increase the wavelength of dunes; whereas injection does the opposite. An increase of up to approximately 30% and a reduction of up to approximately 20% in the dune length is observed for suction and injection, respectively.

A plausible explanation is related to changes of the dune celerity. Experimental data show that a dune moves faster or slower when it propagates into the seepage zone subjected to suction and injection, respectively, which will be explored in the next section. Fig. 5.8 shows the data on seepage effects on dune celerity; the celerity refers to the speed of a point on the dune crest. However, the succeeding dune, which lies outside the seepage zone, still moves at the undisturbed celerity. Thus, the distance between the two dunes tends to be larger or smaller, which results in an elongation or shortening of the dune length depending on the direction of the seepage flow. However, when all of dunes in the flume are subjected to the effect of seepage, the dune length may experience a process of re-adjustment, which leads to the formation of the equilibrium state. In this study unlike those presented for the height and lee-side slope of dunes, the distance-growth of the dune length

along the seepage zone is not available because of the limitation of the apparatus. Additional tests with a longer seepage zone are needed to confirm the above hypothesis.

5.3.6 Seepage Effect on Dune Celerity

Depending on its geometry and the flow properties, a dune propagates at a certain celerity, c_e. The practical importance of knowing the magnitude of c_e is because it, in combination with the dune height and the specific weight of the bed sediment determines the transport rate. When a dune moves into the seepage zone, not only its geometry is modified, its celerity is also changed depending on the seepage flow direction. The data on the dune celerity measured upstream of, downstream of and over the seepage zone are plotted in Fig. 5.8 for both suction and injection.

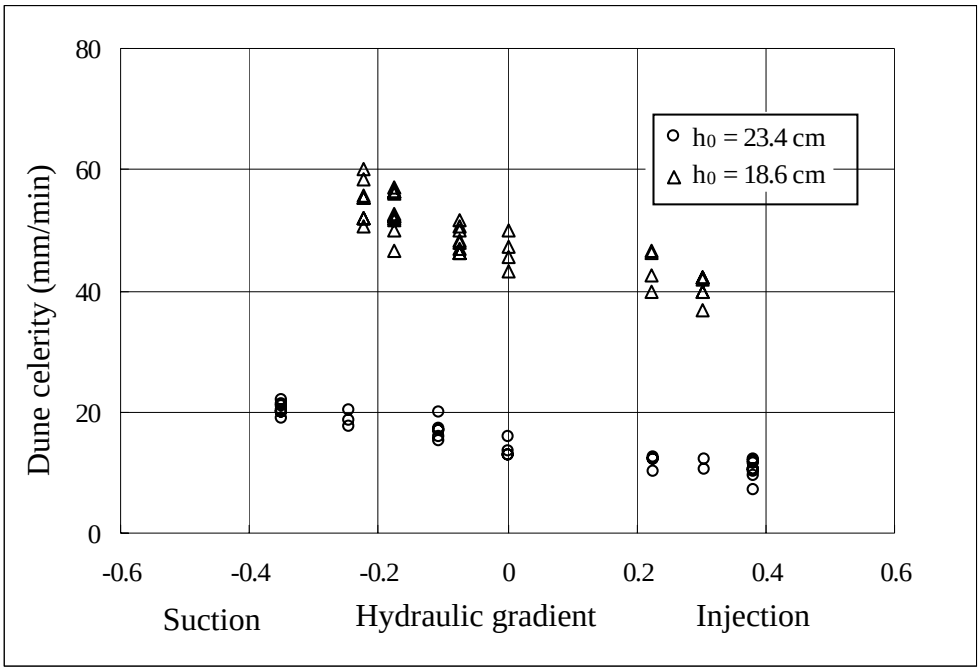

Figure 5.8 Seepage Effects on Dune Celerity

Fig. 5.8 clearly shows that seepage can significantly affect the propagating celerity of dunes: injection decreases while suction increases its magnitude. Since the data include the developing and developed dunes, the points plotted are understandably scattered. Moreover, the points corresponding to different values of h_0 tend to form their own curves. This is not surprising because the dune height, which has a close relationship with h_0, is a dominant parameter in affecting dune celerity.

To better understand this mechanism, the relation between dune celerity and the flow parameter is discussed below. It must first be stated that no agreement has yet been reached, even for the case of no-seepage, on the determination of the value of

c_e. Thus, the present analysis on c_e with seepage is preliminary. To begin with, let us consider the following empirical formula presented in Wuhan University (1961):

$$\frac{c_e}{U} = 0.0144\frac{U^2}{gh_0} \tag{5.1}$$

where U = average velocity of the flow. This formula shows that the dune celerity is in proportion to the average velocity of the flow cubed, which is somewhat consistent with the results of Thomas (1967), although the latter has a more complicated form as:

$$\log\frac{c_e}{U} = 3.342\log\frac{u_* D}{\nu} - A \tag{5.2}$$

in which, u_* = shear velocity; A is a function of water surface slope, J.

In Chapter 6, the average velocity of the flow over a dune-bed is shown to increase and decrease with suction and injection, respectively. In the light of Eq. (5.1) or (5.2), one may infer that dune celerity will correspondingly increase with suction and decrease with injection, which is in agreement with the experimental data in Fig. 5.8.

5.4 IMPLICATION ON SEDIMENT TRANSPORT

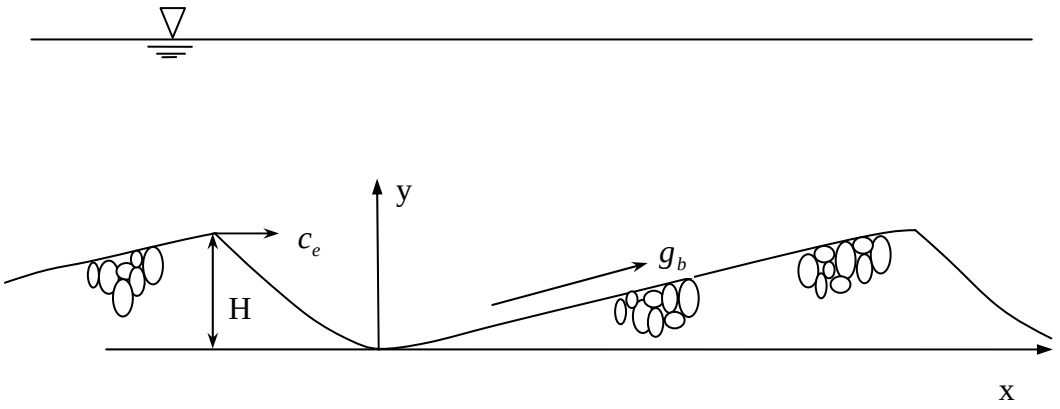

Figure 5.9 Definition Sketch of Sediment Transport over Dunes

Dunes move downstream owing to erosion at their stoss face and deposition on their lee face. If the trough of the dune is used as the datum, the differential equation governing bed-load transport rate for a dune bed (see Fig. 5.9) may be written as

$$\frac{\partial g_b}{\partial x} + \gamma_b \frac{\partial y}{\partial t} = 0 \tag{5.3}$$

where y = elevation of the sand dune boundary above a horizontal datum; x = distance parallel to the direction of flow; t = time; g_b = bed-load discharge per unit width per unit of time; and γ_b = specific weight of bed sediment. Note that in a steady state, one gets

$$\frac{\partial y}{\partial t} + c_e \frac{\partial y}{\partial x} = 0 \tag{5.4}$$

Substituting this expression into Eq. (5.3) leads to

$$\frac{\partial g_b}{\partial x} = \gamma_b c_e \frac{\partial y}{\partial x} \tag{5.5}$$

By integrating Eq. (5.5), one gets,

$$g_b = \gamma_b c_e y + g_0 \tag{5.6}$$

in which g_0 = constant of integration. Assuming that the dunes have triangular shapes, one gets the equation for the average bed-load transport rate between the crests of two adjacent dunes:

$$\overline{g_b} = 0.5\gamma_b H c_e + g_0 \tag{5.7}$$

where $\overline{g_b}$ = average bed-load transport rate between the crests of two neighbouring dunes. g_0 may be interpreted as part of the bed-load which does not contribute to the propagation of dunes. Thus, it may be ignored because it is significantly smaller when compared to the term $0.5\gamma_b H c_e$ (Chien and Wan 1998). Considering this, the final equation for the average bed-load transport rate becomes:

$$\overline{g_b} = 0.5\gamma_b H c_e \tag{5.8}$$

Eq. (5.8) may be used to compute the bed-load transport rate when the average velocities and heights of dunes are known. Moreover, for a shallow flow over a dune bed consisting of coarse material where suspension is negligible, the total sediment transport may be estimated from this formula.

As illustrated in Section 5.3, both the dune celerity and dune height tend to increase with the introduction of suction; whereas the presence of injection leads to smaller values of celerity and height when compared with the no-seepage condition. It can easily be deduced that the average bed-load transport rate defined by Eq. (5.8) becomes larger in the case of suction and vice versa for injection. The modification

of the bed-load transport rate caused by suction can also be inferred from the measurement of bed shear stress which is discussed in Chapter 6. The bed-load transport rate is found to increase with suction, which is consistent with the finding in this chapter. It is worthwhile noting that these results agree with the findings of some investigators on a flat bed: suction increases sediment transport rate (Willetts and Drossos 1975), while injection inhibits the motion of bed particles (Watters and Rao 1971).

5.5 SUMMARY

Detailed investigations on the influence of seepage on dune dimensions are presented in this chapter. The relationship between the hydraulic gradient and angle of repose derived in Chapter 4 is reasonably adopted for prediction of seepage effects on the lee-side slope of dunes. Laboratory data generally support the assumption that seepage effects on the lee-side slope of dunes are the same as that on the angle of repose of sediments. It shows that the slope is reduced when injection is present; while suction increases the slope.

This chapter also explores seepage effects on the development of dune height. The results show that suction increases the equilibrium height of dunes by up to 25%, and injection reduces it by 50%. Although quantitative results on seepage effects on dune lengths cannot be accurately determined due to the limitation of the length

of the test section in the flume, it may be inferred from observation that suction and injection may increase and decrease dune length by approximately 30% and 20%, respectively.

Finally, the response of dune celerity to seepage is also discussed in this chapter. The results show dune celerity increases with suction and decreases with injection. By considering how dune height and celerity are affected by seepage, one may infer that the bed-load transport rate can be significantly modified by seepage.

CHAPTER 6

RESPONSE OF TURBULENT FLOW OVER DUNES TO BED SUCTION

6.1 INTRODUCTION

An erodible sediment bed usually becomes unstable when acted upon by turbulent flow that is capable of initiating bed particle movement. Under this condition, it tends to deform into a variety of configurations, such as ripples and dunes. These features typically have gentle, gradually varying stoss slopes and steep leeside slopes that cause flow separating, creating complex interactions between the flow, bed geometry and sediments. General observations and theoretical considerations show that these large scale bedforms not only make a key contribution to the overall flow resistance, but also significantly influence sediment transport rates in natural

alluvial channels. Because of the importance of dunes, many studies have been conducted to investigate the relationship between flow characteristics and bedform geometry. The characteristics of turbulent flows over dunes have great significance in solving a variety of hydraulic problems; e.g., estimations of flow depth, boundary shear stress, sediment transport rate, etc.

Flow over dunes is well known as a complex flow (Mendoza and Shen 1990) and classically can be described, in the time-average sense, as a separation at the crest and a reattachment in the trough of the bedform, producing recirculation in between. In the divergent zone a wake-like region (shaded region in Fig. 6.1) that extends downstream is formed. Downstream of the reattachment point an internal boundary layer starts to grow within the wake region. In the outer, near-surface region a typical potential-flow overlays the wake, resembling the outer flow of turbulent open channel flow over a flat bed. Fig. 6.1 shows the dominant features of flows over a dune.

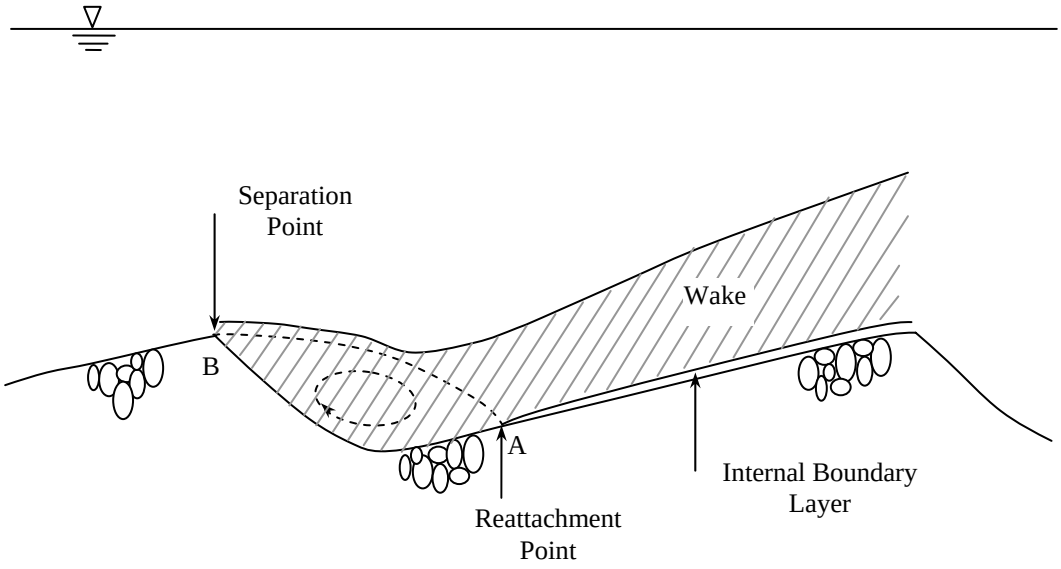

Figure 6.1 Schematic Sketch of Flow over a Dune

Various detailed experimental studies of the fluid flows over dunes have been reported in the literature. Since backward-facing step flows and dune flows share most, although not all, common features, the former has been used as a model of the latter and has been intensively studied. Deserving of mention is the investigations by Raudkivi (1963), Nakagawa and Nezu (1987), Adams and Eaton (1988), Lyn (1993), Nelson et al. (1993), and Bennett and Best (1995). To better understand ripple formation, Raudkivi (1963) conducted some measurements on a backward-facing step flow by using of a hot-film anemometer. However, the hot-film technique is not deemed adequate to measure the turbulence characteristics of reverse flows which are dominant in dune flows or backward-facing step flows. More recently, with the aid of Laser Doppler anemometer (LDA) accurate measurements of backward-facing step flow in an open channel were conducted by Nakagawa and Nezu (1987), and later Adams and Eaton (1988). The mean velocity

and turbulence characteristics were explored in detail. In practice, the mean velocity is not the true time average but calculated arithmetically by summing the velocities of all valid particles and dividing it by the number of particles as defined in Eqs. (3.2) and (3.3); this produces a velocity bias. Adams and Eaton (1988) examined the effect of velocity bias and concluded that such a bias was negligible; therefore no correction in the separated step flow was necessary. To highlight the effect of bed geometry on the turbulence characteristics, two types of artificial periodic bedforms (one of which was unrealistic in having the same sharp slope on both the upstream and downstream face) were investigated by Lyn (1993). Lyn also examined the effect of bed geometry on the wake coefficient. The experiments conducted by Nelson et al. (1993) showed that there was a significant interaction not only between the internal boundary layer and the wake, but also between the topographically induced acceleration and turbulence.

By measuring the downstream and vertical components of velocity in dune flows with much higher spatial resolution, Bennett and Best (1995) presented contour maps of time-average and turbulence characteristics of the flow. Despite these studies on flows over dunes, and many others that are not mentioned in this chapter, their scope is primarily limited to a rigid, wavy and impervious bed boundary.

Seepage flow has been investigated intensively because of its importance in modifying the properties of open channel flow (see Chapter 2). As well known in the literature, seepage can have a significant influence on the near bed flow field, by transferring mass and momentum between the fluid and porous sediments such that

the streamwise velocity profiles deviate significantly from the logarithmic law (Maclean, 1991a; and Cheng and Chiew, 1998a). Moreover, the bed shear stress will increase or decrease with suction or injection (MacLean and Willetts 1986; Maclean, 1991b; Cheng and Chiew, 1998b; and Chen and Chiew, 2004a), while the turbulence intensity is respectively enhanced and reduced (Cheng and Chiew, 1998b; Nezu, 1977).

Very few studies on changes in flows over a porous dune bed have been conducted. Amongst the studies that can be found in the literature is one by Harrison (1968), who noted that the angle of the leeside slope of bedforms increased by 10^o for suction and decreased by 9^o for injection. However, as far as the author is aware, no investigation on seepage effects on bedforms has been documented in the literature.

In this chapter, the results of Series-D experiments are presented. These experiments are designed to investigate the effect of seepage on the turbulence in flows over dune. Measurements of the mean streamwise and vertical velocities, the root-mean-square value of velocity fluctuations and the Reynolds shear stress are made. The results clearly show the influence of seepage on the turbulent properties of the flow. This provides insight into the mechanisms of sediment transport with seepage. In this study, only bed suction is investigated.

6.2 EXPERIMENTAL METHODOLOGY AND PROCEDURE

Series-D is performed in the 30-m-long, 0.7-m-wide, and 0.6-m-deep open-channel flume (see Fig. 3.1) with the objective of investigating the response of turbulent flow over dunes to bed suction. Turbulence characteristics can be quantified only in statistical terms. Thus, sufficiently long period of time is needed to ensure accurate measurements of turbulent flows. However, natural bedforms propagate downstream with slow variations in their geometry; this movable boundary imposes additional difficulties and ambiguities on measurements of a flow over dunes. In order to avoid complications due to boundary uncertainties, artificial dunes, fixed in a typical natural form, are constructed in the flume. Moreover, the use of fixed dunes allows accurate measurements of turbulence with very high spatial and temporal resolution. In fact, it is reasonable to consider fixed dunes as a good approximation because the velocity of their migration c_e which was explored in Chapter 5 is very small in comparison with the stream flow velocity.

However, these artificial dunes must be chosen with care so that the typical flow conditions in the flume are identical to conditions in which such dunes are produced on a mobile bed. In the present study, a total of six artificial dunes with the same dimension, i.e., wavelength λ = 1.4 m, height H = 0.07 m, and angle of leeside slope = 30^0 (see Table 6.1) are constructed. The dimension of these dunes is determined from the test in Series-C on a mobile sediment bed in the same open-channel flume. For further simplification, triangular dune geometry (see Figs. 6.2 and 6.3) is used in the experiment. These bedforms are placed in the flume with

care so that one complete dune with porous boundary discussed in the latter section occupies the center of suction zone as shown in Fig. 6.3

Table 6.1 Summary of Experiment Conditions on Fixed and Mobile Dunes

Experimental conditions	**Mobile bed**	**Fixed bed**
Flow rate, Q, (m^3/s)	0.08	0.08
*Mean water depth, h, (m)	0.23	0.22
Dune wavelength, λ , (m)	1.10~1.55	1.40
Dune height, H, (m)	0.067~0.083	0.07
Dune steepness, H/λ	0.061~0.087	0.05
Angle of leeside slope, α	$32.4\sim33.9^0$	30^0
Dune state	Propagate downstream	Fixed on the bed
*Mean water depth was measured from mean bed level at the center of suction zone		

The procedure for the construction of the artificial dunes is as follows:

(1) Sand with the same diameter (0.9 mm) as that used in the movable bed experiment are shaped according to the geometry described in Table 6.1, but with a slightly smaller height of around 50 mm with the aid of wooden templates;

(2) Cement with a thickness of approximately 50 mm, is cast on top of the sand dunes, except for the part within the seepage zone. The cemented-dunes are molded to the desired dimension;

(3) The surface of the cement-molded sand dunes is covered with a layer comprising the same sediment particles in order to ensure the same surface roughness;

(4) The solitary dune (1.4m long) within the suction zone is not cement-coated but covered with a filter cloth, and overlaid by a stainless steel net. The filter cloth has been found to have no effect on the permeability of the sediment particles used, thus on seepage flow, through a separated permeability test. The purpose is to preserve the same porous boundary, thereby allowing suction to take place over the "un-cemented" dune. Fig. 6.2 shows the photo of the porous dune.

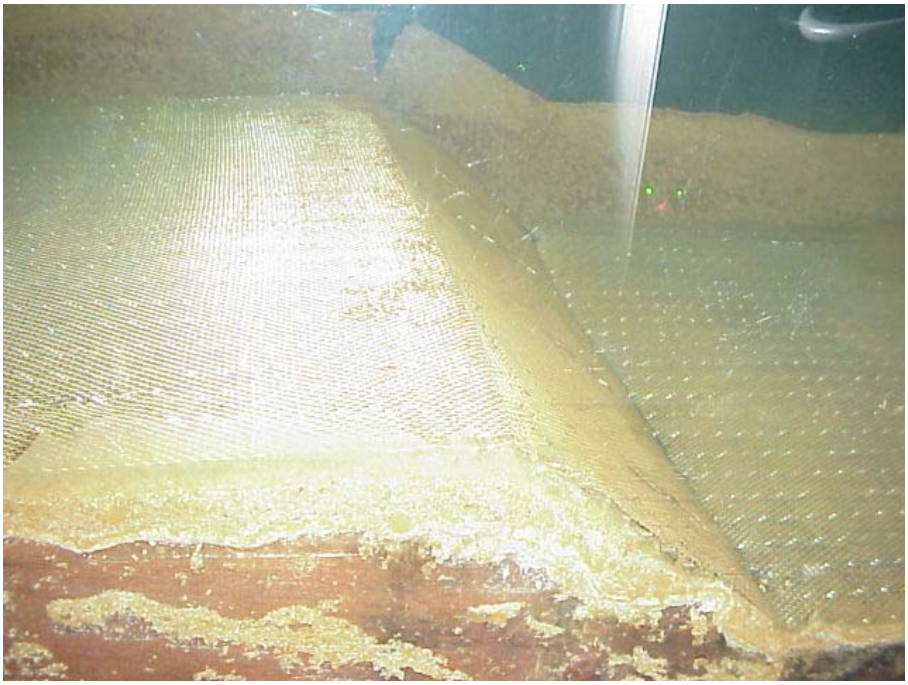

Figure 6.2 Photo of the Porous Dune

When the predetermined flow conditions, which are identical to those used in the movable bed experiments are established, velocity measurements are made at the centerline of the flume over the single dune at the center of suction zone. In order to obtain velocity distribution throughout one dune wavelength with high spatial resolution, measurements are conducted at over 3500 locations as shown in Fig. 6.3. A total of 141 vertical velocity profiles, at intervals of 0.01 m over the dune, are measured. Each profile comprises 20 to 30 points depending on the location along the dune. A Dantec two-component fiber optic Laser Doppler Anemometer (LDA) is used to measure the velocity and turbulence distribution of flow over the artificial fixed dune. A brief description on the properties of the LDA can be found in Chapter 3.

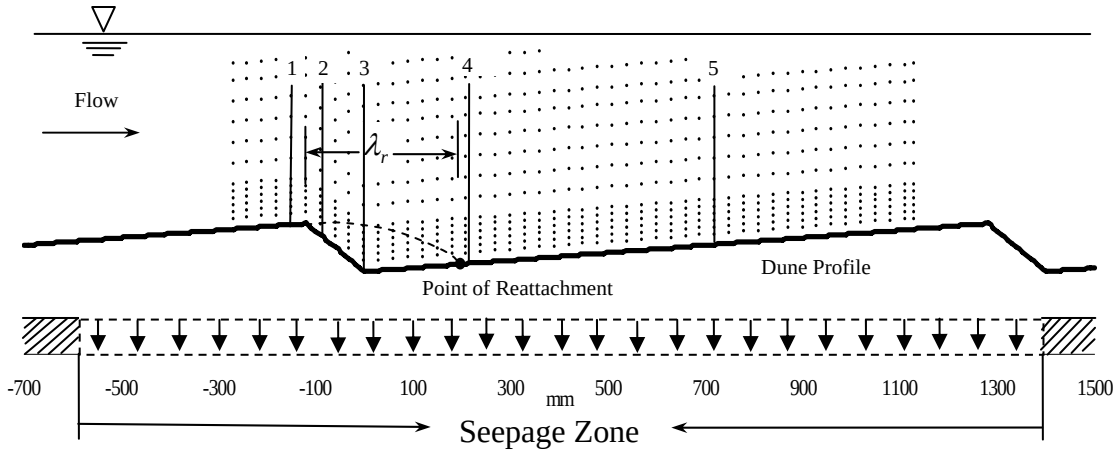

Figure 6.3 Schematic Layout of Sampling Point Distribution over the Triangular Dune

6.3 EXPERIMENTAL RESULTS AND ANALYSIS

Three sets of experimental tests are conducted under the same main flow conditions. Since the suction zone is fairly long, the reduction of the flume discharge due to flow abstraction can have a significant influence on the mean flow field if the suction rate $R = |v_s / U|$, where U = depth-average velocity; v_s = abstraction (or suction) discharge divided by the total surface area of the suction zone, exceeds 0.86% (Chen and Chiew, 2004a). The suction rates applied in the Series-D experiments are selected with care such that suction itself makes a key contribution to the variation of mean flow and turbulence rather than the reducing flow discharge i.e., the loss of mass. To this end, two different bed suction rates are used in the study with $R = 0.29\%$ and 0.45%, which corresponds to 2.4% and 3.75% of the upstream flowrate, respectively. The third test is conducted with zero suction rate.

Five sections along the single dune in the seepage zone are selected to examine the response of the mean flow field and turbulence to suction. Fig.6 3 shows the five locations, noting that the lowest point of the dune (trough) is the location of the origin, thus, the dune crest is located at x = -120 mm. The five points are located at (1) just upstream of the dune crest (x = -250 mm); (2) just downstream of the dune crest (x = -70 mm); (3) within the reverse flow (x = 0 mm); (4) just downstream of the reattachment point (x = 180 mm); (5) 550 mm downstream of the reattachment point (x = 730 mm).

6.3.1 Streamwise and Vertical Mean Velocity Distribution

The streamwise (u) mean velocity distribution for both no-seepage and suction at the five locations are shown in Figs. 6.4(a)-(e), respectively. The profiles with suction in the figures show a steeper rise in the near-bed velocities as compared to that without suction because the faster moving flow is drawn into the bed by flow abstraction. The velocity of flow near the water surface undergoes different changes when compared with that near the bed because of mass conservation although seepage has no direct influence on the outer flow. As a whole, the streamwise mean velocity profile becomes more uniform when compared to that without suction, in good agreement with the findings on turbulent open-channel flow with suction over a flat bed (Maclean, 1991b; Chen and Chiew, 2004a).

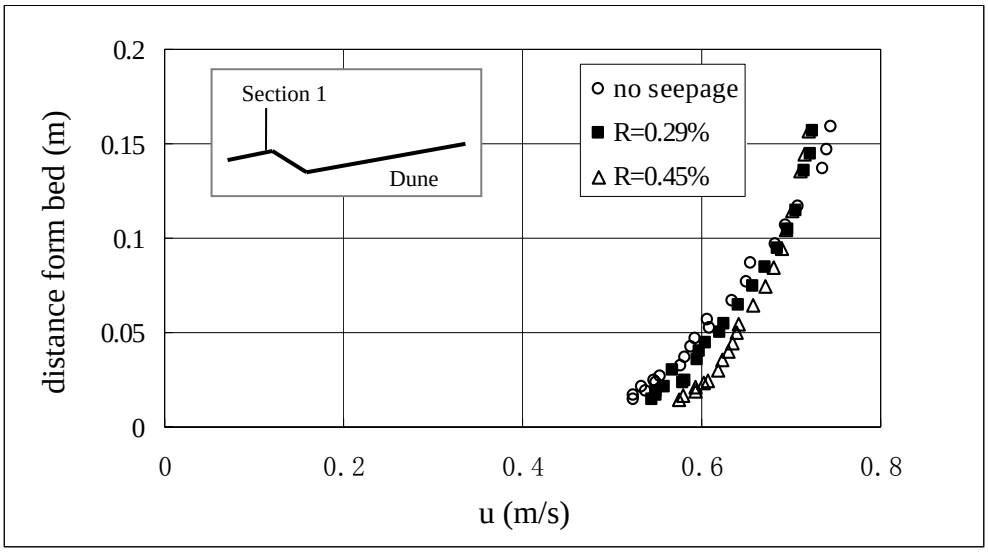

Figure 6.4(a) Comparison of Streamwise Mean Velocity with and without Suction at Section 1

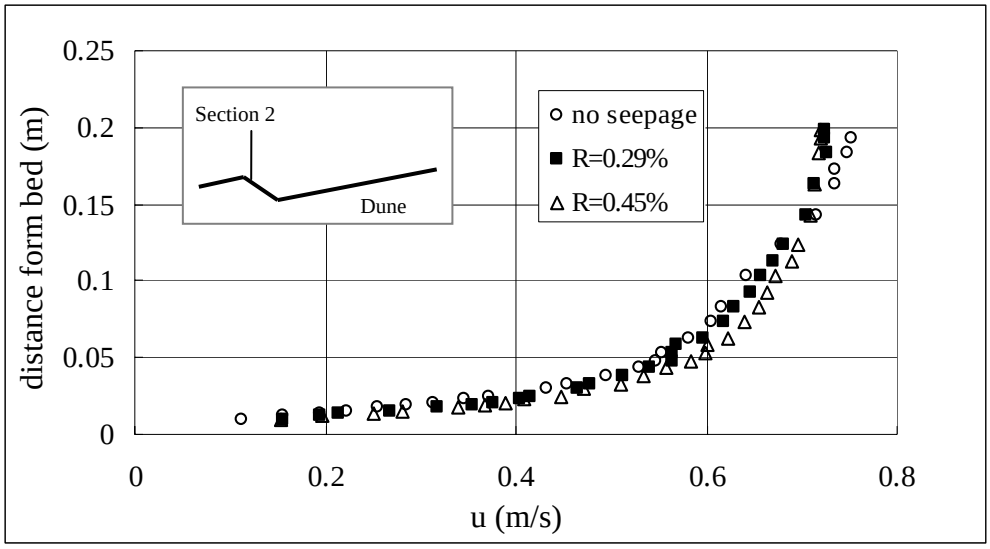

Figure 6.4(b) Comparison of Streamwise Mean Velocity with and without Suction at Section 2

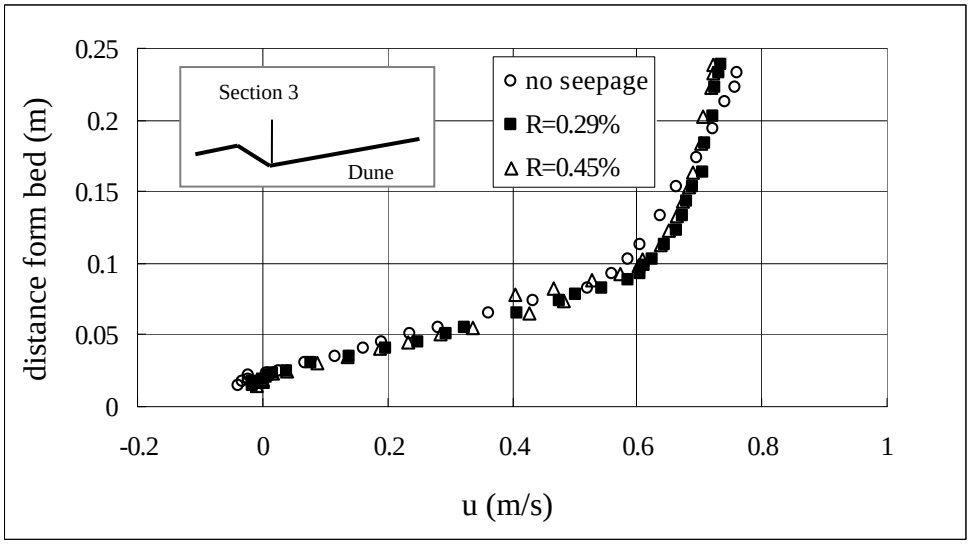

Figure 6.4(c) Comparison of Streamwise Mean Velocity with and without Suction at Section 3

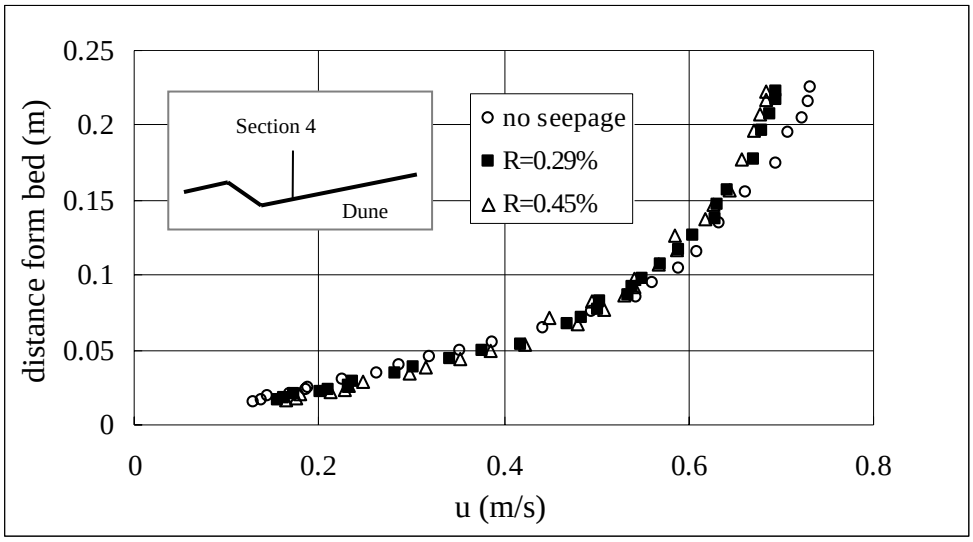

Figure 6.4(d) Comparison of Streamwise Mean Velocity with and without Suction at Section 4

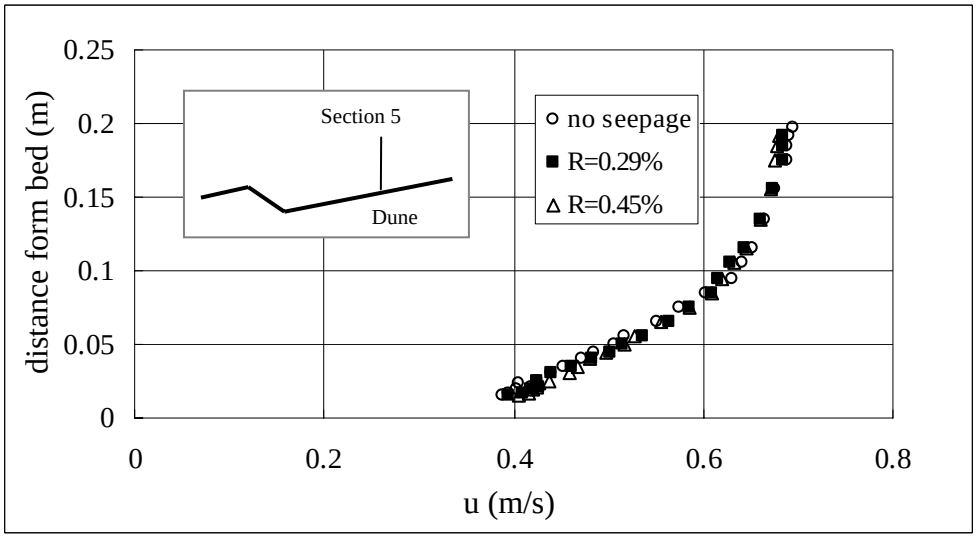

Figure 6.4(e) Comparison of Streamwise Mean Velocity with and without Suction at Section 5

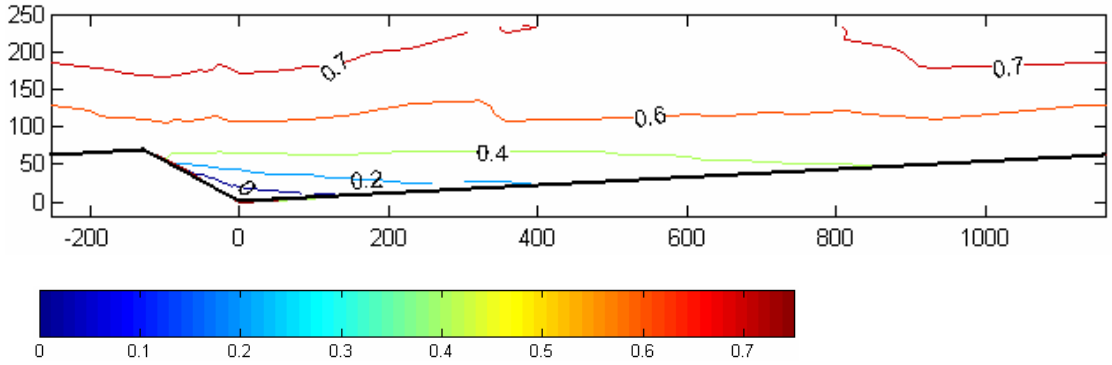

Figure 6.4(f) Contour of Streamwise Mean Velocities without Seepage

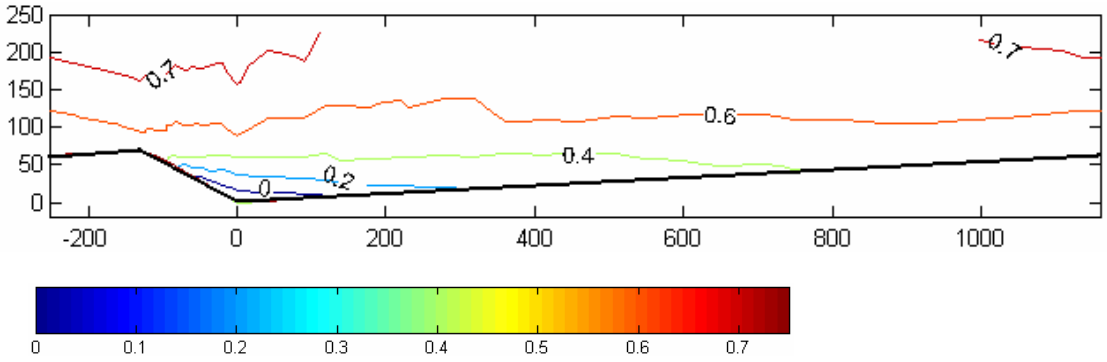

Figure 6.4(g) Contour of Streamwise Mean Velocities with Suction (R=0.29%)

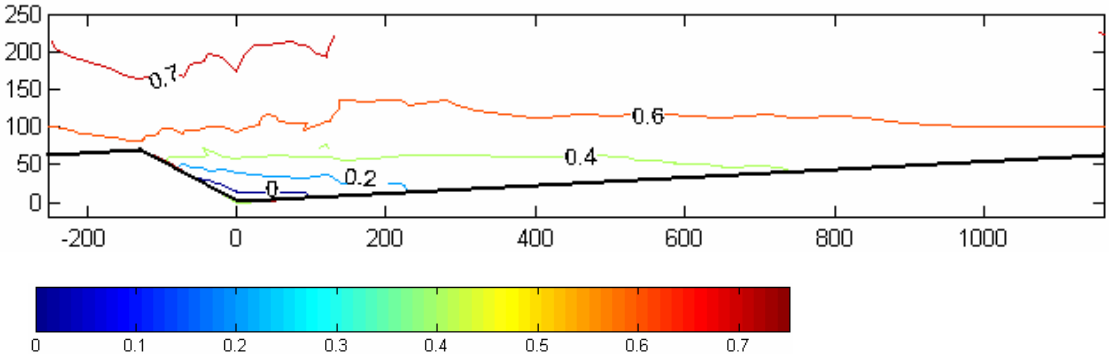

Figure 6.4(h) Contour of Streamwise Mean Velocities with Suction (R=0.45%)

A comparison of the velocity profiles in Figs. 6.4(a)-(e) reveals insignificant variation of velocities at the Section (3) as compared with that at other sections. This difference is discussed in a latter section. As indicated in contours of the streamwise mean velocities with and without suction shown in Figs. 6.4(f), (g), and (h), the general pattern shows little change although significant modifications can be observed near the bed. Taking the contour line at u = 0.2 m/s as an example, it adheres to the bed earlier (farther upstream) with increasing of suction rates, showing that the local velocities are accelerated by suction.

In open channel flow with a flat bed, the magnitude of the vertical component of velocity is generally very small, rendering accurate measurement difficult. For this reason, comparatively less work has been done in this area. Neither Nezu (1977) nor Cheng and Chiew (1998b) reported information on vertical velocity in their experimental studies conducted on a flat bed. In the case of a dune-bed, the magnitude of vertical velocities is large enough, due to topographic effect, to be measured with higher accuracy.

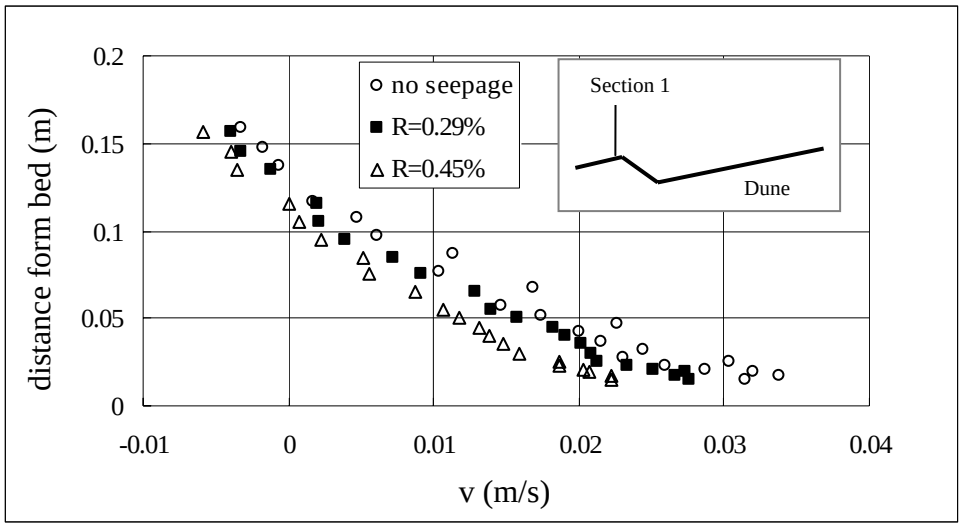

Figure 6.5(a) Comparison of Vertical Mean Velocity with and without Suction at Section 1

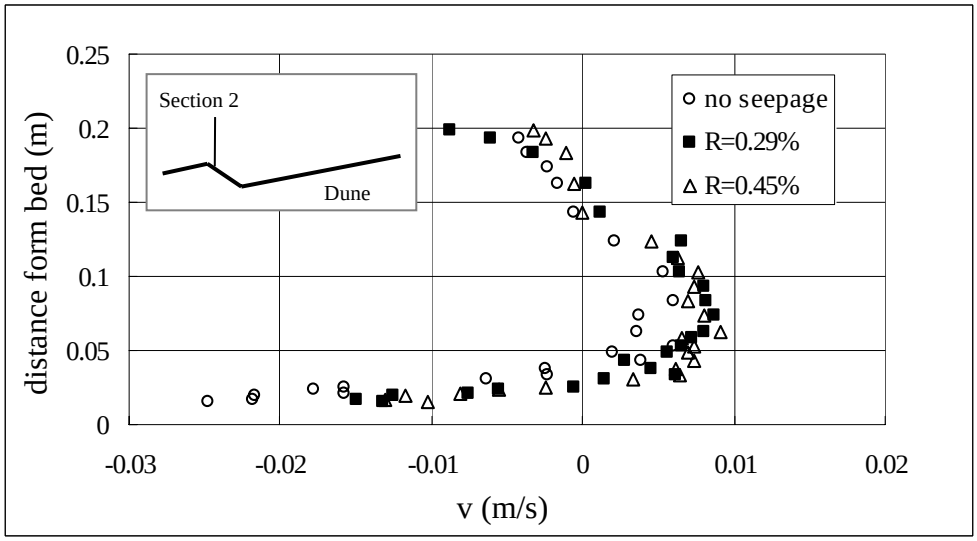

Figure 6.5(b) Comparison of Vertical Mean Velocity with and without Suction at Section 2

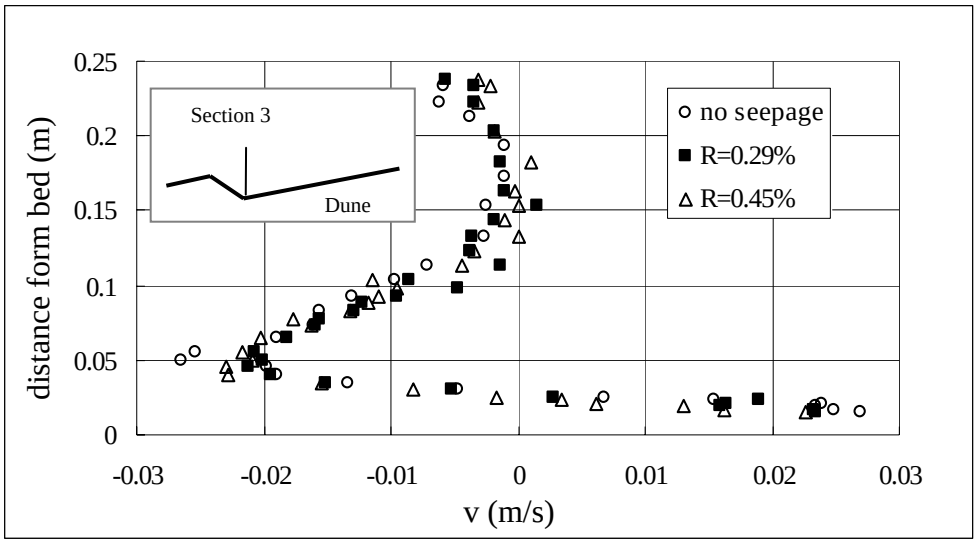

Figure 6.5(c) Comparison of Vertical Mean Velocity with and without Suction at Section 3

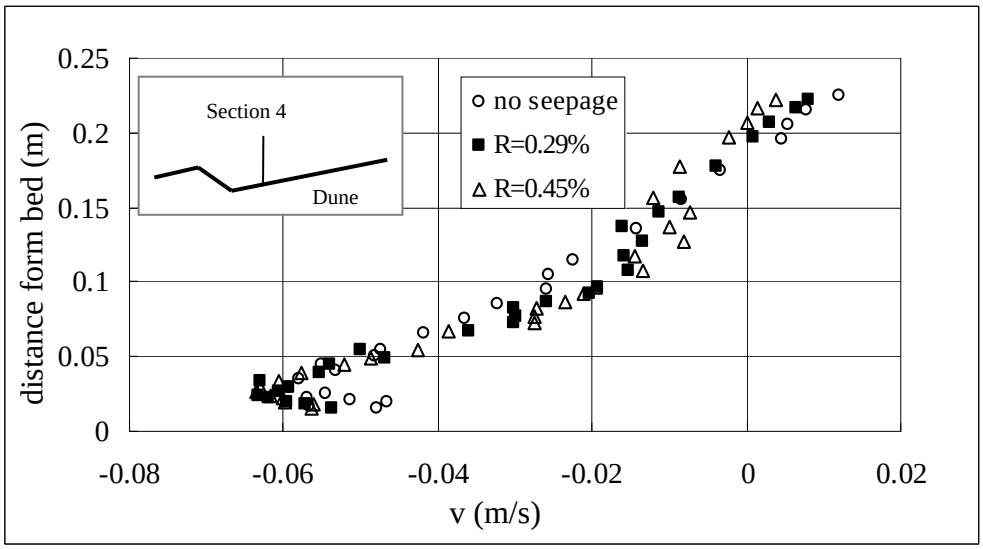

Figure 6.5(d) Comparison of Vertical Mean Velocity with and without Suction at Section 4

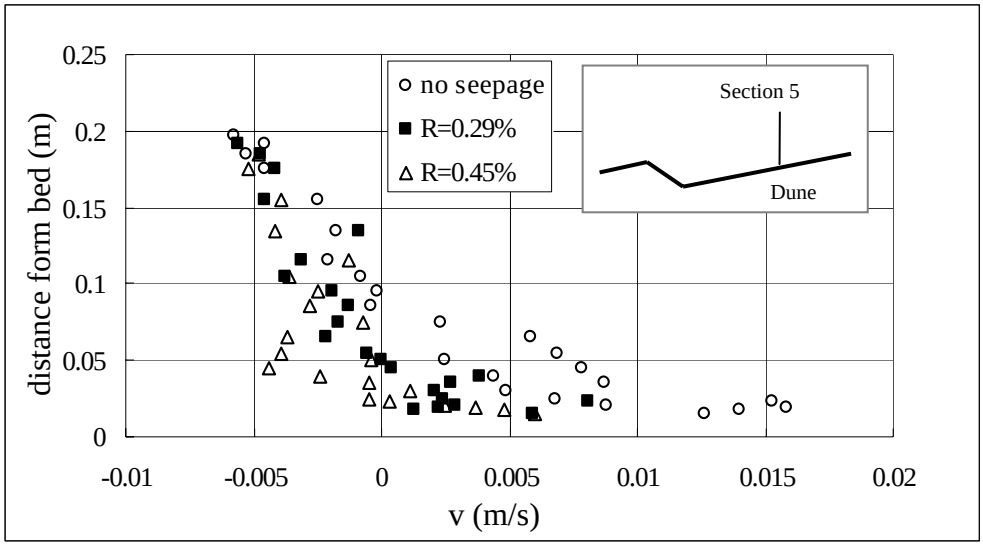

Figure 6.5(e) Comparison of Vertical Mean Velocity with and without Suction at Section 5

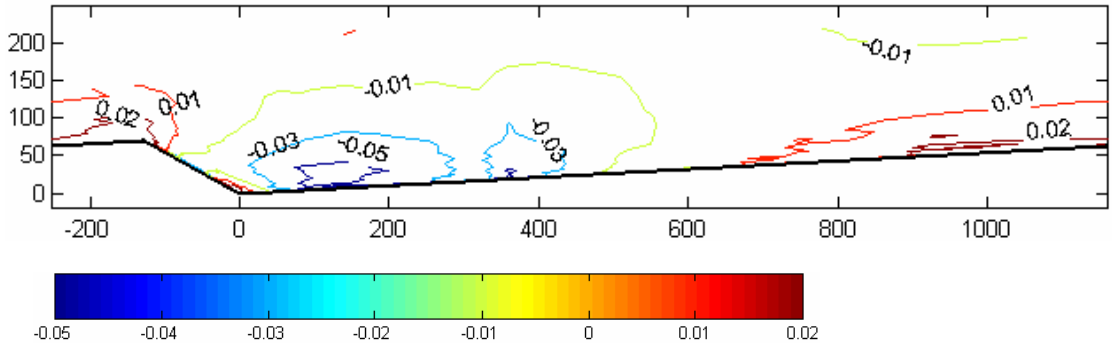

Figure 6.5(f) Contour of Vertical Mean Velocities without Seepage

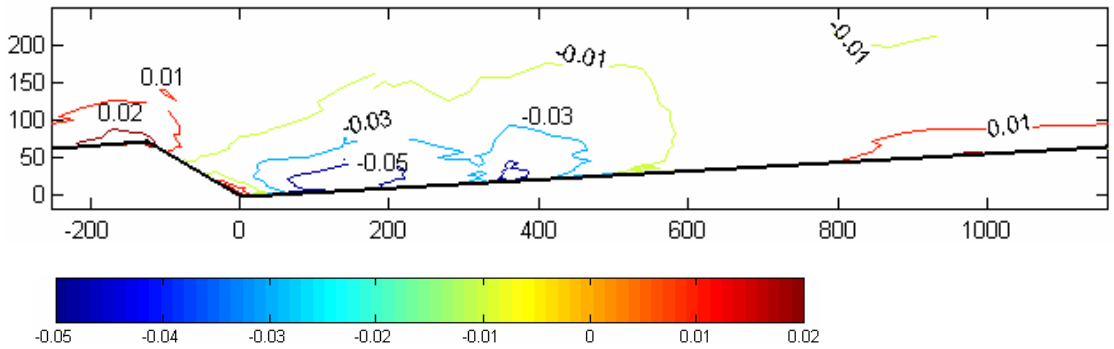

Figure 6.5(g) Contour of Vertical Mean Velocities with Suction (R=0.29%)

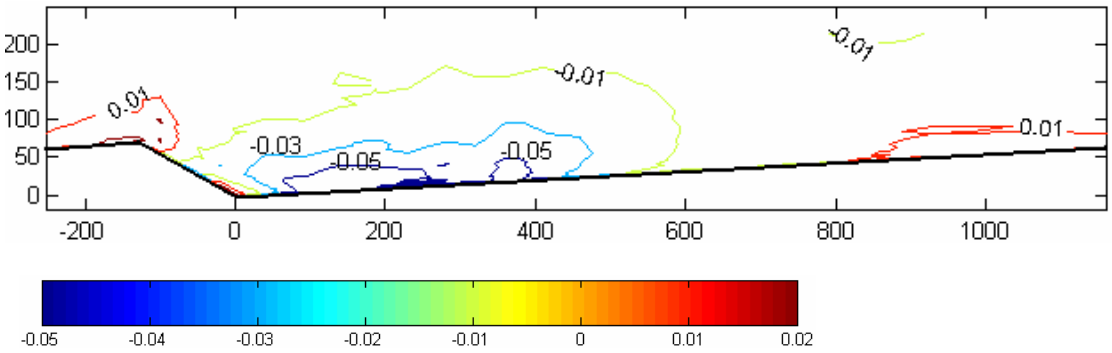

Figure 6.5(h) Contour of Vertical Mean Velocities with Suction (R=0.45%)

Figs. 6.5(a)-(e) show changes of the vertical mean velocity profiles induced by suction at all five locations. The general trend of vertical mean velocities variation is different from that of streamwise mean velocities in that suction always produces smaller or more negative vertical mean velocities in the near-bed region. Since suction is able to influence the vertical mean velocities directly, the deviation of vertical mean velocities is more apparent than that of the streamwise mean velocities. Figs. 6.5(a)-(e) also show the outer flow far away from the bed is not significantly affected by suction. A general layout of the modification of vertical

mean velocities through a single dune length due to suction is shown clearly in Figs. 6.5(f), (g), and (h). The results clearly show that the contour line at v = - 0.05 m/s is stretched by suction and the contour line (v = 0.02 m/s) disappears with suction. It may be inferred from these observations that the introduction of suction always produces more negative or smaller vertical mean velocities near the bed.

6.3.2 Separation Length

The presence of flow separation over the dune crest shows the formation of an eddy at the dune trough. Reattachment of the flow just downstream of the separation cell leads to the development of an internal boundary layer along the stoss side of the succeeding dune. Knowledge of the length of the flow separation is useful in solving a variety of hydraulic problems and also for use in numerical studies. The streamwise spatial resolution of the measurements is fine enough to determine precisely the reattachment point, which is identified by the presence of zero streamwise velocity very near to the bed. It is important to note that the distance of the measuring point from the bed is limited by both the spacing of the laser beams (38 mm) and the location relative to the dune feature. Since the laser light may be intercepted by the boundary waves, the distance of the converging point of these beams has a minimum of 15 mm from the bed if the LDA data are acquired in coincidence mode. This value is too large for measurement of very near-bed streamwise velocity, and thus the precise definition of the reattachment point. To

this end, non-coincidence mode, in which only streamwise components of the flow characteristics can be obtained, is used to reduce the minimal distance to 3 mm.

For the case of no suction, the data in Fig. 6.4(f) may be used to deduce the separation length, λ_r, which is found to be approximately 4 times the dune height ($\lambda_r = 4H$). In the presence of suction, λ_r is reduced to around 3.7 H and 3.4 H for $R = 0.29\%$ and $R = 0.45\%$, respectively (Figs. 6.4g and h). Engel (1981) conducted a series of tests over a fixed bed without suction, for which the values of H/λ varied from 0 to 0.07 and D_{50}/H from 0 to 0.087, respectively. The sand-grain roughness effect (D_{50}/H) was found to be negligible when dunes are steep ($H/\lambda > 0.05$). He further concluded that the separation length for steep dunes was approximately four times the height, in good agreement with the present result without suction.

The results for suction effects on separation length are consistent with general expectations. Suction draws the overlying, often faster-moving flow, toward the bed, resulting in an increase of the local streamwise velocity very near the bed (see Fig. 6.4). Therefore, the location of zero-velocity associated with the reattachment point in the case of no-suction becomes positive due to the introduction of suction. Additionally, suction forces the negative-velocity in the reverse flow zone to be zero, thus causing the formation of the new reattachment point upstream of the original or no-seepage one.

6.3.3 Turbulence Intensities

The profiles of the root mean squared (rms) turbulent fluctuation velocities u' and v' at all five sections for the three suction rates are shown in Figs. 6.6 and 6.7, respectively.

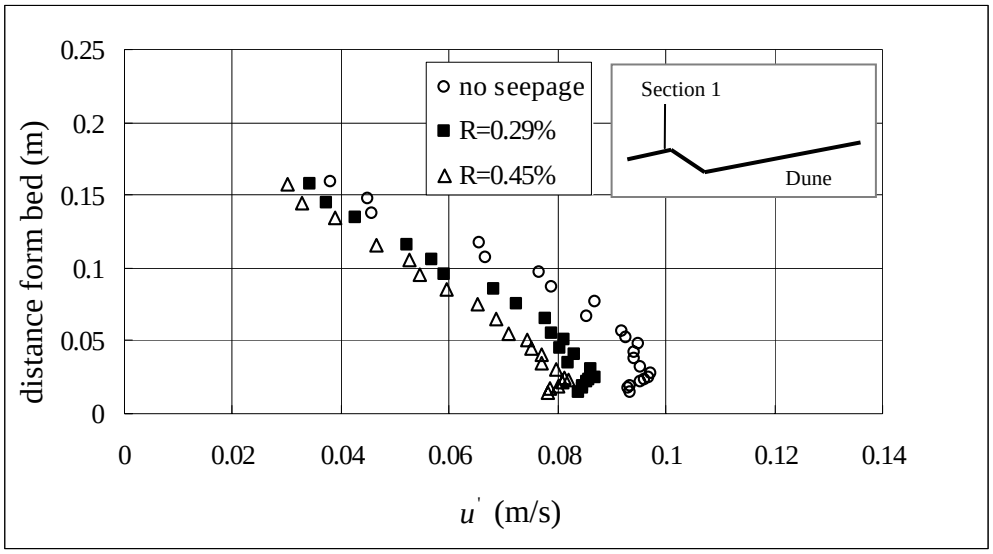

Figure 6.6(a) Variation of RMS Values of Streamwise Velocity Fluctuations at Section 1

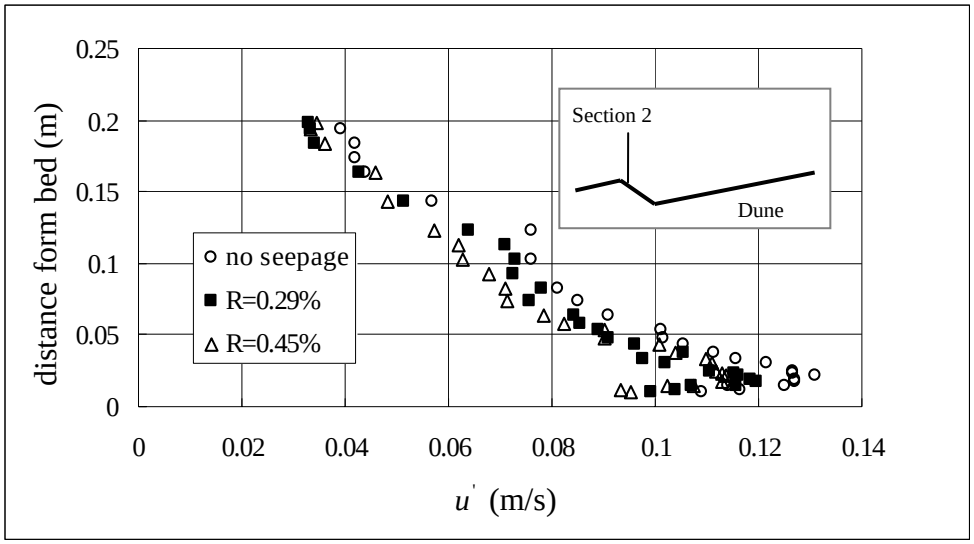

Figure 6.6(b) Variation of RMS Values of Streamwise Velocity Fluctuations at Section 2

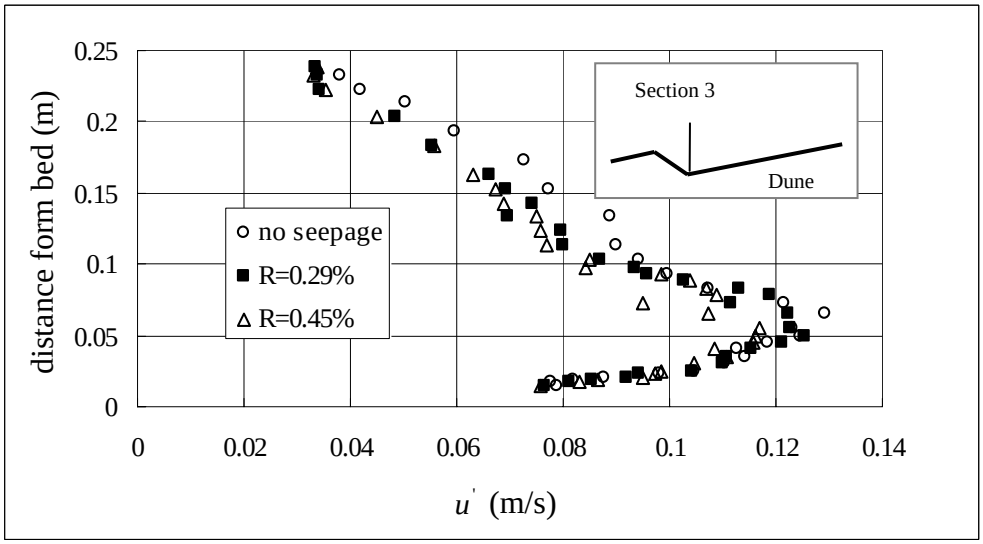

Figure 6.6(c) Variation of RMS Values of Streamwise Velocity Fluctuations at Section 3

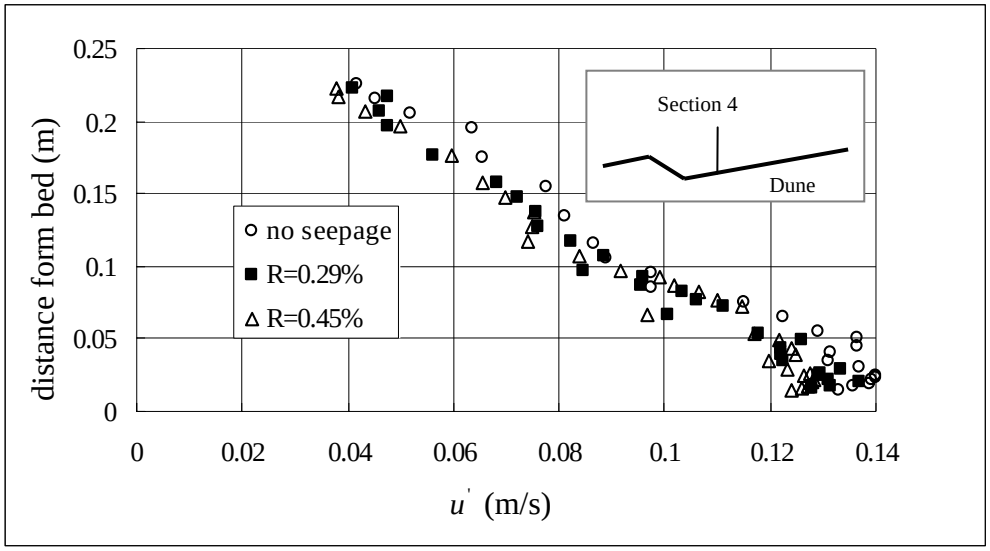

Figure 6.6(d) Variation of RMS Values of Streamwise Velocity Fluctuations at Section 4

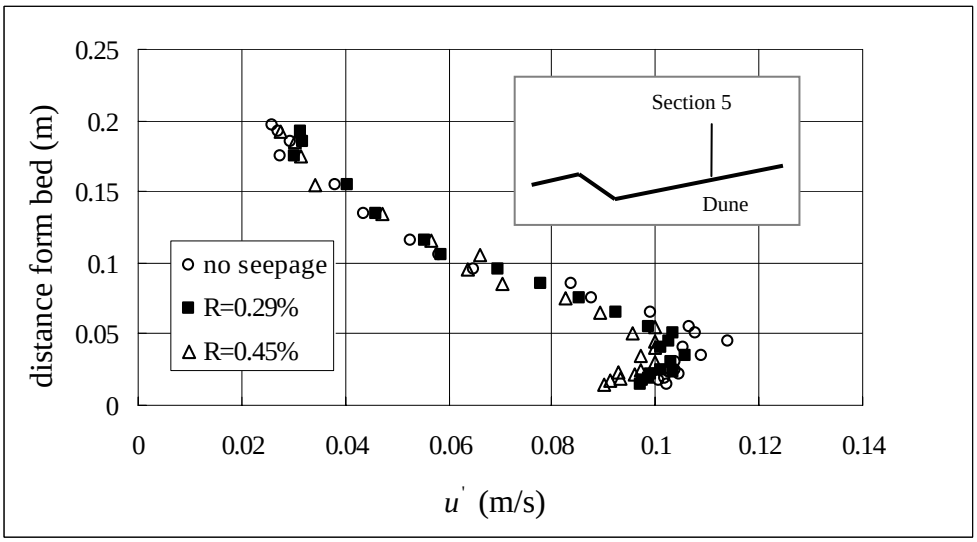

Figure 6.6(e) Variation of RMS Values of Streamwise Velocity Fluctuations at Section 5

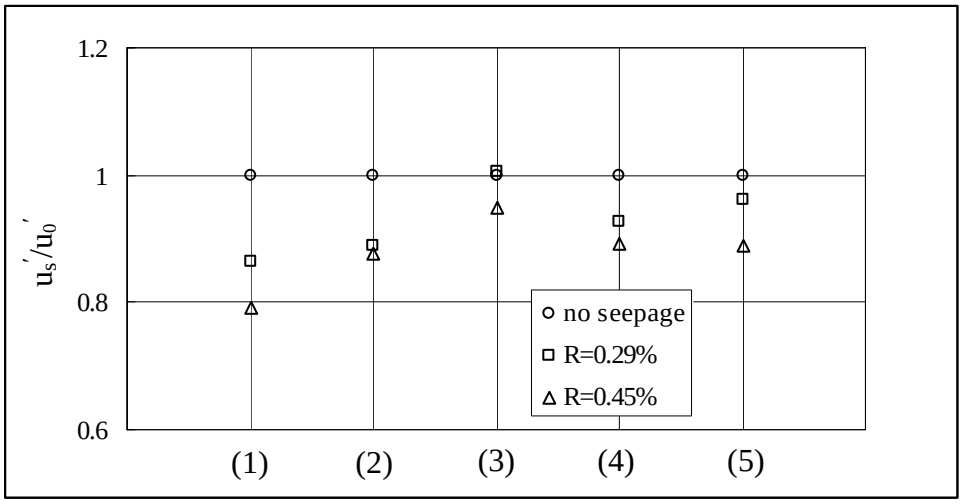

Figure 6.6(f) Variations of Dimensionless RMS Values of Streamwise Velocity Fluctuations at Depth = 50 mm above the Bed

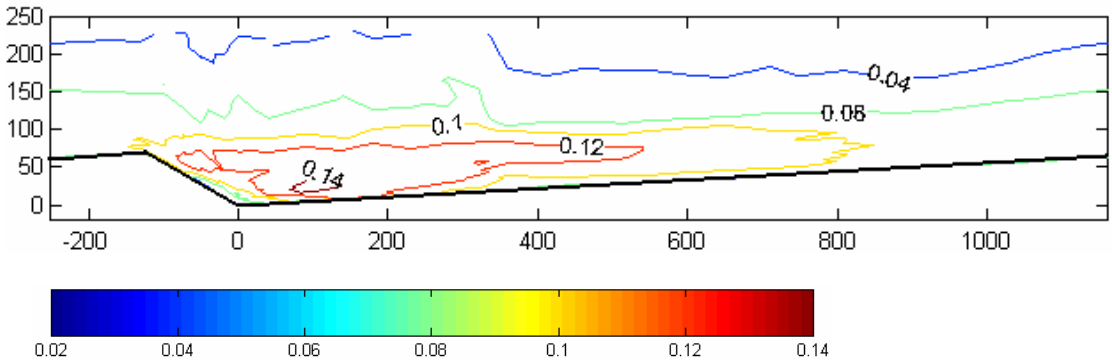

Figure 6.6(g) Contour of RMS Values of Streamwise Velocity Fluctuations without Seepage

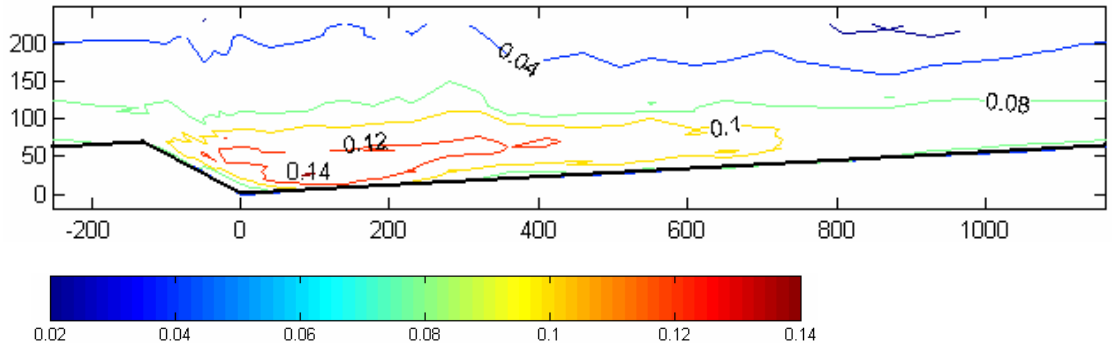

Figure 6.6(h) Contour of RMS Values of Streamwise Velocity Fluctuations with Suction (R=0.29%)

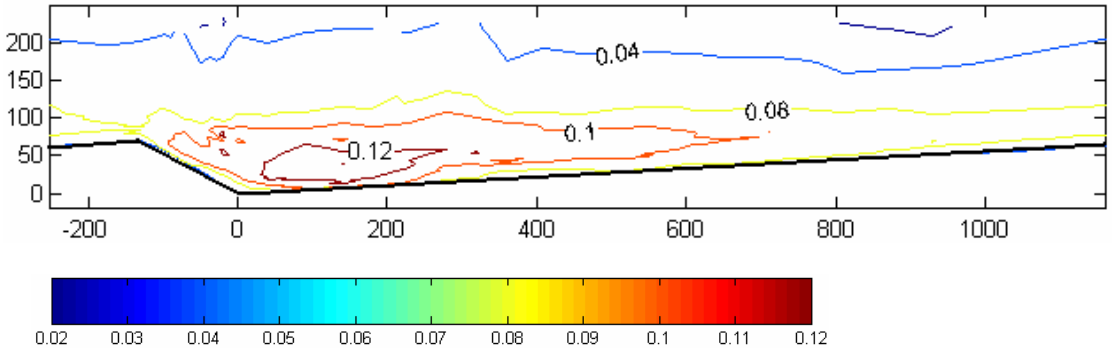

Figure 6.6(i) Contour of RMS Values of Streamwise Velocity Fluctuations with Suction (R=0.45%)

Fig. 6.6 shows the deviation of the rms values of the streamwise velocity fluctuations, indicating that suction can reduce the turbulence intensity near the bed, but has little effect on locations near the water surface. This is consistent with general expectations since mass exchange due to abstraction occurs near the bed rather than at the water surface. One effect produced by suction is the change of the

point of laminar-turbulent transition to a higher Reynolds number (Schlichting 1979); in extreme cases with strong suction, Watters and Rao (1971) reported that the flow in the boundary layer changes from turbulent to laminar. In other words, suction causes the flow to be less turbulent, a phenomenon that is supported by the data in both Figs. 6.6 and 6.7. This agrees well with the general observation of many investigators on the flat bed (Watters and Rao 1971; Nezu 1977; Cheng 1997; Chen and Chiew 2004a) except for the findings of Ramakrishna Rao and Nagaraj (1999). A distinct feature of this effect on flows over a dune is that the magnitude of deviations effected by suction varies with the local position. To further illustrate this phenomenon, the rms values of the streamwise and vertical velocity fluctuations at a depth = 50 mm are extracted from Figs. 6.6 and 6.7. The data at all five sections are tabulated in Table 6.2, and plotted in Fig. 6.6(f) and Fig. 6.7(f), respectively, for the streamwise and vertical rms velocities. In the table and figures, u_s', u_0' = rms value of the streamwise fluctuating velocities with and without seepage, respectively; and v_s', v_0' = rms value of the vertical fluctuating velocities with and without suction, respectively. From the two figures, it is obvious that deviations induced by suction vary with the local position.

Table 6.2 Horizontal and Vertical Fluctuating Velocities at y = 0.05 m for Different Relative Suction Rates, R

Section	Horizontal Fluctuating Velocities, u' (m/s)			Vertical Fluctuating Velocities, v' (m/s)		
	R = 0%	R = 0.29%	R = 0.45%	R = 0%	R = 0.29%	R = 0.45%
1	0.095	0.081	0.074	0.072	0.061	0.057
2	0.101	0.090	0.089	0.073	0.066	0.064
3	0.125	0.125	0.118	0.105	0.102	0.102
4	0.136	0.126	0.122	0.099	0.097	0.092
5	0.108	0.104	0.096	0.080	0.075	0.074

For the location just upstream of the dune crest, i.e., Section (1), the reduction of horizontal rms velocity is significant, by approximately 14% and 21% for R = 0.29% and 0.45%, respectively. The magnitude of change is similar to findings on open-channel turbulence over a flat bed with suction reported by Nezu (1977) and Chen and Chiew (2004b). The change is less apparent at Section (2), which is located just downstream of the dune crest. Within the separation zone (Section 3), the change is almost completely absent. At Section (4), which is near the reattachment point and beyond (Section 5), the change is again observed, with a percentage reduction very similar to those at Section (2). Figs. 6.6(a)-(e) also show that the maximum rms values at a particular section move towards the bed marginally in the presence of suction.

Figs. 6.6(g), (h) and (i) present the contours of the rms values of velocity fluctuations for all three suction rates; they show the general pattern of change due to suction over a single dune length. Fig. 6.6(g) shows that the maximum u'-value, up to 0.14 m/s, occurs around the flow reattachment point, in agreement with the study of Bennett and Best (1995) in the case of no-seepage. Figs. 6.6(h) and 6.6(i) show how these maximum points decrease because suction reduces the turbulent intensity near the bed, as was discussed previously.

A comparison of the rms values of vertical velocity fluctuations with and without suction shows a general pattern similar to that for the streamwise component, as shown in Figs. 6.7(a)-(e) for the five sections, respectively. It is of interest to note that deviations of the vertical component of velocity fluctuation, v' is not more apparent than that of the streamwise component, u', as is illustrated in Fig. 6.7(f). This phenomenon is not the same as that observed for the mean flow velocities discussed earlier. It may be inferred from this observation that suction effects on turbulence intensities are not the same as that on the time-average velocities. The overall changes of the rms values of vertical velocity fluctuations due to suction over a single dune length is shown in Fig. 6.7(g), (h), and (i). The maximum v'-values, up to 0.1 m/s, occur within the flow separation zone, in agreement with the results of Bennett and Best (1995). Figures 6.7(h) and (i) show that the region of these maxima reduces due to suction, similar to the response of the rms values of streamwise velocity fluctuations to suction.

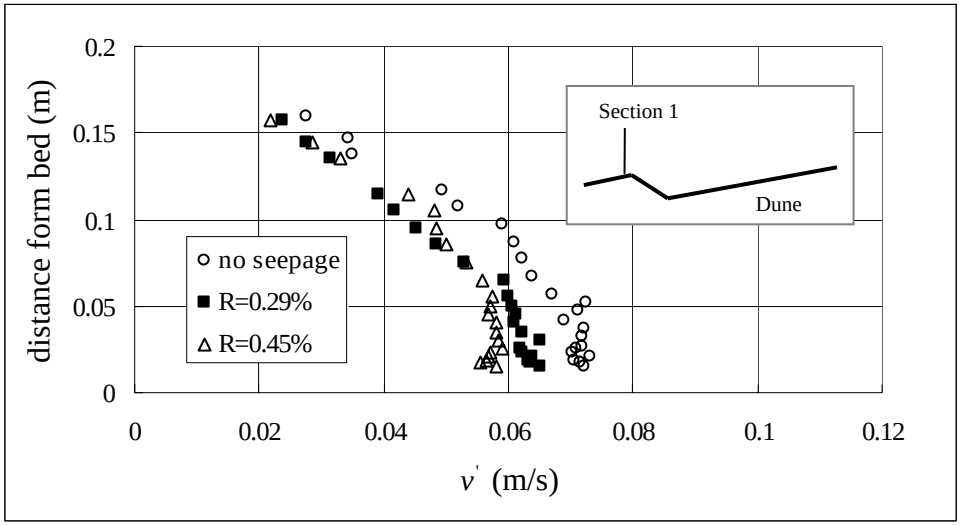

Figure 6.7(a) Variation of RMS Values of Vertical Velocity Fluctuations at Section 1

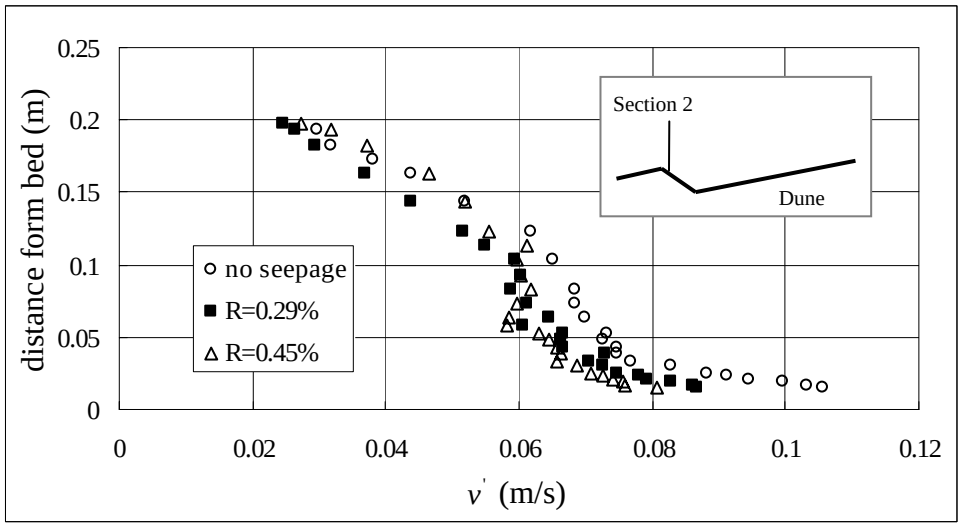

Figure 6.7(b) Variation of RMS Values of Vertical Velocity Fluctuations at Section 2

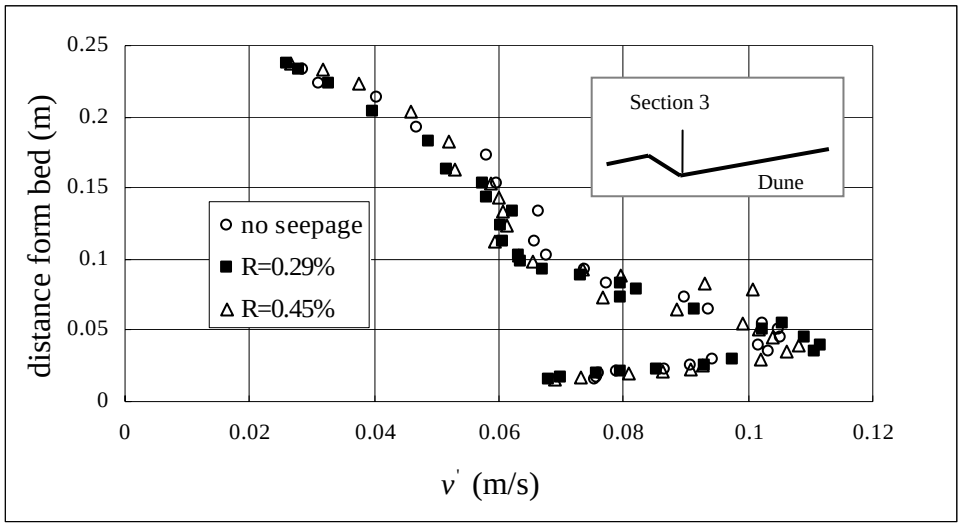

Figure 6.7(c) Variation of RMS Values of Vertical Velocity Fluctuations at Section 3

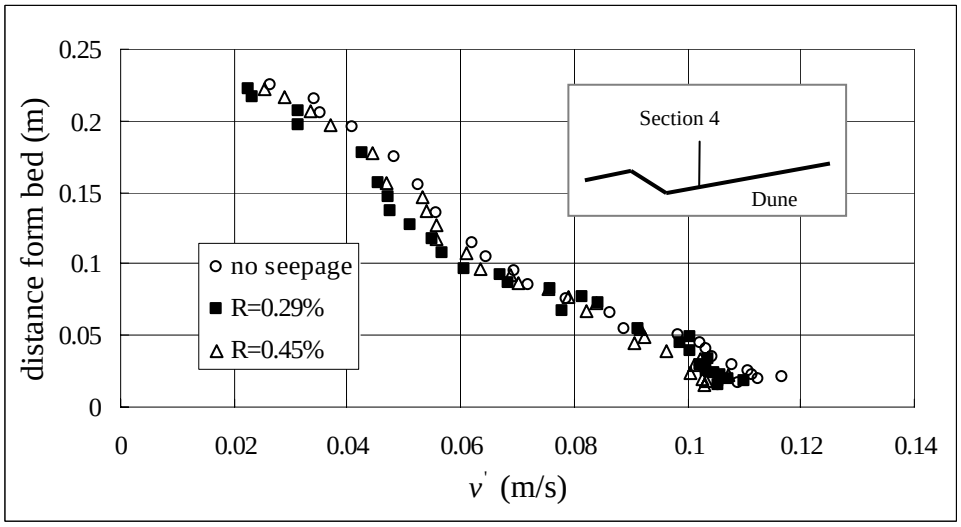

Figure 6.7(d) Variation of RMS Values of Vertical Velocity Fluctuations at Section 4

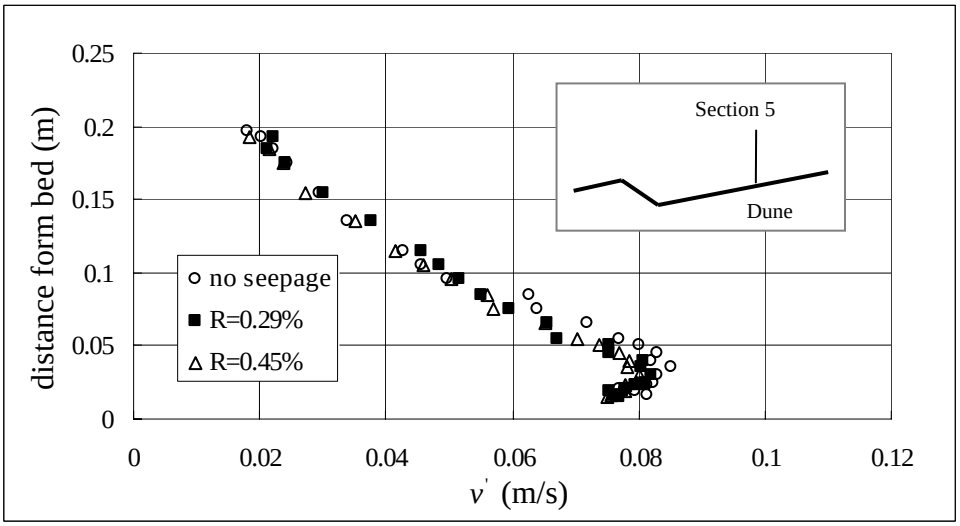

Figure 6.7(e) Variation of RMS Values of Vertical Velocity Fluctuations at Section 5

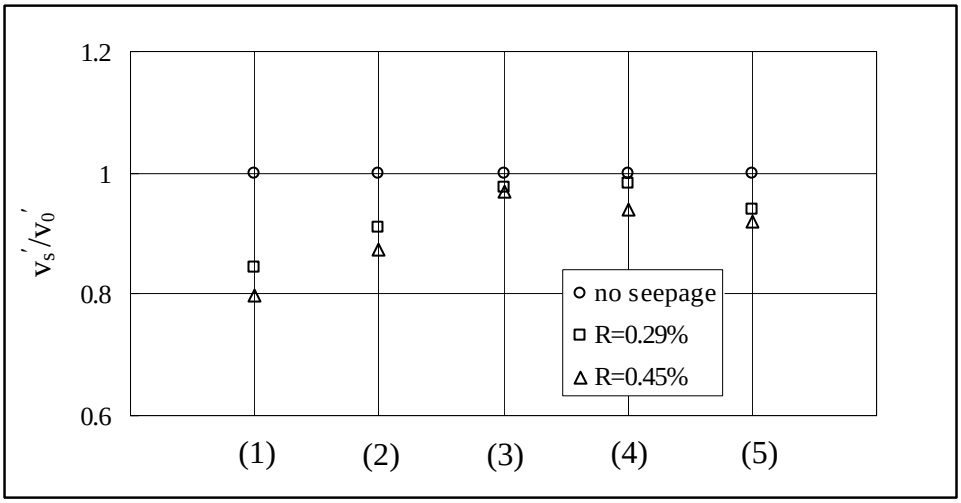

Figure 6.7(f) Variations of Dimensionless RMS Values of Vertical Velocity Fluctuations at Depth = 50 mm above the Bed

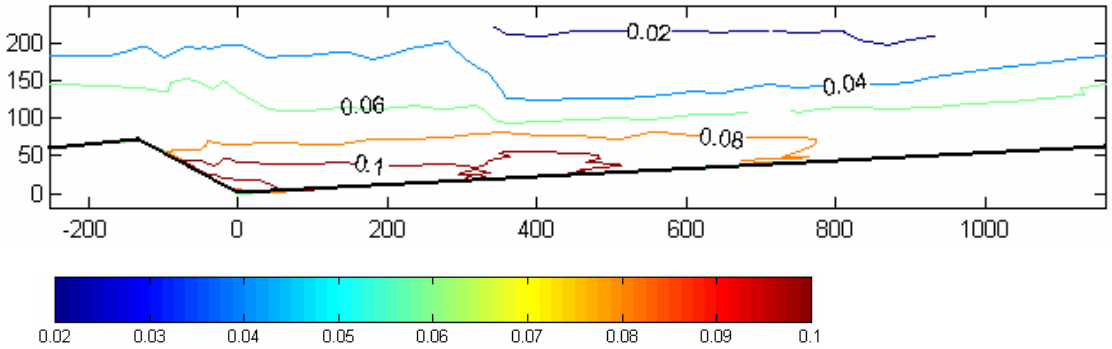

Figure 6.7(g) Contour of RMS Values of Vertical Velocity Fluctuations without Seepage

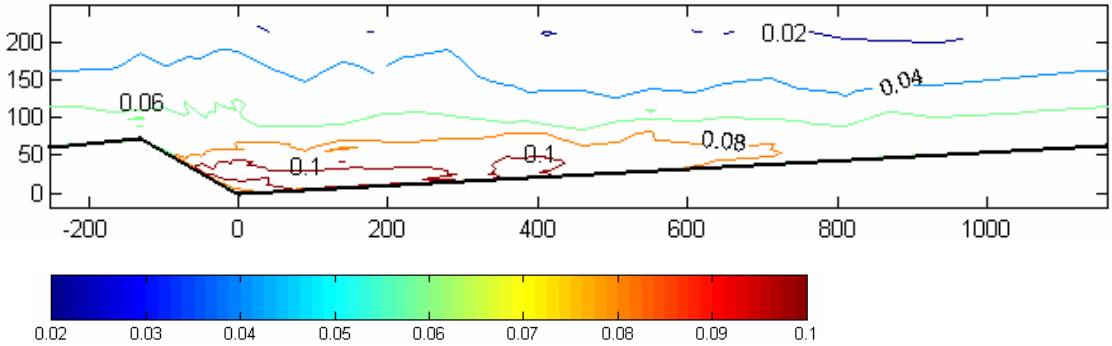

Figure 6.7(h) Contour of RMS Values of Vertical Velocity Fluctuations with Suction (R=0.29%)

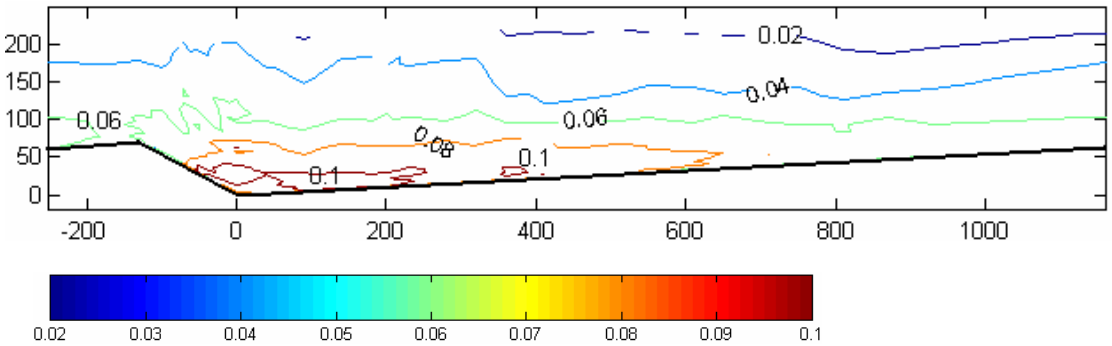

Figure 6.7(i) Contour of RMS Values of Vertical Velocity Fluctuations with Suction (R=0.45%)

6.3.4 Reynolds Shear Stresses

Figs. 6.8(a)-(e) show the vertical profiles of Reynolds shear stresses ($-\overline{u'v'}$) at all the five locations. All five figures, including data with and without suction, expectedly, share the same general trend in that the Reynolds shear stresses increase with distance from the bed until a maximum value is reached at a distance of approximately 0.1h~0.2h. Beyond this value, the Reynolds stress decreases towards zero at the water surface. The only exception to this trend is at the Section (2), where the maximum stress can not be identified. A possible reason is that the location of the maximum value is lower at this section than that at the others and the corresponding turning point is not captured in the measurement.

An overall view of the Reynolds shear stress over a single dune length depicts a vertical shift of the maximum location, which could be attributed to the mixing influence of the flow and the dune boundary. The notable deviation of Reynolds shear stresses caused by suction occurs at the near-bed region, similar to that of the rms value of velocity fluctuations shown in Figs. 6.6(a)-(e) and 6.7(a)-(e). A comparison of the first five curves in Fig. 6.8 shows that suction effects on Reynolds shear stresses decrease significantly when the flow moves into the separation cell and almost vanish altogether at the center of the cell (Section 3). This effect applies not only to Reynolds shear stresses but also the time-average and fluctuating velocities, as shown in Figs. 6.4, 6.5, 6.6 and 6.7. The reason for this phenomenon is discussed in a latter section. Similar to the rms values of velocity fluctuation changes shown in Figs. 6.6(f) and 6.7(f), the Reynolds shear stresses at

0.05m distance for the bed for five sections are also plotted in Fig. 6.8(f), in which τ_{rs}, τ_{r0} = Reynolds shear stress with and without suction, respectively.

A general view on how the Reynolds shear stresses over a single dune length are influenced by suction is shown in Figs. 6.8(g), (h) and (i). Changes in the contour plots associated with Reynolds shear stresses are similar to those associated with the rms value of velocity fluctuations, although smaller changes are again observed in the flow separation cell. A contour map of the spatial distribution of Reynolds shear stresses without suction (Fig. 6.8g) shows that the maximum values, up to 0.006 m^2/s^2, occur near the flow reattachment point; these maximum points are displaced upstream slightly in the presence of suction (Figs, 6.8h and i). This is because of the relocation of the reattachment point upstream due to suction.

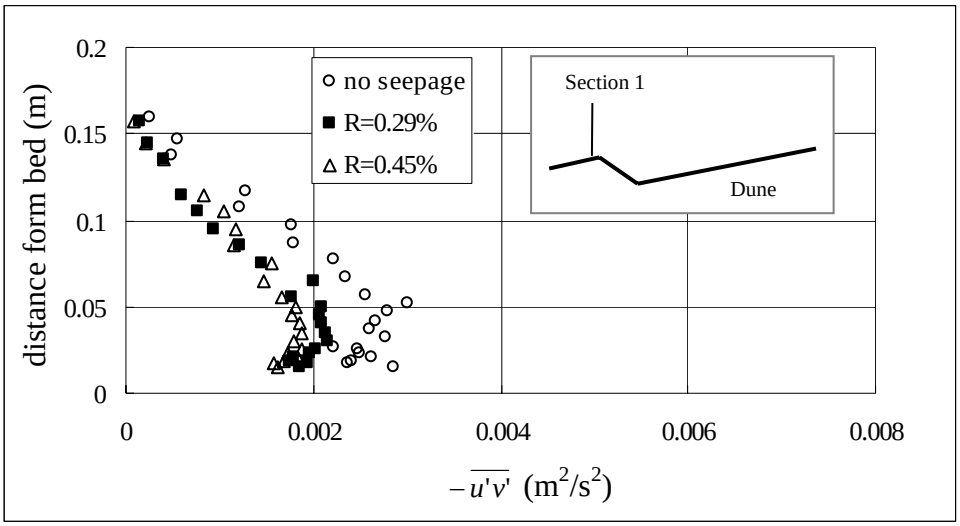

Figure 6.8(a) Variation of Reynolds Shear Stress with Suction at Section 1

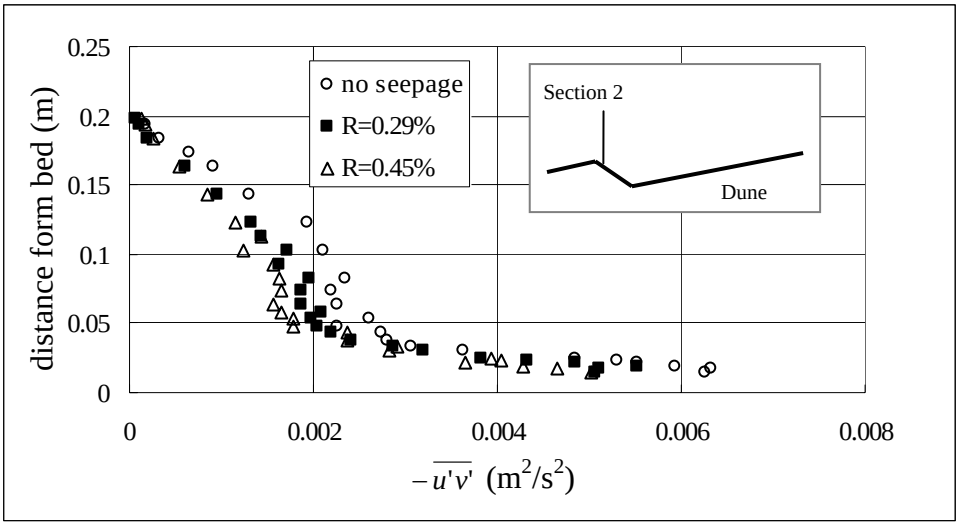

Figure 6.8(b) Variation of Reynolds Shear Stress with Suction at Section 2

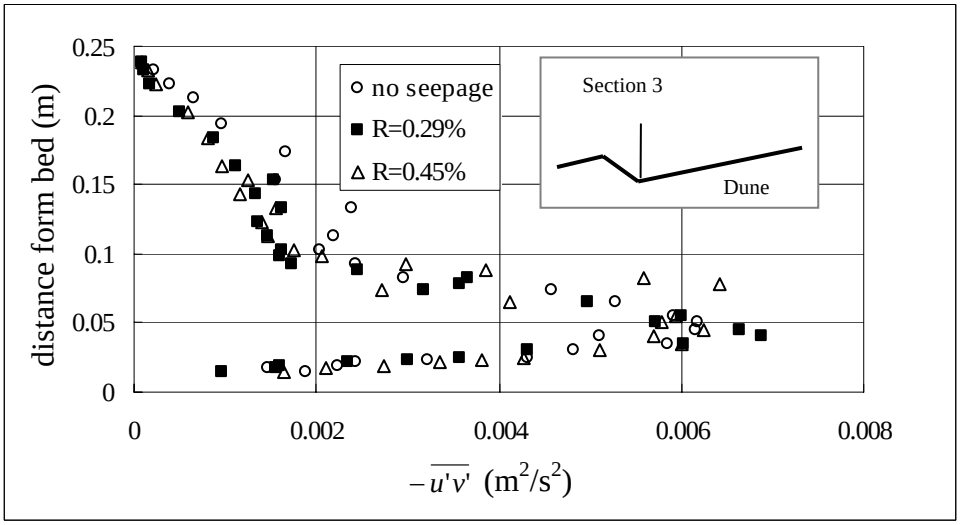

Figure 6.8(c) Variation of Reynolds Shear Stress with Suction at Section 3

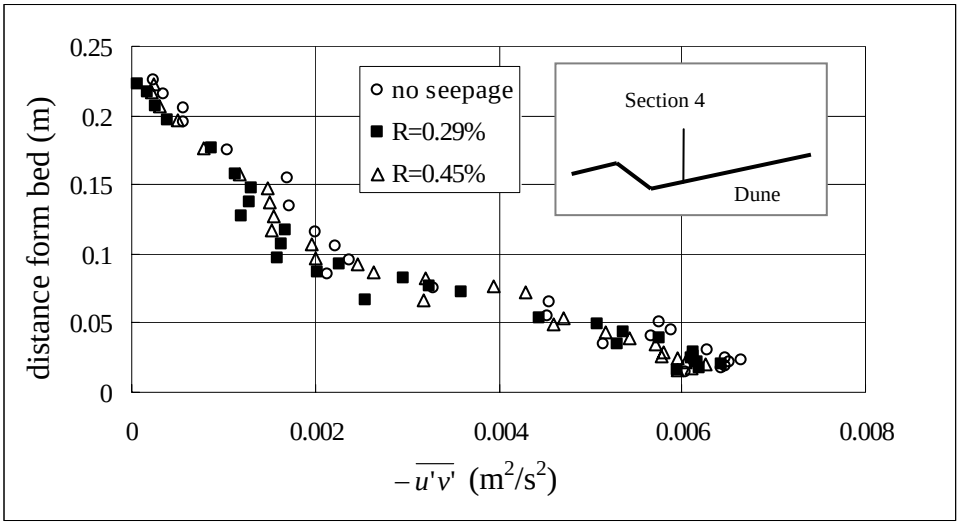

Figure 6.8(d) Variation of Reynolds Shear Stress with Suction at Section 4

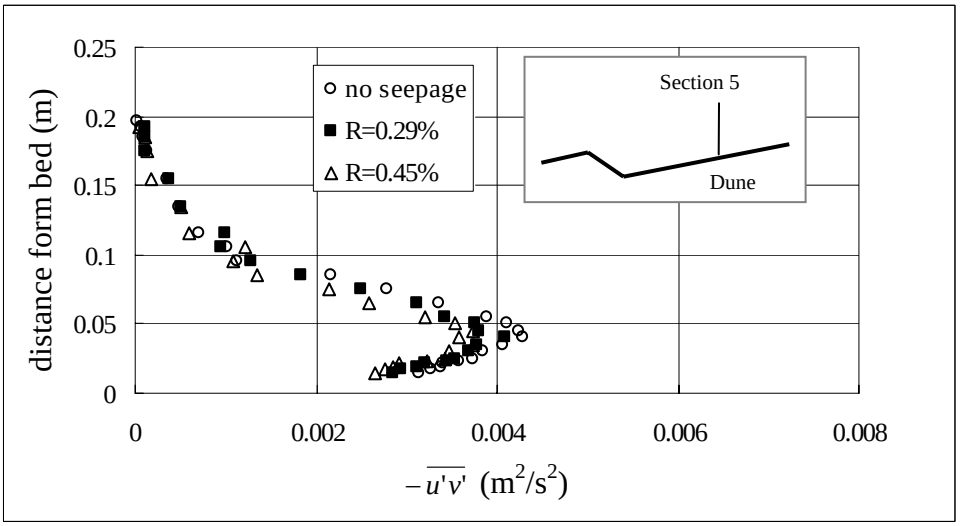

Figure 6.8(e) Variation of Reynolds Shear Stress with Suction at Section 5

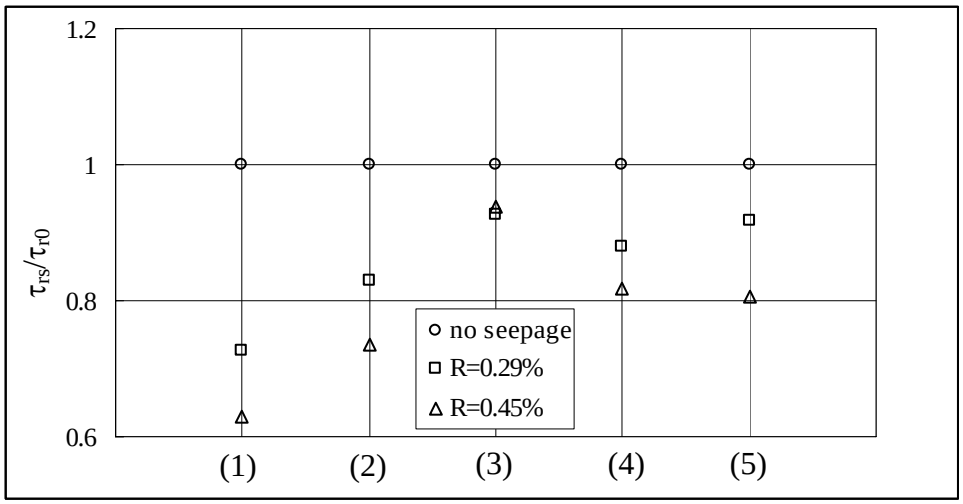

Figure 6.8(f) Variations of Dimensionless Reynolds Shear Stresses at Depth = 50 mm above the Bed

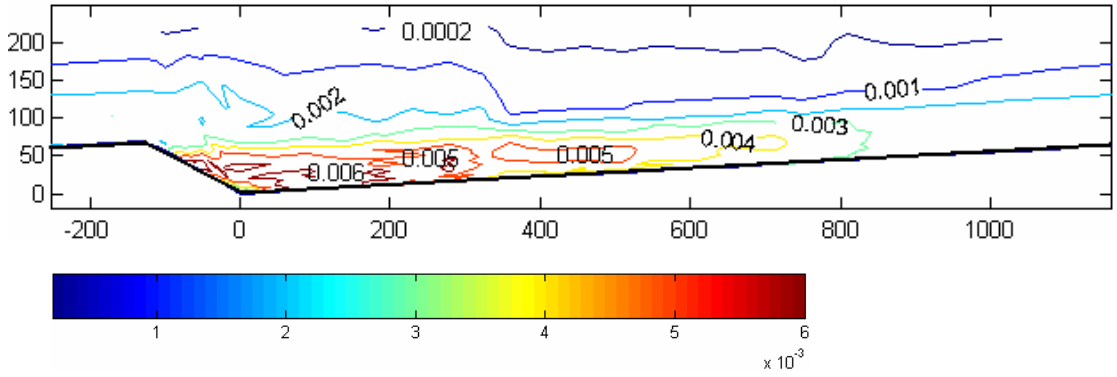

Figure 6.8(g) Contour of Reynolds Shear Stresses without Seepage

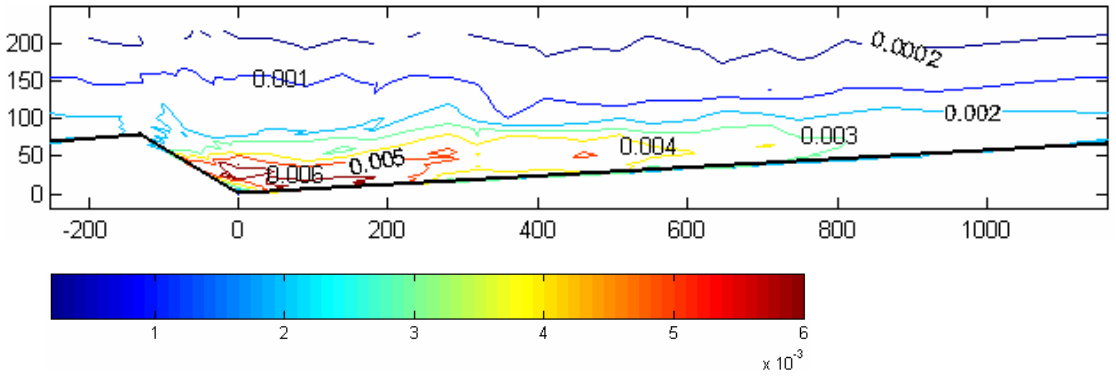

Figure 6.8(h) Contour of Reynolds Shear Stresses with Suction (R=0.29%)

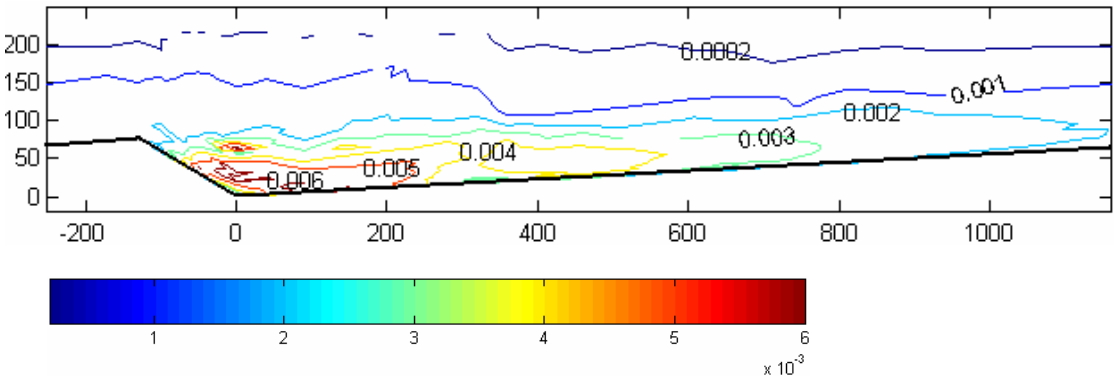

Figure 6.8(i) Contour of Reynolds Shear Stresses with Suction (R=0.45%)

6.3.5 Bed Shear Stress and Implication on Sediment Transport

A detailed investigation of flow in alluvial streams requires an accurate evaluation of the bed shear stresses. The experimental data in the preceding sections of this

chapter clearly show that suction causes significant changes to the near bed velocity as well as the near bed turbulence intensity; as a result, it should also affect bed shear stress. One possible way to determine bed shear stresses is from measured Reynolds shear stress distributions. With this profile, the data may be extrapolated towards the bed to determine the bed shear stresses. The measured data of the Reynolds stress profiles at the five sections in Figs. 6.8(a)-(e) are extrapolated to the bed to determine the bed shear stress for the no-seepage, R = 0.29%, and R = 0.45% conditions, respectively. The results thus obtained are tabulated in Table 6.3, and plotted in Fig. 6.9, in which τ_{bs}, τ_{b0} = bed shear stress with and without suction, respectively. Fig. 6.9 shows an apparent reduction of the bed shear stresses when suction is introduced; although insignificant change is observed within the separation zone at Section (3).

Table 6.3 Bed Shear Stress for Different Relative Suction Rates, R

Section	**Bed shear stress, τ_b (Pa)**		
	R = 0%	**R = 0.29%**	**R = 0.45%**
1	3.9	2.9	2.5
2	9.7	7.7	6.6
3	11.0	11.0	10.8
4	8.0	7.7	7.0
5	6.9	6.1	5.6

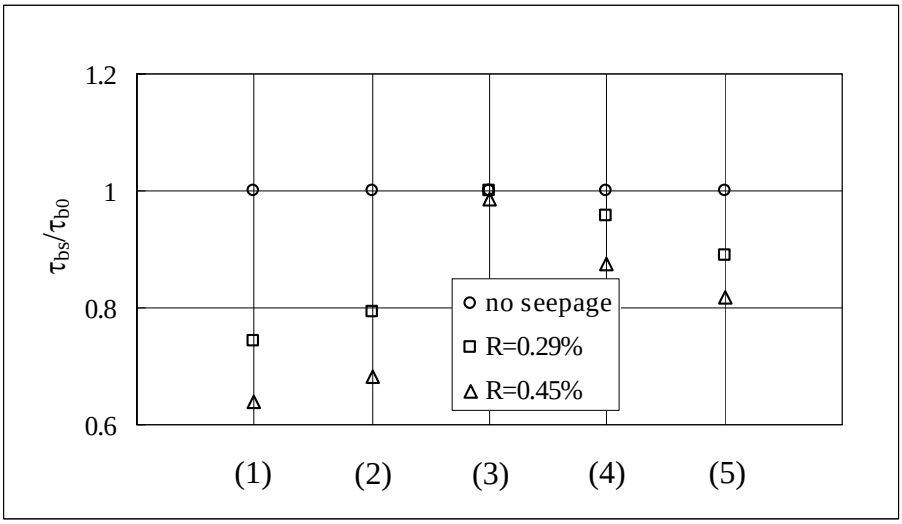

Figure 6.9 Variations of Bed Shear Stress at Depth = 50 mm above the Bed

As was discussed in the earlier sections, suction effects on the time-average and fluctuating velocities as well as Reynolds shear stresses appear to have been nullified within the recirculation or separation zone, i.e., Section (3) in this study. This behavior is clearly shown in Figs. 6.4(c), 6.5(c), 6.6(c), 6.7(c) and 6.8(c) for u, v, u', v' and $-\overline{u'v'}$, respectively. The exact reason for this phenomenon is not known presently but it is reasonable to surmise that the flow property within the recirculation zone has a direct influence on suction effects. A plausible explanation is that suction always tends to aid the formation of boundary layer by causing the flow to adhere to the bed, which results in the reduction of the Reynolds shear stress as well as the turbulence intensity. However, in the separation cell (Section 3), because the suction rate used in the study is not sufficient to prevent separation, suction effects on all turbulent parameters could be less apparent.

For flows over a dune bed, the form and skin drag co-exist, with the latter determining the bed-load transport rate (Einstein and Barbarossa, 1952). The formation of form drag is the result of flow separation at the dune crest, causing a pressure difference across the bedform. Because of the large characterization length scale of pressure over the bedform in comparison with the scale of a sediment particle, form drag is not regarded as an important component in affecting bed load transport (McLean, et al. 1999). However, as shown in the following discussion, form drag is dominant in the total boundary shear stress which is closely related to the turbulence intensity, thus the suspended transport.

Following Einstein and Barbarossa (1955), and Smith and Mclean (1977), the total boundary shear stresses τ_b can be divided into form drag τ_{fd} and spatially-average skin drag τ_{sf} as follows:

$$\tau_b = \tau_{fd} + \tau_{sf} \tag{6.1}$$

The total boundary shear stress can be determined using two different techniques. The first is by using the mean flow depth and water surface slope to calculate the spatially-average mean bed shear stress from the following formula, i.e. Eq. (3.8)

$$\tau_b = \rho g h J$$

In this study the mean flow depth is measured from the mean bed level at the center of seepage zone, and the water surface slope is determined between the location just upstream and that downstream of the seepage zone. A brief description of the method for measuring the water surface slope can be found in Chapter 3. The measured data for the three tests, i.e., for R =0, 0.29% and 0.45% are tabulated in

Table 6.4. With these data, the total shear stresses are computed using Eq. (3.8), which is also shown in the same table.

Table 6.4 Summary of Experimental Flow Parameters

Flow parameter	Case 1	Case 2	Case 3
Mean flow depth, h (m)	0.22	0.218	0.217
Suction rate, R	0	0.29%	0.45%
Water surface slope, J	0.0025	0.0023	0.0021
Bed shear stress from Eq. 3.8 (Pa)	5.37	4.90	4.45
Bed shear stress from Reynolds stress profile (Pa)	4.95	4.58	4.15
Skin drag (Pa)	0.95	1.15	1.22
Form drag (Pa)	4.0	3.43	2.93

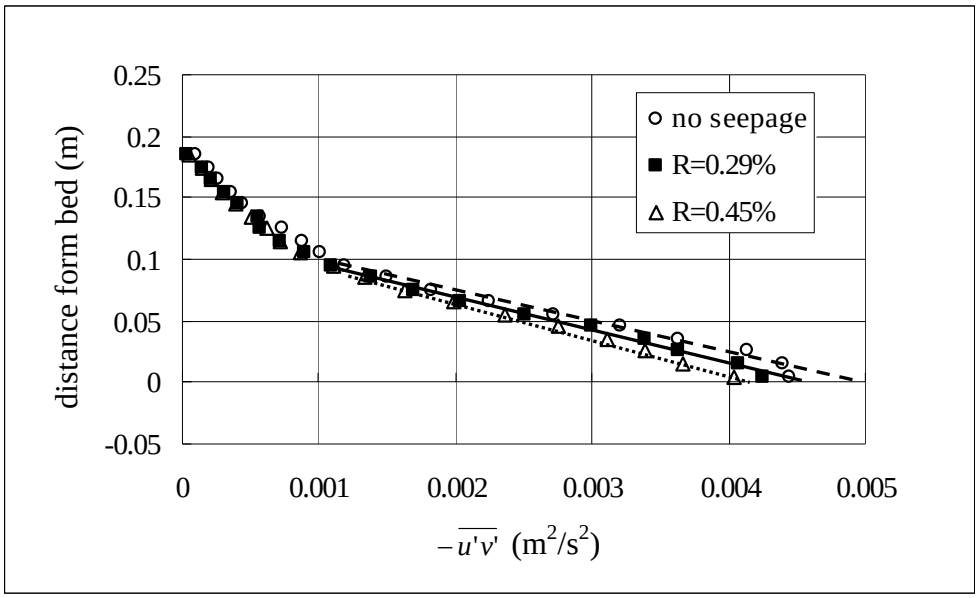

Figure 6.10 Spatially-Average Stresses Profile

The second method to determine the total boundary shear stress is from direct Reynolds shear stress measurements. In the actual application of this method, the values of the Reynolds shear stresses are averaged from the reattachment point to the dune crest along different constant heights above the mean bed level. The results are plotted in Fig. 6.10. Extension of the data to the mean bed height gives the values of τ_b as 4.95, 4.58, 4.15 Pa for the no-seepage, R=0.29%, and R=0.45%, respectively, which are in close agreement with those calculated using Eq. (3.8) (see Table 6.4).

To compute the average skin drag, Smith and McLean (1977) proposed the use of two segments of logarithmic velocity profiles joined at some appropriate matching level, which can be computed using

$$\frac{y_*}{y_0} = 0.1\left[\frac{\lambda}{y_0}\right]^{0.8} \tag{6.2}$$

in which $y_0 = k_s/30.2$ = boundary roughness length; $k_s = D_{84}$, y_* = thickness of the average internal boundary layer. In the present study, with $D_{84} = 1.1$ mm and $\lambda = 1400$ mm, y_* is determined to be 16.9 mm. In the actual calculation, the average skin drag is determined using the law of the wall, (Eq. (6.3), since the flow between the lowest measured point (y =3 mm) and the bed is approximately logarithmic.

$$\frac{u}{u_{*sf}} = \frac{1}{\kappa}\ln\left[\frac{y}{y_0}\right] \tag{6.3}$$

$$\tau_{sf} = \rho u_{*sf}^2 \tag{6.4}$$

where u_{*sf} = skin friction velocity; u = velocity measured at height y; and κ is von Karman's constant = 0.4. The spatially-average skin drag from the reattachment point to the crest of the dune is calculated as 0.95, 1.15, and 1.22 Pa for the no-seepage, R=0.29% and R=0.45%, respectively. Subtraction the skin drag from the total bed shear stress gives the form drag as 4.0, 3.42, and 2.93 Pa for the three cases. The results show that form drag decreases with suction, which confirms that suction causes the flow to adhere to bed boundary, i.e., delay in separation and thus reduction in the difference of pressure between the stoss and lee faces of the dune. Moreover, the increase of the average skin drag implies that the bed-load transport rate increases with suction. In Chapter 5, the bed-load transport rate was estimated from the characteristics of the dune using Eq. (5.6) with the assumption of a triangular dune. The results so estimated reasonably support the

findings inferred from measurements of shear stresses over a fixed dune, i.e., that suction increases the bed-load transport rate.

The effect of both suction and injection on the mobility of sand particles have been investigated on a flat bed by Ramakrishna Rao and Nagaraj (1999). Based on visual observations on the intensity of particle movement, they concluded that suction always enhances the sediment transport. As the suction rate increases, the sediment transport rate in terms of bed erosion also increases, which is consistent with the results of the present study. Further investigation on the bed-load transport rate is needed to confirm those preliminary results. Whether suction will produce a significant increase in sediment transport rate remains uncertain presently.

6.4 SUMMARY

This chapter examines how turbulence characteristics of flow over a fixed dune respond to bed suction. Detailed measurements of the streamwise and vertical components of velocity over a fixed triangular dune with and without suction reveal how suction influences the mean flow and turbulence characteristics. The principal conclusions drawn from the laboratory investigation are:

(1) The streamwise velocity profile becomes more uniform when compared to that without suction; and suction always produces smaller or more negative vertical velocities in the near-bed region.

(2) Suction causes the flow to adhere to the wall resulting in the reduction of separation length. The experimental data show that the separation length to dune height ratio, λ_r/H reduces from 4 for a no-suction case, to 3.7 and 3.4 for suction ratio, R = 0.29% and 0.45%, respectively.

(3) The experimental data show that suction effects on turbulence intensities are not the same as that on time-average velocities. The vertical time-average velocities respond more readily than their counterpart in the streamwise direction; the response of both the streamwise and vertical (rms) turbulence fluctuating velocities to suction is similar.

(4) Both turbulence intensity and Reynolds shear stresses of the flow near to the bed decrease with suction, which confirms that suction causes the flow within the boundary layer to be less turbulent.

(5) Both the time-average and turbulence characteristics of the flow do not respond to suction in the recirculation zone for the suction rates used in the study.

(6) Since the spatially-average skin drag increases when suction flow is introduced, the average bed-load discharge tends to be larger than that without suction, which is consistent with the finding on the mobile bed.

CHAPTER 7

CONCLUSIONS AND RECOMMENDATIONS

7.1 INTRODUCTION

In this study, seepage effects on the angle of repose of sediments, the geometrical dimension of dunes, and the turbulence characteristics of flows over a dune are investigated analytically and experimentally. In total, four series of tests were conducted each with a definite objective and the study consists of three main parts.

First, a review of published studies on flow and sediment transport with seepage is presented to better understand the state-of-the-art in this area of research. Information provided in the review involves the variation of flow velocity and turbulence, bed shear stress, and sediment transport rate, in the presence of seepage

on a flat bed. Contradictory results in published literature are highlighted, and the reason for the differences discussed.

Second, seepage effects on the angle of repose of cohesionless sediments and the geometrical dimension of dunes are examined. A general expression that describes the critical slope of the sediment with seepage is reasonably applied to characterize the influence of seepage on the lee-side slope of dunes. The analytical solution is verified using experimental data. Moreover, the variations of the height and wavelength of dunes caused by seepage are analyzed.

Lastly, the response of time-average velocity distributions, turbulence intensity distributions and Reynolds shear stress distributions over a single dune to bed suction are investigated. The implication on sediment transport rate from measured data is analyzed and compared with findings on a mobile bed.

7.2 SEEPAGE EFFECTS ON DUNE GEOMETRY

(1) To relate the hydraulic gradient of seepage to its velocity for coarse sediment particles, parameters used to define the exponential function are first determined experimentally. The empirical non-linear relationship so established is applied in the analysis of the experimental data associated with angle of repose of sediments and dune geometry.

(2) A theoretical expression (Eq. 4.20) is derived to predict the critical slope (or angle of repose) of cohesionless sediment in the presence of seepage by considering the balance of force, including seepage forces, exerted on a single sphere lying on three packed spherical particles. The critical sandy slope is found to be related to the hydraulic gradient of the seepage applied. The relationship so derived shows that injection reduces the angle of repose of sediments, whereas suction does the opposite. All experimental data reasonably support the theoretical equation when the coefficient in the equation is slightly modified to account for sediment shape and sediment gradation effects.

(3) The development of dunes along the seepage zone is investigated and the length of the seepage zone used in this study is found to be long enough for the development of dune height, but not for the dune wavelength. Experimental results show that the minimum length needed for dunes to reach theirs fully developed height is approximately 30 times the height of the fully developed dunes for a given injection rate; while for a given suction rate, the minimum length is approximately 20 times the height of the fully developed dunes.

(4) Analyses of the laboratory data associated with the fully developed dune height shows that the height of the dune is reduced when injection is present; while suction increases the dune height. The relationship between the hydraulic gradient and angle of repose is reasonably used for predicting seepage effects on the lee-side slope of dunes. The measured data generally support the

assumption that seepage effects on the lee-side slope of dunes are the same as that on the angle of repose of sediments. It shows that the slope is reduced when injection is presented; while suction increases the slope.

(5) The response of the dune celerity to seepage is described: suction increases the celerity; while injection reduces it. These changes may be used to account for the observation that suction appears to increase the wavelength of dunes; whereas injection does the opposite.

(6) In conjunction with the finding on seepage effects on dune height and dune celerity, it may be inferred that the bed-load transport rate can be modified significantly by seepage.

The response of dune geometry to seepage is summarized in Table 7.1.

Table 7.1 Summary of Seepage Effects on Dune Geometry

Dune Properties	Injection	Suction
Angle of repose or lee-side slope of dunes with cohesionless sediments	Decrease	Increase
Fully developed dune height	Decrease	Increase
Dune length	Decrease	Increase
Distance needed for a dune to reach its fully developed stage	30 times the fully developed dune height	20 times the fully developed dune height
Dune celerity	Decrease	Increase

7.3 SUCTION EFFECTS ON FLOW OVER DUNES

(1) Analyses of the experimental results show that suction causes the flow to adhere to the dune-bed boundaries resulting in the reduction of separation length. The experimental data show that the separation length to dune height ratio, λ_r / H reduces from 4 for a no-suction case, to 3.7 and 3.4 for suction rate, R = 0.29% and 0.45%, respectively.

(2) Suction draws the overlying, often faster-moving flow, toward the bed, resulting in an increase of the local streamwise velocity very near to the bed. However, the velocity of flow near the water surface undergoes opposite changes because of mass conservation although seepage has no direct influence on the outer flow. As a whole, streamwise velocity profile becomes more uniform when compared to that without suction; while suction always produces smaller or more negative vertical velocities in the near-bed region.

(3) Both turbulence intensity and Reynolds shear stresses of the flow near to the bed decrease with suction, which confirms that suction can render the turbulent flow in the boundary layer to be more “laminar” or less turbulent. Measured data along the single dune show that changes of both turbulence intensity and Reynolds shear stress are less apparent in the trough of the dune than at the other locations along the dune.

(4) Calculation of the spatially-averaged skin friction stress from the measured Reynolds shear stress shows that skin friction increases with suction. It may be

inferred that the average bed-load discharge tends to be larger in the presence of suction than that without suction, which is consistent with the finding on the mobile bed.

The response of flow and turbulence over a dune to seepage is summarized in Table 7.2.

Table 7.2 Summary of Seepage Effects on Dune Flows

Flow Parameters	**Suction Effects**
Separation length	Decrease with suction
Streamwise velocity	Becomes more uniform
Vertical velocity	Suction produces smaller or more negative vertical velocity in the near-bed region
Turbulence intensity	Decrease with suction
Reynolds shear stress	Decrease with suction
Skin drag	Increase with suction

7.4 RECOMMENDATIONS

(1) Published works are uncertain as to whether seepage reduces or enhances sand-bed stability on flat bed, conflicting results are still present. Some suggestions for further studies have been proposed in Chapter 2. The complex interactions between the flow and permeable boundary caused by seepage raise important issues that require further consideration. The issues directly concern evaluation of velocity distributions, bed shear stress variation, etc.

(2) Experimental results show that the seepage zone used in the study is not long enough for the length of dune to reach its equilibrium stage. Further investigations on the distance-growth of the dune length should be conducted with a longer seepage zone.

(3) The sediment transport rate in this study is indirectly obtained from the measured dune height and its propagating celerity with certain assumptions, including a triangular fixed dune or from measurement of Reynolds shear stresses. Directly measuring the sediment transport rate in a seepage zone and the zone just upstream of it is necessary to study how seepage affects the local sediment transport rate. The results will either confirm or deny the present hypothesis.

(4) For turbulent flows over dunes, only suction effects are explored in this study; the present results have shed light on the mechanism of sediment transport in

the case of suction. Further research on injection effects on the turbulence characteristics over dunes should be undertaken.

REFERENCES

1. Adams, E., and Eaton, J. (1988). "An LDA study of the backward facing step flow, including the effects of velocity bias." Journal of Fluids Engineering, 110(Sept.), 275-282.
2. Allen, J. R. L. (1968). Current ripples. Their relation to patterns of water and sediment motion, North-Holland Publishing Co., Amsterdam, The Netherlands.
3. Allen, J. R. L. (1984). Sedimentary structures, their character and physical basis, Developments in sedimentology, Elsevier, Amsterdam: New York.
4. Antonia, R. A. and Zhu, Y. (1995). "Effect of concentrated wall suction on a turbulent boundary layer." Physics of fluids, 7(10), 2465-2474.
5. Bass, J. H. (1993). "Dimensional analysis of current ripples in recent and ancient depositional environments." PhD thesis. Department of Geology, University of Utrecht, 199pp. Utrecht, The Netherlands.
6. Bennett, J. P. (1995). "Algorithm for resistance to flow and transport in sand-bed channels." Journal of Hydraulic Engineering, ASCE, 121(8), 578-590.

7. Bennett, S. J., and Best, J. L. (1995). "Mean flow and turbulence structure over fixed, two-dimensional dunes: implications for sediment transport and bedform stability." Sedimentology, 42, 491-513.
8. Chen, X. W. and Chiew, Y. M. (2004a). "Velocity distribution of turbulent open channel flow with bed suction." J. of Hydraulic Engineering, ASCE, 130(2), 140-148.
9. Chen, X. W. and Chiew, Y. M. (2004b). "Turbulence Characteristics of Open Channel Flow with Bed Suction." J. of Engineering Mechanics, ASCE (under review).
10. Cheng, N. S. (1997). "Seepage effect on open-channel flow and incipient sediment motion." A thesis submitted to Nanyang Technological University in fulfillment of the requirements for the degree of Doctor of Philosophy.
11. Cheng, N. S. (2003). "Application of Ergun Equation to Computation of Critical Shear Velocity Subject to Seepage." J. of Irrigation and Drainage Engineering, Vol. 129(4), 278-283.
12. Cheng, N. S., and Chiew, Y. M. (1998a). "Turbulent open-channel flow with upward seepage." Journal of Hydraulic Research, IAHR, 36(3), 415 - 432.
13. Cheng, N. S., and Chiew, Y. M. (1998b). "Modified logarithmic law for velocity distribution subjected to upward seepage." Journal of hydraulic Engineering, ASCE, 124(12), 1235-1241.
14. Cheng, N. S., and Chiew, Y. M. (1999). "Incipient sediment motion with upward seepage." Journal of Hydraulic Research, IAHR, 37(5), 665-681.

15. Chien, N., and Wan, Z. H. (1998). Mechanics of sediment transport, ASCE Press, Virginia.
16. Chiew, Y. M. (1991). "Bed features in nonuniform sediments." Journal of Hydraulic Engineering, ASCE, 117(1), 116-120.
17. Chiew, Y. M. (1995). "Mechanics of Riprap Failure at Bridge Piers." Journal of Hydraulic Engineering, ASCE, 121(9), 635-643.
18. Chu, Y. S., and Gelhar, L. W. (1972). "Turbulent pipe flow with granular permeable boundaries." MIT Report, Ralph M. Parsons Lab., No.148.
19. Clarke, J. H., Menkes, H. R., and Libby, P. A. (1959). "A provisional analysis of turbulent boundary layers with injection." J. of the Aerospace Sciences, 22(4), 255-260.
20. Coleman, S. E., and Melville, B. W. (1994). "Bed-form development." Journal of Hydraulic Engineering, 120(5), 544-560.
21. Coleman, S. E., and Melville, B. W. (1996). "Initiation of bedforms on a flat sand bed." Journal of Hydraulic Engineering, 122(6), 301-310.
22. Dantec (2000) BSA Flow Software: Installation and User's guide, 6th edition, Denmark.
23. Das, B. M. (1979). Introduction to Soil Mechanics. The Iowa State University Press.
24. Dey, S. and Zanke, U. C. E. (2004). "Sediment Threshold with Upward Seepage". J. of Engineering Mechanics, ASCE, 130(9), 1118-1123.
25. Durst, F., Melling, A., and Whitelaw, J. H. (1987). Principles and Practice of Laser-Doppler Anemometry, 2nd edition, G. Braun, Karlsruhe.

26. Eagleson, P. S., and Dean, R. G. (1959). "Wave-induced motion of sediment particles" Trans. Am. Soc. Civil Engrs. Paper, 1959 (3225) 1162-1186.

27. Einstein, H. A. , and Barbarossa, N. (1952). "River channel roughness." Trans., ASCE, 117, 1121-1146.

28. Engel, P. (1981). "Length of flow separation over dunes." Journal of the Hydraulics Division, ASCE, 107(HY10), 1133-1143.

29. Engelund, F. (1970). "Instability of erodible beds." Journal of Fluid Mechanics, 42(2), 225-244.

30. Engelund F. and Fredsϕe (1982) "Sediment ripples and dunes." Ann. Rev. Fluid Mech. 14:13-37.

31. Espinoza, J., and Martínez, P. (2000). "Experimental study of turbulent macro-structures behind dunes." 2000 Joint Conference on Water Resources Engineering and Water Resources Planning & Management, ASCE.

32. Fredsϕe, J. (1974). "On the development of dunes in erodible channels." Journal of Fluid Mechanics, 64(1), 1-16.

33. Fredsϕe, J. (1975). "The friction factor and height length relations in flow over a dune-covered bed." Prog. Report 37, Institute of Hydrodynamics, Technical University of Denmark.

34. Fredsϕe, J. (1980). "The form of dunes." Proceedings of International Symposia River Sedimentation, Beijing, Paper B-12, 13pp.

35. Garde, R. J., and Ranga Raju, K. G. (1977). Mechanics of sediment transportation and alluvial stream problems, John Wiley and Sons, New York.

36. Haque, M. I., and Mahmood, K. (1986). "Analytical study on steepness of ripples and dunes." Journal of Hydraulic Engineering, ASCE, 112(3), 220-236.
37. Haque, M. I., and Mahmood, K. (1987). "Sediment convection-diffusion and bedform length." Journal of Hydraulic Engineering, ASCE, 113(11), 1381-1401.
38. Harrison, S. S. (1968). "The effects of groundwater seepage on stream regime – a lab study." A thesis presented to University of North Dakota, in partial fulfillment of the requirements for the degree of Doctor of Philosophy.
39. Ji, Z. G., and Mendoza, C. (1997). "Weakly nonlinear stability analysis for dune formation." Journal of Hydraulic Engineering, ASCE, 123(11), 979-985.
40. Julien, P. Y., and Klaassen, G. J. (1995). "Sand-dune geometry of large rivers during floods." Journal of Hydraulic Engineering, ASCE, 121(9), 657-663.
41. Karim, F. (1999). "Bed-form geometry in sand-bed flows." Journal of Hydraulics Engineering, ASCE, 125(12), 1253-1261.
42. Kennedy, J. F. (1963). "The mechanics of dunes and antidunes in erodible-bed channels." Journal of Fluid Mechanics, 16(4), 521-544.
43. Kennedy, J. F. (1969), "the formation of sediment ripples, dunes and antidunes." Ann. Rev. Fluid Mech. 1:147-168.
44. Kim, K. and Sung, H. J. (2003). "Effects of periodic blowing from spanwise slot on a turbulent boundary layer." AIAA Journal, 41(10), 1916-1924.
45. Kovács, G. (1981). Seepage hydraulics. Elsevier Scientific Publishing Company, U.K.

46. Krogstad, P.-Å. And Kourakine, A. (2000). "Some effects of localized injection on the turbulence structure in a boundary layer." Physics of Fluids, 12(11), 2990-2999.

47. Lambe, T. W., and Whitman, R. V. (1979). Soil mechanics. SI version, John Wiley & Sons, New York, N.Y.

48. Landry, W., and Werner, B. T. (1994). "Computer simulations of self-organized wind ripple patterns." Physics D, 77, 238-260.

49. Ling, C. H., Jan, C. D., Chen, C. L., and Shen, H. W. (1992). "Numerical simulation of a sphere moving down an incline with identical spheres placed equally apart." Proc., 9th Conf. On Engrg. Mech., ASCE, New York, N.Y. 764-767.

50. Lovera, F., and Kennedy, J. F. (1969). "Friction factor for flat bed flows in sand channels." Journal of Hydraulic Division, ASCE, 95(4), 1227-1234.

51. Lyn, D. A. (1988). "A similarity approach to sediment-laden flows in open channels." Journal of Fluid Mechanics, 193, 1-26.

52. Lyn, D. A. (1992). "Turbulence characteristics in sediment-laden open-channel flows." Journal of Hydraulic Engineering, ASCE, 118(7), 971-988.

53. Lyn, D. A. (1993). "Turbulence measurements in open-channel flows over artificial bed forms." Journal of Hydraulic Engineering, ASCE, 119(3), 306-326.

54. Maclean, A. G. (1983). "Local erosion over a submerged intake in an alluvial channel." Thesis presented to the University of Aberdeen, at Aberdeen,

Scotland, in fulfillment of the requirements for the degree of Doctor of Philosophy.

55. Maclean, A. G. (1991a). “Open channel velocity profiles over a zone of rapid infiltration.” Journal of Hydraulic Research, IAHR, 29(1), 17-27.
56. Maclean, A. G. (1991b). “Bed shear stress and scour over bed-type river intake.” Journal of Hydraulic Engineering, ASCE, 117(4), 436-451.
57. Maclean, A. G., and Willetts, B. B. (1986). “Measurement of boundary shear stress in non-uniform open channel flow.” Journal of Hydraulic Research, IAHR, 24(1), 39-51.
58. McLean, S. R., and Smith, J. D. (1986). “A model for flow over two-dimensional bed forms.” Journal of Hydraulic Engineering, ASCE, 112(4), 300-317.
59. McLean, S. R., Wolfe, S. R., and Nelson, J. M. (1999). “Predicting boundary shear stress and sediment transport over bedforms.” Journal of Hydraulic Engineering, 125(7), 725-736.
60. Mendoza, C., and Shen, H. W. (1990). “Investigation of turbulent flow over dunes.” Journal of Hydraulic Engineering, ASCE, 116(4), 459-477.
61. Mercer, A. G. (1971). “Analytically determined bed-form shape.” Journal of the Engineering Mechanics Division, ASCE, 97(EM1), 175-180.
62. Miller, R. L., and Byrne, R. J. (1966). “The angle of repose for a single grain on a fixed rough bed.” Sedimentology, Elsevier Publishing Company, Amsterdam, 6 (1966) 303-314.

63. Nakagawa, H., and Nezu, I. (1987). "Experimental investigation on turbulent structure of backward-facing step flow in an open channel." Journal of Hydraulic Research, IAHR, 25, 67-88.

64. Nakagawa, H., Tsujimoto, T., and Murakami, S. (1988). "Effect of suction or injection through bottom of a stream on bed load transport processes." Proc., Int. Conf. On Fluvial Hydraulic, Budapest, 70-75, IAHR, Delft, Netherlands.

65. Nelson, J. M., McLean, S. R., and Wolfe, S. R. (1993). "Mean flow and turbulence fields over two-dimensional bed forms." Water Resources Research, 29(12), 3935-3953.

66. Nezu, I. (1977). Turbulent structure in open channel flow. PhD thesis, Kyoto University, Kyoto, Japan.

67. Niño, Y., Atala, A., Barahona, M., and Aracena, D. (2002). "Discrete particle model for analyzing bedform development." Journal of Hydraulic Engineering, ASCE, 128(4), 381-389.

68. Oldenziel, D. M., and Brink, W. E., (1974). "Influence of suction and blowing on entrainment of sand particles." Journal of the Hydraulics Division, ASCE, 100(HY7), 935-949.

69. Parker, G. (1975). "Sediment inertia as cause of river antidunes." Journal of the Hydraulics Division, ASCE, 101(HY2), 211-221.

70. Prinos, P. (1995). "Bed-suction effects on structure of turbulent open-channel flow." Journal of Hydraulic Engineering, ASCE, 121(5), 404-412.

71. Ramakrishna Rao, A. and Nagaraj, S. (1999). "Stability and mobility of sand-bed channels affected by seepage." J. of Irrigation and Drainage Engineering, 125(6), 370 – 379.

72. Ramakrishna Rao, A., Subrahmanyam, V., Thayumanavan, S., and Namboodiripad, D. (1994). "Seepage effects on sand-bed channels." J. of Irrigation and Drainage Engineering, 120(1), 60-79.

73. Raudkivi, A. J. (1963). "Study of sediment ripple formation." Journal of Hydraulic Division, ASCE, 89(HY6), 15-33.

74. Raudkivi, A. J. (1997). "Ripples on stream bed." Journal of Hydraulic Engineering, ASCE, 123(1), 58-64.

75. Raudkivi, A. J., and Witte, H. H. (1990). "Development of bed features." Journal of Hydraulic Engineering, ASCE, 116(9), 1063-1079.

76. Reynolds, A. J. (1965). "Waves on the erodible bed of an open channel." Journal of Fluid Mechanics, 22(1), 113-133.

77. Richards, K. J. (1980). "The formation of ripples and dunes on an erodible bed." Journal of Fluid Mechanics, 99, 597-618.

78. Richardson, J. R., Abt, S. R., and Richardson, E. V. (1985). "Inflow seepage influence on straight alluvial channels." Journal of Hydraulic Engineering, ASCE, 111(8), 1133-1147.

79. Rotta, J.C. (1966). "Control of turbulent boundary layers by uniform injection or suction of fluid." ZAMM 46, T 213 - T 215.

80. Schlichting, H. (1979). Boundary layers theory, 7th Ed., McGraw-Hill, Inc., New York.

81. Shen, H. W. (1971). River mechanics, vol. 1, Colorado State University, Fort Collins, Colo.

82. Shen, H. W., and Julien, P. Y. (1993). "Erosion and sediment transport." Handbook of Hydrology, edited by Maidment, D. R., Ch. 12, pp. 12.1-12.61, McGraw-Hill Inc..

83. Simons, D. B., and Richardson, E. V. (1961). "Form of bed roughness in alluvial channels." Journal of the Hydraulics Division, ASCE, 87(HY3), 87-105.

84. Smith, J. D., and McLean, S. R. (1977). "Spatially averaged flow over a wavy surface." Journal of Geophysics Research, 82, 1735-1746.

85. Terzaghi, K., and Peck, R.B (1967). "Soil mechanics in engineering practice." Second Ed., John Wiley & Sons, New York, N.Y.

86. Thomas, Z. (1967). "Velocity of motion of sand banks." Proc 12th Congress of IAHR, Vol. I, Fort Collins, Colorado, Sept. 1967.

87. van Rhee, C., and Bezuije, A. (1992). "Influence of seepage on stability of sandy slope." Journal of Geotechnical Engineering, 118(8), 1236-1240.

88. van Rijn, L. C. (1982). "The prediction of bedforms and alluvial roughness." Proceedings of Euromech 156, Mechanics of Sediment Transport, Istanbul, 133-136.

89. Vanoni, V. A. (1975). "Sedimentation engineering." ASCE Manual and Reports on Engineering Practice No. 54, ASCE, New York, N. Y.

90. Watters, G. Z. and Rao, M. V. P. (1971). "Hydrodynamic effects of seepage on bed particles." J. of the Hydraulics Division, ASCE, 101(3), 421-439.

91. Willetts, B. B., and Drossos, M. E. (1975). "Local erosion caused by rapid forced infiltration." Journal of the Hydraulic Division, ASCE, 101(HY12), 1477-1488.

92. Wuhan University, River Mechanics. Industry Publishing Company, China, 1961.

93. Yalin, M. S. (1972). Mechanics of sediment transport, Pergamon Press, Inc., London, England.

94. Yalin, M. S. (1977a). Mechanics of sediment transport, 2nd edition, Pergamon Press, Inc., London, England.

95. Yalin, M. S. (1977b). "On the determination of ripple length." Journal of the Hydraulics Division, ASCE, 103(HY4), 439-442.

96. Yalin, M. S. (1985). "On the determination of ripple geometry." Journal of Hydraulic Engineering, ASCE, 111(8), 1148-1155.

97. Yalin, M. S., and Karahan, E. (1979). "Steepness of sedimentary dunes." Journal of the Hydraulics Division, ASCE, 105(HY4), 381-392.

98. Zippe, H. J., and Graf, W. H. (1983). "Turbulent boundary-layer flow over permeable and non-permeable rough surfaces." Journal of Hydraulic Research, IAHR, 21(1), 51-65.